PHD

Interpretation of sub-bottom signals

Savory, P. G.

Award date:
1986

Awarding institution:
University of Bath

INTERPRETATION OF SUB-BOTTOM SIGNALS

submitted by P.G. Savory

for the degree of PhD

of the University of Bath

1986.

P.G. Savory

ProQuest LLC
789 East Eisenhower Parkway
P.O. Box 1346
Ann Arbor, MI 48106-1346

SUMMARY

An investigation into acoustic means of examining the buried sediment layers that make up the sea bed has been undertaken; the approach taken was both experimental and theoretical. A successful sediment facility was developed, in the laboratory, which consisted of an echo sounder and data collection system, together with graded sands which were prepared into water saturated layers. The echo sounder was used as a sub-bottom profiler to record reflections from these layers at normal incidence. The depth of the layers were of the order of a few centimetres and the echo sounder was operated at a frequency of 165 kHz.

Particular emphasis was put on the requirement for high resolution and to this end a deconvolution technique was used to improve the recorded signals. The deconvolution was carried out on a desk top computer and it was shown that the resolution can be improved, but the extent of the improvement depends on the bandwidth of the signals used.

Techniques were used to derive the acoustic parameters of attenuation and impedance from the output of the deconvolution; these results have shown agreement with independently made measurements on the same types of graded sands. The technique proposed can calculate both parameters together given the opportunity to re-survey an area each time a new layer is deposited.

ACKNOWLEDGEMENTS

I am grateful to have this opportunity to thank many of the people who helped me with this work.

Firstly I wish to thank Professor H.O.Berktay, my supervisor, for his encouragement, constructive criticism and patience.

I also wish to thank Mr. B.Ring and the technicians in the Physics department for their help, especially Mr. B.Gay who assisted with building the experimental equipment.

There are many people who made useful suggestions towards this work and in particular I wish to thank Dr. V.Humphrey, Dr. N. Pace and Dr. P. Thorne for their interest in this work and for their advice.

The financial support of the SERC is also acknowledged.

Finally I would to like to thank my sister, Maggie, and my mother and father who have encouraged me throughout this work.

CONTENTS

LIST OF FIGURES

LIST OF SYMBOLS

u, U Displacement of sediment solid skeleton and fluid respectively.

P, Q, R Sediment elastic coefficients.

ρ_{11}, ρ_{22} are effective densities of solid and fluid respectively.

ρ_{12} Coupling parameter between solid and fluid movements.

h Porosity.

ρ_m Effective density of sediment.

ρ True density of sediment.

c Velocity of acoustic waves.

B Bulk modulus.

B_1 Liquid bulk modulus.

B_s Solid bulk modulus.

τ Arbitary delay between two signals.

δ Dirac delta.

$*$ Denotes convolution.

* Complex conjugate.

ω Frequency domain variable in radians per second.

j Denotes imaginary part of.

t Time domain variable.

W Half window width in frequency domain.

r Reflection coefficient.

T Transmission coefficient.

C_m Coefficients of small value expansion for tanh(x).

d Depth of a layer.

α Attenuation coefficient.

Z Acoustic impedance.

a_n Actual amplitude loss in a given layer, n.

$\Gamma_1(t)$ Observed primary outputs.

γ_n Individual primary output from interface, n.

χ Comparative layer reflectivity coefficient.

k Wave number.

J_1 Bessel function of order one.

θ_B Half power beamwidth.

λ Wavelength.

a Transducer element radius.

Q 'Q' factor.

A(t) Envelope of reference signal.

$\phi(t)$ Phase of signal.

ω_o Carrier frequency in radians per second.

p In-phase component of signal.

q Quadrature component of signal.

r(t) Reference pulse (or wavelet).

R(ω) Fourier transform of reference.

x(t) Measured signal before deconvolution.

X(ω) Fourier transform of x(t).

y(t) Deconvolved signal.

Y(ω) Fourier transform of y(t).

i(t) Impulse response.

I(ω) Fourier transform of i(t).

H(ω) Window function in frequency domain.

h(t) Inverse Fourier transform of H(ω).

N Number of points in inverse transform.

f_o matched resonant frequency of ceramic element.

f_o' open circuit resonant frequency of ceramic

ϕ ideal transformer ratio of ceramic.

S surface area of the element face.

Z_c acoustic impedance of the element.

C_o static capacitance of the element.

e_{33} stress per electric field of the element.

ϵ_{33} dielectric constant of the element

ϵ_o dielectric constant of free space.

D thickness of the element.

R_m mechanical impedance of the element.

CHAPTER 1 INTRODUCTION

Geophysical surveys of the sea bed for purposes such as the location of buried pipes or cables, pre-construction site survey or the monitoring of shipping channels can be achieved by acoustic means. Reflection seismic surveying is a rapid means of generating an extremely useful graphical display of bottom and sub-bottom features based on acoustic reflections.

Acoustic waves are attenuated in the sea bed and the penetration achieved depends on the frequency used. The attenuation increases with frequency and hence lower frequencies are used for deeper penetration, at the expense of resolution, and high frequencies are used for shallow penetration where resolution is important. In deep seismic work a maximum frequency of about 100 Hz may be used to achieve penetrations of the order of a kilometre , whilst for high resolution work a frequency of about 10 kHz may be used with useful results obtained for the first ten metres or so of the sea bottom. This work is concerned with the high resolution end of the scale and is generally referred to as sub-bottom profiling.

The work described here has evolved, to some extent, from previous work in Bath University, where a sub-bottom profiler had been developed to obtain intensity modulated pictures of the first 10 - 15 metres of sediments. The implementation of this sub-bottom

profiler was achieved by housing the acoustic equipment in a towed body, referred to as a fish, and the equipment was controlled from the towing vessel by means of electrical connections inside the towing cable.

The acoustic equipment transmitted a 12 kHz pulse using a piezo-electric transducer constructed from two tubular elements. The transducer had physical dimensions of the order of one wavelength at 12 kHz, and it was positioned at the focal point of a pseudo-parabolic reflector, approximately 1 m across, to produce a beamwidth of 8 degrees. The beam was directed vertically downwards to insonify the sea bed at normal incidence; the system achieved penetrations of typically 15 metres and a resolution of about 40 cms was claimed in some situations. The towing speed was typically set at 3 metres per second, which enabled large ranges to be surveyed very rapidly compared to any other method; a pulse repetition frequency of 5 Hz and a towing height of about 20 metres above the sea bed meant that successive areas insonified on the sea floor overlapped considerably which achieved some averaging of the returned signals.

The advantages gained by towing the fish were that the fish could be positioned away from the noise generated by the towing vessel, and the movement of the towing vessel was largely decoupled from the fish; a quieter and more stable sonar platform was the result. Furthermore, by placing the fish close to the bottom the

resolution was improved by reducing the insonified area, and the amplitudes of the returned signals were increased because of the shorter paths involved; also reverberation effects in the top water layer were outside the time window of the useful returns.

There was no signal processing applied to the results obtained, apart from a dynamic range compression, and the main aim of this project was to investigate the possibility of obtaining information about the elastic parameters of the sediment layers by processing the signal returns obtained in sub-bottom profiling. To this end an experimental programme of work was undertaken in the laboratory by building a 'scaled' echo sounder and using graded sands to model a layered sea bottom. This model was then used to record reflections from these layers, at normal incidence, so that the effects of signal processing techniques could be examined by simulation on a desk-top computer. Different methods are used for analysing echoes from these sub-bottom layers depending on the application, however insonification at normal incidence with shallow penetration using narrow beams is a great simplification to the general application and much of the processing effort required in deep seismic work is not required here.

In this work sediments are generally taken to mean sands where the mineral grain diameters are within the range of 50 μm to 500 μm. This corresponds to a

typical sandy beach found around the British coastline and represents a large proportion of the Continental Shelf sea bed. The model to be built was to be approximately a one tenth to one fifteenth scale of the sea going system so that an operating frequency of about 150 kHz would be required, penetrating into sand layers to a depth of a few tens of centimetres and with a resolution of a few centimetres.

The literature survey discusses both the theoretical and experimental work that has been carried out to give an insight into the propagation of sound through typical sediments. The literature survey also discusses some high resolution sub-bottom profilers developed elsewhere together with their results, which indicate areas where useful work may be directed.

The theoretical work is described in chapter 3 and a method of processing the received signals to improve the resolution is described, using a deconvolution technique. Then, two different methods of obtaining the parameters of the sediment layers are put forward, one method uses an integration technique and can potentially output a continuous acoustic impedance profile. The other method relies on the identification of each echo, and then generates equations which can be solved for both acoustic impedance and attenuation; this is particularly applicable to regularly monitored sediments in harbours and estuaries.

The experimental equipment is described in chapter 4 which explains how the modelled sediment layers were set up in the laboratory; the transducer design, calibration and manufacture is explained together with the electronics system built to drive it. The receiving electronics used a demodulation technique before the signals were recorded, and then the signals were converted to digital form for storage and use by the computer. An estimate of the performance expected in terms of resolution is made.

Chapter 5 describes the main measurements that were taken in the laboratory and firstly shows the received signals in their unprocessed state. The received signals are then deconvolved using the method described in chapter 3 and the results are shown for the cases of one, two and three layers. These results are then used to obtain the acoustic impedance and attenuation of each of the buried layers which can be compared with results obtained previously from measurements on the individual sands.

Chapter 6 examines the performance of these techniques in terms of what they achieve. An improvement in resolution of about 2:1 can be achieved and the acoustic parameters were deduced to within about ten per cent, but it was not possible to improve any further on this because of the limited bandwidth of the signals used.

CHAPTER 2 LITERATURE SURVEY

2.1 Introduction

The purpose of this literature survey is to examine the work that has been done in areas which are relevant to this project and to learn from the conclusions and progress of other authors; in this respect the relevant literature has been divided into four areas. The first concerns work on individual single sands and starts by looking at the theoretical work that has been done; fitting the theoretical results to experimental measurements helps to generate an understanding of the mechanisms going on. The next area concerns work on layers or shaped boundaries with more than one sediment type and reveals useful information about the properties of waves in these layered media. The third area discusses the methods used for obtaining measurements of sediments at sea and the results lead to an appreciation of the properties with which this work will be dealing. The last area discusses profiling systems which have been built, together with the results and progress made.

2.2 Sediment Properties

In his classical work of 1956 Biot[1,2] presented a theoretical treatment for acoustic wave propagation in saturated sediments by modelling such a sediment as a skeletal frame of solid, with fluid in the interstices.

The equations he derived for the propagation of the dilatational waves may be written in the form

$$\nabla^2(P.u + Q.u) = \frac{\partial^2}{\partial t^2}(\rho_{11}.u + \rho_{12}.U) \quad \text{2.2.1}$$

$$\nabla^2(Q.u + R.u) = \frac{\partial^2}{\partial t^2}(\rho_{12}.u + \rho_{22}.U) \quad \text{2.2.2}$$

where the damping terms have been omitted for simplicity, u and U represent the displacement of the solid skeleton and fluid respectively. The parameters P,Q and R represent elastic coefficients, ρ_{11} and ρ_{22} relate to the densities of the solid and fluid via the porosity and ρ_{12} is a coupling parameter.

Rotational waves are also predicted, but, because of the statistical isotropy of the material, they are uncoupled from the dilational waves and obey independent equations of propogation.

A qualitative application of Biot's theory was not forthcoming, in the interpretation of experimental results, until the work of Yew and Jogi[3] in 1976. Yew and Jogi solved Biot's equations which predicted two dilationatial waves (a fast slightly dispersed one and a slower, heavily dispersed and attenuated one). The results of their experimental work showed that only the fast wave was observed in the laboratory, however they had difficulty in obtaining agreement with Biot's predicted wave speeds mainly because of the problem of determining the parameters. In particular ρ_{12}, the solid/fluid coupling parameter is an unknown quantity,

however they did demonstrate that its magnitude is small and that its contribution to the magnitude of wave speeds is 13% at the most.

Meticulous measurements have been made at spot frequencies over a range of sediment types and in particular Thomas and Pace[4], Hampton[5], Nolle et al[6] and McCann and McCann[7] have presented graphs showing the relations between attenuation and velocity versus grain size, porosity and density. Only Thomas and Pace[4] have made attenuation measurements over a range of frequencies using a correlation technique.

Three attenuation mechanisms have been acknowledged,

1) ~~Raleigh~~ Rayleigh scattering, which is characterised by a fourth power dependence on frequency, is negligible for grain sizes much less than the wavelength and can be ignored for grain sizes less than 1 mm at frequencies under 1 MHz, see Nolle et al[6].

2) Solid friction losses occurring at the points of contact of the grains are identical in nature with those in polycrystalline rocks and are characterised by a linear variation of attenuation with frequency over the range 1 to 10^9 Hz, see McCann and McCann[7].

3) Viscous losses depend on the acoustic velocity differential of the solid skeleton and the fluid and are expected to vary as the square root of frequency for frequencies down to a few tens of kHz

with grain sizes above about 20 μm, see Thomas and Pace[4] and Stoll[10].

The viscous loss mechanism depends on the permeability of the sediment and uniformity of the mineral grains, however at frequencies above about 1 kHz the results of McCann and McCann[7] and Hamilton[25] suggest that the solid friction mechanism is dominant for sediments of diameter greater than 20 μm; although for a well sorted sediment, or for diameters less than 20 μm, viscous losses may become important.

Nolle et al[6] addressed the question of particle movement by examining the velocity of acoustic waves. The velocity is given by,

$$c = [\ B/\rho_m\ ]^{1/2} \qquad 2.2.3$$

where B is the bulk modulus given by

$$1/B = h/B_l + (\ 1-h\ )/B_s \qquad 2.2.4$$

where B_l is the liquid bulk modulus

B_s is the solid bulk modulus

and h is the porosity

ρ_m is the effective density of the sediment and for particles at rest is given by,

$$\rho_m = \rho/(h/k) \qquad 2.2.5$$

where ρ is the true density of the mixture

k allows for stagnant pore spaces which cannot allow the liquid to pass in the direction of the wave and is always greater than unity.

Nolle took a typical value for k of 4.3 from the work of Ferrero and Sacerdote[8] which predicts much lower

velocities from equation 2.2.3 than those measured. He concluded that the definition used for the effective density in equation 2.2.5 must have been incorrect and that the particles are not at rest.

Urick pointed out, however, that in the case where the particles are small compared with the wavelength and move with the fluid then ρ_m should be taken as the total mass of solid and liquid per unit volume. Using this definition of ρ_m in equation 2.2.3 gives results much closer to those observed by Nolle, suggesting that the particles must move substantially with fluid.

The emerging picture of a water saturated sediment is of a skeletal frame of grains, supported by point contacts, with a large proportion of pore spaces open for fluid flow. When insonified the skeletal frame flexes slightly with the fluid flow to give a linear dependence of attenuation on frequency, and a sound wave velocity depending on the effective bulk modulus and some effective density of the mixture.

2.3 Layered Models

Having established a model of the interactions taking place within a homogeneous sediment it is necessary to consider interactions between sediment layers. The modelling of sediments in a laboratory is difficult because of the problems of obtaining realistically sorted sands, achieving compaction and de-aeration.

A method of preparing sands used by Nolle[6] was to boil the water/sand mixture to remove air, then to transfer the mixture to a vibrating box underwater which compacted the sand; the vibration was continued until the acoustic parameters ceased to change. Hampton[5] used an evacuation technique to remove air and simply left the sediment to settle to achieve compaction, while Thomas and Pace[4] used a combined evacuation and vibration technique.

The practical difficulties encountered have limited work on layered sediments in the laboratory, however Barnard, Bardin and Hempkins[11] have examined single layers . In particular they worked with three boundaries which were,

1) a pressure release boundary

2) a semi-infinite sand bottom

3) a solid sub-bottom covered with a fluid sediment.

Using a 100 kHz sonar with a 300 μs pulse they measured reflection coefficients over a range of grazing angles from 20° to 70°; normal incidence was not considered. They compared their results with calculated values from the Rayleigh reflection coefficient for oblique incidence, allowed for attenuation and took into account shear waves where appropriate, as described by Brekhovskikh[12]. Their conclusion was that, for these well defined models, the

simple reflection coefficients are adequate to predict the results.

Hilterman[13,14] and Woods[15] have both investigated various structured boundaries using spark sources with models of paper and wood in air. Their results clearly show the effects of delayed echoes returned from off axis insonification of the structure which produce a hyperbola for each point reflector. They do not consider penetration of the structure but demonstrate a resolution limitation with beamwidth.

Smith[16] develops a theoretical model of a more complex system using a ray tracing technique. His model allows for penetration in up to three layers, and also allows for sloping bottoms and curved top layers. He produced synthetic reflection profiles from this model. One important conclusion from Smith's work is that he considers the only multiple reflection with a significant amplitude to be the water multiple.

A theoretical model by Rutherford and Hawker[17] of a three layer model of water/sediment/basement has been used to investigate the effects of varying sound speed and density gradients on the bottom loss. The model has been developed further by Hawker[18] to allow for the possibility of shear waves and by Hawker, Williams and Foreman[19] to allow fo variation of absorption with depth. The results over a range of grazing angles are complicated, however at normal incidence the models predict that no shear waves will be exited, and they

also predict a simple increase in attenuation for increasing attenuation gradient. The total attenuation for a layer with a linearly increasing attenuation coefficient is given by the attenuation of an equivalent homogenous layer, with an attenuation coefficient equal to the mid-way value of the actual layer.

Fryer[20] considered a theoretical model consisting of a stack of homogenous, isotropic layers sandwiched between a fluid half space above and a solid half space below. His solution showed that conversion of compressional energy to shear energy is unimportant, for the case of elastic constants varying continuously, above about 20 Hz. In agreement with Hawker[18], he also showed that no shear waves will be excited at normal incidence.

Mitchell and Lemmon[21] investigated the limits within which ray theory is a good approximation to wave theory. They derived a model with an arbitary number of absorbing fluid layers with variable sound velocity. overlying an iso-velocity half space. Comparing their results with Fryer[20] they found that ray theory results were indistinguishable from wave theory above about 20 Hz.

Cron and Nuttal[22,23] examined phase distortion of a pulse reflected from lossy bottoms, by treating the system as a linear filter. Calculating the distortion over a range of incident angles and attenuation coefficients, they found that for a normally incident

pulse insignificant distortion will result unless the bandwidth of the pulse is greater than the inverse of the attenuation (in Nepers/Hz), since frequency components at opposite ends of the spectrum will undergo substantially the same amount of attenuation.

2.4 Measurements from sea samples

The acoustic properties of real sediments can be obtained from core samples or they can be measured using data from sonobuoys. A problem caused by collecting core samples is that the sample is inevitably disturbed by the coring process and some early core samples gave velocity values which showed a great deal of scatter, see Schreiber[24]. However these problems have been largely overcome and extremely consistent results have been obtained by Hamilton[25,26]. The problem of converting a velocity value, measured in a laboratory from a core sample, to what it would have been in situ has been elucidated by Hamilton[27].

The conversion method assumes that whilst the sample is in situ the salinity of the bottom water is about the same as that within the pore spaces of the sediment, and this does not change from in situ to the laboratory. Hence the only changes in sound velocity in the bottom water and pore water are due to temperature and pressure changes. The effects of temperature and pressure changes on the mineral grains themselves are insignificant. Hence both water and sediment velocites

can be converted from laboratory to in situ values by making corrections for temperature and pressure using standard tables for speed of sound, but the ratio will remain the same. The identity of the ratio of the laboratory and in situ values was proved experimentally, by Hamilton.

In situ measurements of sediment surface velocity were made by Tucholke and Shirley[28] while taking core samples. Transducers were fastened to the corer and measurements were taken across the core as the corer penetrated the sediment and a velocity profile recorded. They compared their results with laboratory measurements on the same sample, corrected to in situ values, and they reported reasonable agreement.

Sonobuoy data has been collected world wide by Houtz et al[29], Hamilton et al[30] and Hamilton et al[31]. The sonobuoy method uses the sonobuoy as a remote vehicle for supporting a hydrophone. A shipborne source continuously transmits pulses, typically of length 1 ms and at intervals of 1 second, while the ship steams away from the sonbuoy.

The pulses partially penetrate the sea bottom and are reflected from each interface below it, to be recorded by the hydrophone, see figure 2.4.1. The length of the path of each return is different, and as the distance between the ship and the hydrophone increases there is a different rate of change of path

length for each return, depending on the geometry and the velocities in each layer.

The solution for the velocities in each layer assumes that each layer is iso-velocity and then takes refactoin into account at the boundaries. The minimum layer thickness is limited to about 1/10 of the depth of the water layer because of errors in the water column. An improvement by Bryan[54] is to place both source and receiver on the sea bed which reduces the length of each run but nevertheless reduces the minimum layer to about 1/25 of the water depth. These methods calculate a velocity at the mid-point of each layer and hence the velocity at the top of the top layer, which is of critical importance, is not known. An independently derived sediment surface velocity is required and these can be obtained by divers in shallow water or alternatively measured from core samples taken in the area.

These measurements have shown large variations in sediment properties and Houtz[32] has noted variations in velocity measurements from sonobuoy data from 0.6 to 3 km/s world wide. In general large velocity gradients are found in calcareous sediments while low velocity gradients are found in terrigeneous sediments.

Jones Leslie and Barton[33] made some reflection measurements in 1963 at five different locations over angles of incidence from 0° to 45°. They could not find any variation in reflection coefficient with angle

of incidence at four of these locations where the bottom was mud or sand although they did where the bottom was hard packed coral-sand. However they claim an accuracy of 10 % in their measurements for reflection coefficients greater than 0.7, but this accuracy decreased as the reflection coefficient decreased and they could not distinguish between coefficients of 0.1 and 0.15 . It is worth noting that at one location they found a reflection coefficient of -0.85 indicating a pressure release boundary caused by entrapped gas in the bottom mud, probably generated from biological matter. This phenomenon is not uncommon and demonstrates a requirement to be able to detect inversions of the returned signals.

It is not useful to produce regression equations for acoustic parameters based on measured grain size, sorting, porosity etc. because of the great variability found. However, Hamilton[25] does present graphical data of velocity and attenuation versus each of porosity , grain size and density showing wide ranges of values. Large variations of acoustic parameters with each physical parameter were also found by Tucholke[37] who found a great deal of scatter in his core sample measurements taken in the Western Atlantic. He noted that no one parameter can adequately describe the acoustic environment, however his results were in general agreement with Hamilton's and showed the same trends. Hamilton considers that in silt-clays of all

the pressure induced changes porosity reduction is by far the most important; near the surface the volume of water present is the most significant factor in the increase of bulk modulus with depth. In sands there is little reduction in porosity in the upper tens of metres and the main effect of pressure is to increase rigidity due to intergranular pressure.

Hamilton has been most prolific in collecting and presenting data over many years and his papers[26,34,35,36] effectively contain all the present knowledge concerning attenuation, velocities and reflection coefficients compared with physical parameters such as grain size, porosity etc. These papers are summarised in his latest paper[25].

He presents regression equations of the form,

$$\text{Velocity, } V = A + B(\text{Depth}) + C(\text{Depth})^2 \qquad 2.4.1$$

where he tabulates values of A, B and C, for three different sediment types.

For fine sands he presents,

$$\text{Velocity, } V = 1806(\text{Depth})^{0.015}\ ms^{-1} \qquad 2.4.2$$

for the velocity in the top 20 m, where depth is in metres. This equation predicts zero velocity for zero depth but it should be noted that the experimental measurements were made from core samples which had been cut into 10 cm lengths. The velocity measurement made on the top core sample was taken to be at the mid-point which is at a depth of 5 cm. This top measurement was corrected to an in situ value and the velocity obtained

was 1727 ms^{-1}. The figure of 0.015 for the power of the depth had been established previously, as a best fit to experimental data, and substituting the values of 1727 ms^{-1} at a depth of 0.05 m gave the constant of 1806 ms^{-1}. Hence this equation should not be used at depths less than 5 cm. For other sediments he considers penetrations of several hundred metres and does not show detail in the first few metres.

These results enable a mean velocity gradient to be calculated by subtracting the top and bottom velocity values for a layer, or as Houtz[32] points out integration gives a local gradient, at a particular depth in the layer.

Attenuation versus frequency has been measured by Hamilton[25] and he presents data over six orders of magnitude of frequency which show a dependence on the first power of frequency, supporting the solid friction attenuation mechanism decribed by McCann and McCann[7]. There is the possibility of non linearity at frequencies below 1 kHz where no measurements appear to exist. Viscous losses theoretically exhibit an f^2 dependence at low frequencies and an f^{4} dependence at high frequencies, The exact cross over point is not well defined but lies within the range 1 to 20 kHz, see Stoll[10].

2.5 Profiling Systems

There is a wide range of applications for profiling systems which have different requirements. At one end of the scale are systems requiring deep penetration at the expense of resolution, which is generally in the field of oil exploration. Deep penetration has its own problems[38] mainly caused by distortion of the transmitted pulse, refraction of the pulse and the wide beamwidths which generate a hyperbola for each point scatterer on the seismic section. These problems are not discussed here because it is the other end of the scale that is of interest here. The work here requires high resolution at shallow penetrations. This is in support of surveys of buried pipes or cables, site survey before underwater construction and monitoring of navigation channels. Having restricted the situation to shallow penetration many problems are averted, in particular there is not usually any significant distortion of the transmitted pulse[22,23] and reverberations in the water layer do not usually occur within the time window of interest.

In order to obtain high resolution it is necessary to use a high frequency and to insonify a small area on the sea floor (the footprint). The frequency cannot be increased indefinitely because the attenuation increases with frequency and the useful range is reduced, hence there is a trade off between penetration required and resolution. Typically frequencies of 3 or 4 kHz are

used for penetrations down to about 100 m and 10 or 12 kHz for penetrations of 10 m or so. There are existing systems which have been commercially available for about 10 or 15 years operating at these sort of frequencies. These systems are packaged in a towed body, called a fish, which is towed behind a ship as close to the sea bottom as possible in order to reduce the size of the footprint.

More recently the parametric array has been developed and these have some significant advantages over conventional systems. Typically two primary frequencies of the order of 200 kHz and separated by a few kHz are transmitted into the water. The two signals mix in the water due to the non linear propogation effects to produce a narrow beamwidth signal at the difference frequency of a few kHz. A sum frequency is also produced but is rapidly attenuated in the water.

The advantage gained is a beam at a few kHz with about the same beamwidth as the original primary frequencies, with no observable sidelobes, generated from an acoustic aperture much smaller than would be required by conventional means (typically a factor of 16 times smaller). The penalty paid is a much reduced source level because of the low efficiency of the difference frequency generation and the limit on the maximum acoustic intensity available at the higher primary frequencies - if the primary frequencies are at

intensity levels well above the cavitation threshold the difference frequency pattern can become almost omnidirectional.

The uses and applications of the parametric acoustic source have been discussed by Konrad[74] and these include a depth sounder for deep water mining, a doppler navigation system and a side scan sonar. The particular advantage for high resolution sub-bottom profiling is the narrow sidelobeless beams that can be obtained at relatively low frequencies where absorption remains reasonably low. The Raytheon Company, Portsmouth have reported[76] useful results in high resolution sub-bottom profiling in water depths of 6000 m, using difference frequencies in the range 3.5 to 12 kHz. A system developed at the University of Birmingham[77] in colaboration with Vickers Oceanics Ltd. used a chirped pulse with a swept band of 6.6 kHz and a centre frequency which could be selected to be 5, 10 or 15 kHz. This system showed little advantage at 15 kHz but showed significantly more detail at 10 kHz than at 5 kHz, and the conclusion was that this system could be a very useful tool in applications involving shallow penetration into sediments

A parametric sub-bottom profiler has been developed in Norway as a joint project between Simrad A/S and the University of Bergen sponsored by the Norwegian Council for Scientific and Industrial Research. Pettersen, Hovem, Lovik and Knudsen[47] describe the system which has

a selectable difference frequency over the range 1 to 7 kHz giving beamwidths of 10 to 5 degrees respectively. The signal level is increased by using a 10 m long cable with 40 hydrophones to receive on, and the received signal is filtered and replica correlated with the transmit pulse, before it is displayed. The results from the first trial in 1975 were encouraging and they found that a frequency of about 3 kHz gave an optimum penetration at 40 m.

Returning to conventional systems, the Marine Physical Laboratory of Scripps Institution of Oceanography have a deep tow instrumentation system which started as a simple towed echo sounder in 1962 and has been steadily improved until it now carries up to 20 sensors or sampling systems including the associated control, processing and display equipment aboard ship. This very sophisticated system is of particular interest because of the 4 kHz profiler added in 1972. The equipment and the results obtained have been discussed by Tyce[39] and Tyce, Mayer and Spiess[40].

Attention is drawn to a high lateral variability found in deduced parameters. Indeed over lateral distances of a few metres they report 7 dB changes in overall reflected energy as well as 10 dB changes from individual reflectors. They also reported anomalously high amplitudes, which indicate a reflection coefficient greater than one (assuming 0.25 dB/m attenuation). They put forward the possibility of interference between

layers in order to explain these results, and they added a 6 kHz profiler in 1977, so that they could investigate this possibility. The results of the 4 and 6 kHz profilers indicate quite different sub-bottom features supporting the idea of multilayer interference. Indeed interactions at one frequency can show an apparent feature where none exists at another frequency.

In order to relate physical properties to acoustic properties they examined 10 m core samples, measuring density and velocity to compute a reflection coefficient series at 10 cm steps. Convolving this with the 4 kHz wavelet they obtained good agreement with the observed profile at 4 kHz. However generating synthetic 2 and 6 kHz profiles in the same manner they found that the energy profiles bore no resemblance to the 4 kHz one. Tyce reported that none of these bore any resemblance to the original reflection coefficient series.

In 1982 Marchisio and Hodgkiss[41] used this same reflection coefficient series to assess the performance of various deconvolution techniques. They took the same series and added four large synthetic reflectors to the measured series in such a manner that they could show that the reflected output from the original series was essentially the same as the output from the altered structure, at a particular frequency. This demonstrated that the output from a given structure was not unique and the two series provided a good test for their deconvolution techniques to see whether they could

distinguish between them. They found that their processing methods showed a trade off between stability and resolution; however, all of the methods used recovered that portion of the reflection coefficient spectrum that lay within the frequency band of the transmit pulse.

Huntec (70) Ltd of Canada have been involved in both land and marine geophysical instrumentation since 1970. In 1974 the firm started a 5 year project in conjunction with the Bedford Institute of Oceanography (Dartmouth, Nova-Sotia, Canada) called Seabed '75, to "quantify vertically reflected acoustic energy in terms of the parameters of the sea floor". Hutchins, McKeown and King[42] describe the objectives and the sytem more fully. A towed system has been developed incorporating a powerful boomer source with a bandwidth from 800 Hz to 10 kHz and a beamwidth of 11 degrees. The system has shown penetrations of up to 100 m in soft bottoms. This was a complex deep tow system carrying many sensors and techniques have been developed to remove tow fish motion, (Hutchins[43]). The boomer has been investigated by Simkin[44] and one of the features of this type of boomer is that the bandwidth is dependent on the angle off axis where it is measured. The effective beamwidth can be varied by the use of filters at the input stage to the receiver, at the expense of some bandwidth, and azimuthal resolution can be controlled.

Of interest are one of the display techniques which were described Parrot, Dodds, King and Simpkin[45] in their evaluation of the 5 year project. They calculate two reflectivities by summing the returned energies, r_1 and r_2, in two time windows from 0 to 0.64 ms and 0.64 to 1.60 ms on the assumption that these windows correspond to coherently reflected and scattered reflections respectively; the outgoing pulse being 0.3 ms. In this way the median and 20th and 80th percentile points for each r_1 and r_2 can be evaluated for each window by averaging over it and the previous 19 windows. This was in an effort to average out some of the statistical variations of the sort noted by Tyce, and also to provide the interpreter with more data. These r_1 and r_2 values have been shown to provide a characteristic result for bottoms of the same type.

Another interesting idea is the development of a sonogram. A sonogram is calculated by windowing (in time) the return into many short windows at successively longer delays from the start of the return pulse. The frequency spectrum is calculated for each window and a plot of amplitude of frequency components versus time delay is made. This plot can be a three dimensional plot where the X and Y axes are time and frequency and the amplitude is the Z axis. Then a contour plot can be made and this is the method favoured by Dodds[46]. Dodds describes the method more fully and demonstrates

how the sonogram can be used to calculate an attenuation coefficient.

The attenuation measurement relies on dividing the spectrum at time t_1 by the spectrum at t_2 to obtain the attenuation at each frequency component. Assuming attenuation is proportional to the first power of frequency then fitting a straight line through the origin to this divided spectrum should yield an attenuation coefficient for the medium between the instants t_1 and t_2. Some caution must be used because of the finite bandwidth of the transmitted signal. The results are encouraging but show large standard deviations of up to 60 % and do not agree well with predicted values from Hamilton[25,26]. A positive correlation with grain size is shown but they note that no one parameter fully characterises a sediment, in agreement with Hamilton.

2.6 Summary

Interest in the acoustic properties of sediments has been both theoretical and experimental. The theoretical work has been difficult to apply because of the problem of defining the parameters of the equations, in particular those that relate to the physical shape of the sand grains, however work has shown that normal incidence insonification leads to much simpler reflection loss mechanisms and the problems associaated with energy conversion to shear waves are absent.

Measurements on sediments from core samples have been made widely available and methods for correcting the results to in situ values have been developed. Measurements at sea have been made world wide using sonobuoys and the results are now extremely consistent, however they do show large variations world wide.

Measurements of reflected responses from sediments at sea have produced much useful information on sediment layering, however examination of the fine scale features reveals large variations on a scale of only a few metres horizontally, which are presently explained by interference between multiple reflections. Measurements on sediment layers in a laboratory have been difficult because of the problem of preparing realistic sediments, and there are few reports of measurements of reflected signals from precisely known layers. In particular there is little laboratory work aimed specifically at explaining the results of sub-bottom profilers.

Some techniques for presenting the acoustic parameters derived from the reflected output signals of sub-bottom profilers have been developed, however they do not appear to be widely used and some poor results have been obtained for the attenuation of buried layers.

A useful area of work would therefore be the setting up of an experimental facility that would enable layered sands to insonified at normal incidence, followed by attempts to improve the returned signals and

to deduce the acoustic parameters of the buried sand layers from them.

CHAPTER 3 THEORETICAL TREATMENT

3.1 Introduction

3.1.1 Expected signals and assumptions.

In this chapter a method for deriving the acoustic parameters of a layered sediment from the measured reflected signals of a sub-bottom profiler is described.

Consider first the type of signal expected: the sub-bottom profiler transmits a short pulse, in a narrow beam, vertically downwards to insonify a patch (or footprint) on the sea floor. Some of this energy will be reflected and some will be transmitted into the layered sediment.

The transmitted energy will continue, and as it encounters each interface it will undergo partial transmission and partial reflection again. Any reflected energy will travel back up towards the transducer, undergoing partial transmission and partial reflection at each interface above it, and some energy will eventually escape through the top surface. Any energy not escaping after one reflection will have been reflected downwards and may subsequently be reflected upwards again at any lower interface. There are an infinite number of paths that the energy could follow (not neccessarily within one layer), however if the energy is to escape through the top surface it must have undergone an odd number of reflections. Thus the complete reflected output is generated from all paths

which have undergone an odd number of reflections. Those that have under gone one reflection only are called primaries and are generally larger in amplitude than the multiple reflected outputs.

The reflected signals arriving at the profiler may be expected to be a series of exact replicas of the transmitted signals whose amplitudes depend only on the reflection, transmission and attenuation coefficients that they have undergone; however, this is only an approximation and there are several justifications to be made before this approximation can be accepted.

The assumption of a flat bottom, or planar, layer is made although it is known that the sea floor is seldom flat. In particular, if the roughness of the sea floor approaches the dimensions of the acoustic wavelength then scattering rather than reflection may be expected. For normal incidence the returned intensity may be reduced by as much as 5 dB (Urick[7]) while distributing the total scattered energy considerably in angle. For the laboratory work the size of the sand particles will be small enough to ensure that scattering is negligible, see section 4.2.

The planar assumption also has difficulties on a much larger scale than a wavelength. If the bottom is curved it will tend to focus the reflected energy in a manner which is a function of the bottom topology, resulting in substantial errors in any reflection coefficients predicted from observed outputs. This

effect is less pronounced in narrow beam systems at short ranges, which insonify a small footprint on the sea bed. The laboratory echo sounder insonifies a circle of 9 cm radius to the -3 dB point, at 0.5 m depth, see section 4.3, and topographic focusing should not be a problem.

The assumption of plane waves is also made, although the acoustic sound source essentially generates spherical waves which decrease in intensity as a function of range, within the far field. Firstly it is assumed that all the measurements will be within the far field, and the laboratory system will have approximately 55 wavelengths between the transducer and the top layer which puts the top layer well within the far field for a transducer with an acoustic aperture of about 5 wavelengths. The sea going system would typically have a somewhat larger number of wavelengths, and the far field assumption is justified in this case as well. Secondly, if apparent losses due to spherical spreading are taken into account, a spherical wave can be treated as a good approximation to a plane wave at a moderate number of wavelengths from the source (see Officer[72]). The correction for spherical spreading is then carried out by extrapolating back all signal amplitudes to the value that they would have had at some reference point. The reference point is conveniently taken as one metre and then the corrected amplitude is given by,

$$\text{corrected amplitude} = \frac{\text{actual amplitude} \times \text{actual range}}{\text{reference range (1 m)}}$$

Fine scale layering can cause a simple model based on the Rayleigh reflection coefficient to be in error if two successive layers are separated by a distance less than the length of the incident signal. In this case the layers cannot be resolved without special processing because the interference between the returns from the two layers will prevent the returned energy being representative of the actual impedance contrasts involved.

The signal will undergo attenuation as it passes through each layer but it is known (Hamilton[25]) that attenuation is linearly dependent on frequency and hence the high frequency components will be attenuated more than the low frequency components. If the signal undergoes a sufficiently long path then the signal will be severely distorted and this is a major problem where deep penetration is concerned. However, insignificant distortion will occur, at normal incidence, if the bandwidth of the pulse is less than the inverse of the attenuation, measured in Nepers/Hz, (Cron and Nuttal[22,23]), and for shallow penetration systems the distortion is negligible.

Noise is present whether it is environmental acoustic noise or noise in the electronics system and this may swamp many of the small returns, especially from multiple reflections between layers. This introduces an unavoidable limit on the dynamic range;

there is also a limit imposed by the lowest quantisation level of the signal/data capturing system. In the laboratory system noise will play a minor role, but in the sea going system it cannot be ignored.

In this work it will be assumed that the amplitude of each return will depend only on the reflection and transmission coeffients at each boundary, the attenuations within each layer and a spreading loss.

3.1.2 Proposed processing

It is required to estimate the acoustic parameters of the layers in the presence of the uncertanties described above. This is a two part process; the first being to convert the recorded signals to an estimate of the impulse response; the second is to deduce the acoustic parameters from the impulse response.

The aim of the first part is to remove the effects of the transmitted wavelet as far as possible. The second part is necessary because the impulse response is not the same as the reflection coefficient series due to effects caused by the transmission and attenuation coefficients of the sediment. Compensation for these effects requires a knowledge of the exact path followed by the energy which produced each return; this may not be possible with multiple reflections if there are two possible paths with the same total travel times. The layer depths themselves cannot be known precisely

because there is no information available on the sound velocity in the sediment. The layer depths can be calculated based on an assumed velocity, or just left in terms of travel times. This causes a problem with attenuation because, even if an overall loss within a layer is known, it will be in terms of loss per unit time when what is really required is loss per unit distance.

The signal to noise ratio in sea going systems is increased by adjusting the p.r.f. and towing speed so that adjacent footprints overlap considerably. In the laboratory a similar effect can be achieved by summing a large number of returns whilst the echo sounder is kept stationary. The process to be used for estimating the impulse response depends on the model of the layered sediment being used.

There are two basic models which have been termed parametric and non-parametric by Mendel[70]. The parametric models are characterised by two signals travelling in opposite directions in each layer such that the upgoing wave is the superposition of the downgoing wave in that layer and the transmission of an upgoing wave from the layer below, and likewise for the downgoing wave.

It is possible to relate the up and downgoing waves in adjacent layers by the reflection coefficient at the boundary of the layers. However simple solutions are strongly dependent on the assumption of equal travel

times in the layers and noise free observations of both input and output signals; more robust solutions require the inversion of a Toeplitz type matrix which requires the Levinson algorithm and only works if the top reflection coefficient is unity.

This may be applied in deep penetration work where this top reflection coefficient may represent the sea/air interface but in shallow penetration work the sea/air interface is not involved. For these reasons this model has not been considered further, and it was decided to adopt a non parametric model which applies to a lossless layered medium with horizontal homogeneity and constant velocity insonified by plane waves. This model will fit the sort of signals that are expected in this work, as described earlier, provided that an allowance is made for spreading loss and that attenuations within layers are calculated separately. In a non parametric model the outputs are the sum of time shifted and scaled replicas of the input signal. A non-parametric representation can be written as a convolution summation, first proposed by Robinson[73] in 1954, as

$$x(t) = \sum_{t=1}^{n} i(t).r(n - t) \qquad \text{3.1.1}$$

where x(t) is the output sequence,

r(t) is the input sequence

and i(t) is the impulse response.

Having accepted a convolution type model it is natural to solve it by using a de-convolution technique; this is decribed in section 3.2 where it is seen that a window is required. The width of this window can be varied in order to optimise the results. It is worth noting that related processess were considered such as autocorrelation and relica cross correlation (or matched filtering) but it is found that auto correlation does not give the best resolution and is more suitable for detecting hidden periodicities; replica cross correlation does not give a significant improvement unless the BT product is large, although it is useful in detecting signals hidden in noise.

Two possible methods for deducing the acoustic parameters from the impulse are described. The first is the 'Acousticore' method (in section 3.3), and secondly an algebraic estimation method is proposed (in section 3.4) based on comparing adjacent returns from successive layers. These are the processes that have been used on the experimental measurements and a summary of the processes is included at the end of this chapter (in section 3.5).

3.2 Deterministic Deconvolution

3.2.1 Description of the method.

Consider the signal, x(t), which is output from the convolution model stated in equation 3.1.1; let the

impulse response represent two reflectors so that,

$$i(t) = \delta(t) + \Omega.\delta(t - \tau) \qquad \text{3.2.1}$$

where the first reflector has zero delay and unit amplitude , Ω is the amplitude of the second reflection and τ is the delay of the second reflection with respect to the first.

Let the input be, r(t), which will represent the transmitted pulse and will be referred to later as the reference pulse. Thus x(t) will consist of the signal, r(t), combined with a replica of r(t) which has been delayed and attenuated, thus,

$$x(t) = r(t) + \Omega.r(t - \tau) \qquad \text{3.2.2}$$

It has already been stated that this model assumes a lossless layered medium with horizontal homogeneity and constant velocity insonified by plane waves. In practice a correction for a 1/R spreading loss will have been made to Ω, and then Ω will be representative of the combined reflection, transmission and attenuation coefficients of the layers. This deconvolution process will estimate Ω and τ only without separating the contributions of each amplitude loss mechanism.

Equation 3.2.2 can be re-written as,

$$x(t) = r(t) * [\delta(t) + \Omega.\delta(t - \tau)] \qquad \text{3.2.3}$$

where * represents convolution.

In frequency domain this becomes,

$$X(\omega) = R(\omega).(1 + \Omega.\exp(-j\omega t)) \qquad \text{3.2.4}$$

i.e. the transform of the wavelet is multiplied by the transform of the impulse response.

It follows that having obtained $X(\omega)$ it is necessary to divide by $R(\omega)$ and transform back to time domain to separate out the impulse response[46],

$$i(t) \Leftrightarrow I(\omega) = \frac{X(\omega)}{R(\omega)} \qquad \text{3.2.5}$$

In order to implement this in practise it is necessary to incorporate a window function, in frequency domain, after the division. It is also necessary to have a prior knowledge of $R(\omega)$ and to assume that the transmitted pulses will not undergo any distortion. These points are discussed below and a schematic block diagram of the deconvolution process is shown in figure 3.2.1.

3.2.2 Windowing in frequency domain

A window in frequency domain is equivalent to a bandpass filter and the purpose is to exclude those parts of the spectrum where the result of the division is likely to be in error. In parts of the spectrum where the signal to noise ratio is low the division is dominated by noise and it is possible to generate meaningless results, this is explained further in chapter 6. The specification of the window is somewhat arbitary, however if the window function is $H(\omega)$ then having applied the window to the spectrum the signal obtained, $Y(\omega)$, is given by,

$$Y(\omega) = \frac{X(\omega)}{R(\omega)} . H(\omega)$$

and transforming back to time domain gives,

$$y(t) = i(t) * h(t) \qquad \text{3.2.6}$$

Hence the result calculated is the required impulse response convolved with the transform of the window used. It is required to select the window so that the deconvolved output, y(t), is as close as possible to the impulse response, i(t).

For example, the shape of a Hamming window, centred on ω_o, is given by a raised Cosine bell as,

$$H(\omega) = 0.54 + 0.46 \times \mathrm{Cos}[(\omega - \omega_o)\pi / W]$$

$$\text{for} \quad \omega_o - W \leq \omega \leq \omega_o + W$$

$$H(\omega) = 0 \qquad \text{for} \quad \omega < \omega_o - W$$

$$\text{and} \quad \omega > \omega_o + W \qquad \text{3.2.7}$$

Where ω is the index along the frequency axis and

W is the half window width.

There are many other standard window functions which could be used, Harris[49], this one was chosen to introduce minimum ambiguities, with time sidelobes specified to be - 40 dB below the main lobe. This was considered sufficient bearing in mind that the data collection system, discussed in section 4.4.2, only had 48 dB dynamic range. The window allows inputs from parts of the spectrum between $\omega_o \pm W$, where the window will be centred on the carrier frequency, so this whole range can be considered as total bandwidth. In order

to relate this to the - 3 dB bandwidth put,

$H(\omega) = 0.54 + 0.46 \times \mathrm{Cos}[(\omega-\omega_o)\pi/W] = 0.707 \ (\equiv -3 \text{ dB})$

then $|\omega - \omega_o| = 0.38 \times W$

i.e. the -3 dB bandwidth is 0.38 of the total bandwidth.

3.2.3 Windowing problems

One of the problems caused by the convolution of the impulse response of the sediment with the transform of the window is that the polarity of the wavelet may be hidden; hence it may not be possible to detect an inversion of the wavelet, such as would be caused by a reflection from a softer acoustic medium.

If the deconvolution is carried out on a signal with a carrier frequency, ω_o, then the window has to be centred on ω_o and the transform of the window is multiplied by a sinusoid at the carrier frequency. The number of cycles of the sinusoid within this transform depends on the ratio ω_o/W; if $\omega_o/W \gg 1$ there are a large number of cycles and it is not easy to identify which way up the wavelet is unless the signal to noise ratio is very good. This is discussed further in section 4.5.

If alternatively the whole process is carried out at baseband, described in section 4.4.1, then an amplitude and phase may be calculated, but the phase is with respect to that of the demodulating oscillator. Thus in order to detect an inversion the phase of the demodulating oscillator must be locked to the instant of

transmission and the signal delay known to within at least ± π/2 of phase. In this situation the phase of the original carrier relative to the envelope must be known to detect an inversion.

3.2.4 The transmitted wavelet.

This method requires that the transmitting system be realised to produce identical signals for every transmission, in order to know $R(\omega)$, in advance. The wavelet can be recorded from a reflection off a 'perfect reflector' or directly using a hydrophone, in the latter case the response of the hydrophone must be allowed for, see section 4.3.2.

The shape of the wavelet may change as it passes through the medium either (1), because of different attenuation characteristics across the signal bandwidth or (2), as a result of interference with multiple reflections. No allowance has been made for these features in this model, but (1) can be justified in the case of shallow penetrations and small bandwidth where the difference in overall attenuation across the bandwidth is small, (Cron and Nuttal[22,23]). In deep penetration work this may not be justified and this method would require the wavelet to be continually re-estimated at intervals of travel time.

For (2) it is justified to ignore the water multiple if it is arranged that this return will be delayed sufficiently so that it is outside the time

window of interest. Smith[16] considers that the water multiple is the only multiple with a significant amplitude, but Tyce[39,40] has found that multiple reflections within layers cause quite variable results, and the measurements to be used here may suffer in the same way.

3.3 The Acousticore Technique

3.3.1 Application

The deconvolved signals represent, as discussed previously, a measure of the impulse response of the sediment. These signals can be used to determine, quantitatively, the acoustic impedances of various layers. The "Acousticore" technique has been developed by Wright and Miles[59] and Wright[60] for this purpose. They use the fact that the acoustic impedance can discriminate between consolidated sediments, gravel, sand, clay and silt, directly from measurements (such as those made by Hamilton[61] and Shumway[62]), for purposes such as sand and gravel assay, preconstruction site survey and sea floor engineering. Their application of the method requires the measurement of both the outgoing and received signals in order to deconvolve the signals before application of the algorithm. Hence this technique requires that the measured reflected signals be already de-convolved.

3.3.2 Acousticore model

The impedance profile is modelled as a lossless, continuous, monotonically varying function of acoustic travel time. The model is analysed by decomposing it into 'n' layers, and the continuous profile is obtained by considering arbitarily many steps in the limit as 'n' tends to infinity.

The assumption of a lossless medium is clearly violated in sediments and some allowance must be made, although Wright achieves good results with the lossless model to a depth of 20 feet in sand and mud. Leeman[58] has made the assumption that attenuation is constant per unit travel time and independent of frequency in his application to ultrasound scanning of human tissue. This is the simplest allowance to make but is only true if the velocity is constant, as well as the attenuation coefficient. In practice the velocity is likely to be in range 1550 to 1800 ms^{-1} for the sands likely to be encountered here[4] and the attenuation 40 to 80 dB m^{-1} at an operating frequency of 165 kHz, see section 4.3. This therefore would not appear to be a very good approximation, particularly as typical attenuation losses in a 10 cm layer are of the same order as the reflection loss expected, at this frequency. In practise attenuation will have to be measured separately and a method for this is described in section 3.4.

The initial impedance is taken as Z_o, and in this application will be that of water, the impedance of the

n^{th} layer is Z_n and the travel time to the n^{th} interface is t_n, see figure 3.3.1. The Rayleigh reflection coefficient at the n^{th} interface is given by,

$$r_n = \frac{Z_n - Z_{n-1}}{Z_n + Z_{n-1}} \qquad \text{3.3.1}$$

and in order to make the analysis simpler the time intervals are chosen in such a manner that all the reflection coeffients can be made equal and,

$$r_1 = r_2 = \ldots\ldots\ldots r_n = r \qquad \text{3.3.2}$$

Note that all the r's are taken as the same sign which forces the impedance change to be monotonic. It is important to distinguish between true layers and modelled layers:- this method is being applied to a continuous monotonic impedance change within one true layer, the 'n' interfaces referred to are the modelled layers.

3.3.3 Singly reflected components

Considering outputs which have undergone a single reflection only, $\Gamma_1(t)$, by putting multiple reflections within a layer to zero, the output from this model for an incident impulse can be written, see figure 3.3.2, as

$$\begin{aligned}\Gamma_1(t) = {} & r.\delta(t - 2t_1) + r.(1 - r^2).\delta(t - 2t_2) \\ & + r.(1 - r^2)^2.\delta(t - 2t_3) \\ & \ldots\ldots + r.(1 - r^2)^{n-1}.\delta(t - 2t_3)\end{aligned} \qquad \text{3.3.3}$$

where the dirac delta is used to represent time delay and it is recalled that the two way transmission

coefficient at an interface, T^2, is given by,

$$T^2 = 1 - r^2 \qquad \text{3.3.4}$$

Integrating equation 3.3.3 to time $2t_n$ gives

$$\int_0^{2t_n} \Gamma_1(t).dt = r + r.(1 - r^2) + r.(1 - r^2)^2 + \ldots\ldots + r.(1 - r^2)^{n-1} \qquad \text{3.3.5}$$

Recognising this as a geometric progression,

$$\int_0^{2t_n} \Gamma_1(t).dt = \frac{1}{r}.[1 - (1 - r^2)^n] \qquad \text{3.3.6}$$

The term $(1 - r^2)^n$ may be expanded as a Binomial series since $|r^2| < 1$ for any real layer, then

$$\int_0^{2t_n} \Gamma_1(t).dt = \frac{1}{r}.[1 - (1 + n.(-r^2) + \frac{n.(n-1).(-r^2)^2}{2!} + \ldots)]$$

$$\therefore \int_0^{2t_o} \Gamma_1(t).dt = nr - \frac{n.(n-1).r^3}{2!} + \frac{n(n-1)(n-2)r^5}{3!} + \ldots \qquad \text{3.3.7}$$

Now combining equations 3.3.1 and 3.3.2,

$$\frac{Z_n}{Z_o} = \left(\frac{1 + r}{1 - r}\right)^n \qquad \text{3.3.8}$$

and taking logarithms of both sides,

$$LOG\ (\ Z_n/Z_o) = n.LOG(\ 1 + r\ ) - n.LOG(\ 1 - r)$$

expanding the log terms on the right hand side in a Taylor series,

$$LOG\ (\ Z_n/Z_o) = n.(\ r - \frac{r^2}{2} + \frac{r^3}{3} - \ldots\ ) - n.((-r) - \frac{(-r)^2}{2} + \frac{(-r)^3}{3} - ..)$$

$$\therefore \tfrac{1}{2}\text{LOG}\left(Z_n/Z_o\right) = n.r + n.\frac{r^3}{3} + n.\frac{r^5}{5} + \ldots \qquad 3.3.9$$

Comparing equations 3.3.7 and 3.3.9 to a first order approximation, in the limit of arbitarily many impedance steps Wright states,

$$\lim_{n\to\infty} \int_0^{2t_n} \Gamma_1(t).dt = \tfrac{1}{2}\text{LOG}\left(Z_n/Z_o\right) \qquad 3.3.10$$

where $\Gamma_1(t)$ are the singly reflected components only.

3.3.4 Multiple reflections

Whilst still confining the method to one true layer, the effects of multiple reflections between the modelled layers are examined. Consider the triply reflected components, $\Gamma_3(t)$: first the outputs from the original model in figure 3.3.3 for an incident impulse can be written,

$$\sum_{t=0}^{4t_n} \Gamma_3(t_n,t) = \sum_{j=1}^{n-1} \sum_{k=j+1}^{n} \sum_{i=j+1}^{n} (-r^3)(1-r^2)^{i+k-j-2} \times \delta(t - 2(t_i+t_k-t_j)) \qquad 3.3.11$$

where i,j,k are the indices of the first, second and third layer that the particular component has reflected from.

Thus for a downward reflection at a given layer, j, there are n-j possible layers for each independent upward reflection at i and k, see figure 3.3.3. Hence

the total number of possible triple reflected outputs is given by,

$$\text{Total number} = \sum_{j=1}^{n-1} (n-j)^2$$

extending the top limit of the summation to n (since n-j = 0 if j=n), and expanding,

$$\text{Total number} = \sum_{j=1}^{n} (n^2 - 2jn + j^2)$$

$$\text{Hence total number} = \frac{n^3}{3} - \frac{n^2}{2} + \frac{n}{6} \qquad \text{3.3.12}$$

Now each of these triply reflected outputs has an amplitude of $(-r)^3 . (1-r^2)^{i+k-j+2}$ where in the limit of arbitarily many impedance steps the transmission factor, $(1-r^2)^{i+k-j+2}$ reduces to unity and equation 3.3.11 reduces to

$$\sum_{t=0}^{4t_n} \Gamma_3(t_n,t) = (-r)^3 . \left(\frac{n^3}{3} - \frac{n^2}{2} + \frac{n}{6} \right) \qquad \text{3.3.13}$$

Re-writing,

$$\sum_{t=0}^{4t_n} \Gamma_3(t_n,t) = -\frac{(n.r)^3}{3} + \frac{n^2.r^3}{2} - \frac{n.r^3}{6} \qquad \text{3.3.14}$$

and comparing equation 3.3.14 with equation 3.3.9 to a first order approximation, in the limit of arbitarily many impedance steps Wright states

$$\lim_{n\to\infty} \int_0^{4t_n} \Gamma_3(t_n,t).dt = \frac{-1}{3}.(\tfrac{1}{2}\text{LOG}\ (Z_n/Z_o))^3 \quad \text{3.3.15}$$

For higher order multiple reflections a similar calculation yields

$$\lim_{n\to\infty} \int_0^{6t_n} \Gamma_5(t_n,t).dt = \frac{2}{15}.(\tfrac{1}{2}\text{LOG}\ (Z_n/Z_o))^5 \quad \text{3.3.16}$$

and

$$\lim_{n\to\infty} \int_0^{8t_n} \Gamma_7(t_n,t).dt = \frac{-17}{315}.(\tfrac{1}{2}\text{LOG}\ (Z_n/Z_o))^7 \quad \text{3.3.17}$$

recognising these coefficients in the series expansion of tanh(x) Wright suggests that in general,

$$\lim_{n\to\infty} \int_0^{2_m t_n} \Gamma_{2m-1}(t_n,t).dt = C_m.(\tfrac{1}{2}\text{LOG}\ (Z_n/Z_o))^{2m-1} \quad \text{3.3.18}$$

where m is the number of reflections and C_m are the coefficients in the small value expansion for tanh(x). Then the total relection impulse response, i(t), is written as the sum of the odd number reflections,

$$i(t) = \sum_{m=1}^{\infty} \Gamma_{2m-1}(t) \quad \text{3.3.19}$$

This derivation has so far been applied to a continuous monotonic imedance profile. If two contiguous regions of impedance transition are

considered the primary returns from each region are separated in time, since the single reflection impulse response function has a total duration equal to twice the travel time through a region. Since the second region may represent either a monotonic increase or decrease Wright concludes that equation 3.3.10, for the primaries only, is true for any continuous impedance profile.

The higher number responses are more complicated and equations 3.3.15/16/17 do not hold true for any continuous imedance profile.

Now if the higher order outputs are insignificant then the primaries approximate the total output and equation 3.3.10 is an approximation to a complete solution for i(t). Wright shows that the higher order reflections can be ignored to within about ten per cent for impedance ratios up to 3 : 1, using his model of lossless layers. The higher order reflections are small in the application here, because of attenuation within the layers. This attenuation must be corrected for, if the acousticore method is to be applied, by reducing all outputs to what they would have been if there were no attenuation. In this case these higher order outputs are not so insignificant and this ten percent error will still occur in this application. However this ratio covers all sands that will be used here, but does not extend to the impedance of the bottom of the tank, and it may be expected that the calculated

value of the impedance of the bottom of the tank will be in error. In practice this limits the application to comparitively soft sediments and excludes accurate measurements of rock bottoms.

3.4 Calculation of Sediment Parameters

3.4.1 Parameters

Having calculated the impulse reflection response from a given layered medium it is now required to find the parameters of each layer. A reflection from any given layer will have undergone losses from transmission through other layers and absorption in other layers before it can be observed outside the medium. Whilst it is relatively straightforward to predict the observed outputs given the reflection coefficients and absorption coefficients for each layer the inverse procedure is more difficult and prone to errors.

It is worth limiting the calculations to those which have undergone a single reflection only, called primaries. Outputs which have undergone more than one reflection represent multiple reflections within one or more layers and, as will be seen later, in section 6.3, they are unlikely to be of a large enough amplitude to be useful in the application considered here.

In order to describe a layered medium each layer is defined by its depth, d, acoustic velocity, c, attenuation coefficient, α, and acoustic impedance, Z.

Derived from these properties is the actual attenuation in each layer, a, given by

$$a = \alpha.d.f$$

where f is the operating frequency in kHz.

If α is in units of $dBm^{-1}kHz^{-1}$ then 'a' becomes a fraction measured in dB.

Also derived from the four basic properties are the reflection coefficients and two way transmission coefficients at each layer, determined by the acoustic mismatch. The reflection coefficient is given by the Rayleigh reflection coefficient, R, where

$$R = \frac{Z_1 - Z_2}{Z_1 + Z_2} \qquad 3.4.1$$

where Z_1 and Z_2 are the acoustic impedances of the medium on each side of the boundary , with Z_2 being the medium in which the wave is travelling.

The two way transmission coefficient, T^2, is linked to the reflection coefficient by,

$$T^2 = 1 - R^2 \qquad 3.4.2$$

The properties of each layer can be given a suffix to identify them and in this application it is convenient to start numbering from the bottom since when an additional layer is added the existing layers all

retain their suffix. The bottom interface has the suffix 0 and the layer immediately above the suffix 1. These definitions are summarised in figure 3.4.1, for the case of three layers, which shows an additional suffix, w, appended to the top interface to show that the layer above it is water. Also shown are the individual primary outputs, γ, which make up the total primary output, $\Gamma_1(t)$, given a suffix corresponding to the interface which generated them; hence by numbering from the bottom γ_n is observed at the output before γ_{n-1} and γ_0 is the last primary output.

3.4.2 Output equations

The equations relating the observed outputs, γ, to a unit impulse input can be readily written down by examination of figure 3.4.1.

Consider a one layer case for a unit input then,

$$\gamma_1 = R_{1w} \qquad \text{3.4.3}$$

Output γ_0 has passed through interface number 1 twice and layer 1 twice before being reflected from interface number 0, hence

$$\gamma_0 = T_{1w}^2 . a_1^2 . R_0 \qquad \text{3.4.4}$$

Similarly for a two layer case,

$$\gamma_2 = R_{2w} \qquad \text{3.4.5}$$

$$\gamma_1 = T_{2w}^2 . a_2^2 . R_1 \qquad \text{3.4.6}$$

$$\gamma_0 = T_{2w}^2 . T_1^2 . a_2^2 . a_1^2 . R_0 \qquad \text{3.4.7}$$

and the three layer case,

$$\gamma_3 = R_{3w} \qquad \text{3.4.8}$$

$$\gamma_2 = T^2_{3w}.a^2_3.R_2 \qquad \text{3.4.9}$$

$$\gamma_1 = T^2_{3w}.T^2_2.a^2_3.a^2_2.R_1 \qquad \text{3.4.10}$$

$$\gamma_0 = T^2_{3w}.T^2_2.T^2_1.a^2_3.a^2_2.a^2_1.R_0 \qquad \text{3.4.11}$$

These equations can be written in matrix form so that the structure is clearer to see and to show how additional layers are effected,

$$\begin{bmatrix} a^2_3a^2_2a^2_1 & 0 & 0 & 0 \\ 0 & a^2_3a^2_2 & 0 & 0 \\ 0 & 0 & a^2_3 & 0 \\ 0 & 0 & 0 & 1 \end{bmatrix} \begin{bmatrix} T^2_3T^2_2T^2_1 & 0 & 0 & 0 \\ 0 & T^2_3T^2_2 & 0 & 0 \\ 0 & 0 & T_3 & 0 \\ 0 & 0 & 0 & 1 \end{bmatrix} \begin{bmatrix} R_0 \\ R_1 \\ R_2 \\ R_3 \end{bmatrix} = \begin{bmatrix} \gamma_0 \\ \gamma_1 \\ \gamma_2 \\ \gamma_3 \end{bmatrix}$$

Hence the equations for four layers are obtained by extending the matrices to order five and multiplying the diagonals of the square matrices by a_4 and T_4 respectively, and inserting a '1' in the end diagonal positions.

In shorthand notation these equations become,

$$\mathbf{a}.\mathbf{T}.\mathbf{R} = \boldsymbol{\gamma} \qquad \text{3.4.12}$$

3.4.3 Solutions to parameter equations

The immediate problem of solving equations 3.4.12 is that there are more unknowns than equations. The measured quantities are the γ's and the unknowns the R's and the a's; the T's are linked directly to the R's and

are not therefore additional unknowns. Much of the literature on theoretical solutions relies in the assumption of lossless media, Mendel[7o], such that all the a's are equal to unity. In more practical work an average value for all the a's is taken based on some measurement of a locally taken sample. Neither solution is very accurate for this type of work as the values of 'a' and 'R' are of the same order of magnitude for typical layers, as will be shown later.

However, considering a solution where an average value of the a's is assumed equation 3.4.12 has solution

$$R = a^{-1}.T^{-1}.\gamma \qquad \text{3.4.13}$$

Taking the inverse of these diagonal matrices the solutions for the three layer case may be written,

$$R_{3w} = \gamma_3 \qquad \text{3.4.14}$$

$$R_2 = \frac{\gamma_2}{a_3^2.T_{3w}^2} \qquad \text{3.4.15}$$

$$R_1 = \frac{\gamma_1}{a_3^2.a_2^2.T_{3w}^2.T_2^2} \qquad \text{3.4.16}$$

$$R_o = \frac{\gamma_o}{a_3^2.a_2^2.a_1^2.T_{3w}^2.T_2^2.T_1^2} \qquad \text{3.4.17}$$

The solution requires starting at the top and working down so that the value of R_{3w} from equation 3.4.14 can be used to calculate T_{3w} ready for substituting into equation 3.4.15 and so on. The set of equations for N layers follows in the same pattern.

The errors incurred by substituting forwards in this manner are discussed later.

There is another possible solution which reduces this successive substitution and can be extended, in certain limited applications, to calculate the attenuation in each layer. Consider, first, the general case of N layers which yield N+1 equations for $\gamma_0 \ldots \gamma_N$ as in equation 3.4.11, now if adjacent pairs of these are divided a set of N equations are derived of the form,

$$T_{k+1}^2 . a_{k+1}^2 . R_k = \frac{\gamma_k . R_{k+1}}{\gamma_{k+1}} \qquad \text{for } k = 0 \ldots N-1 \qquad \text{3.4.18}$$

If these are solved from the top down starting with $k = N-1$ then $\gamma_{k+1} = R_{k+1}$ by comparison with the three layer solution, and equation 3.4.18 becomes equivalent to 3.4.15 for the three layer case. The remaining equations can be solved in a similar manner by passing just one parameter, R, from one equation to the next. This may yield a smaller accumulated error than in the first case, see later; however it is still necessary to assume values for attenuation.

In some practical situations it is possible to make successive measurements, over a period of time, as extra layers build up at a given location. This situation exists in certain harbours and estuaries where clearances in shipping lanes are monitored, and the

situation can be copied in a laboratory. In this case then, equations 3.4.18 can be solved from the bottom up.

Starting with the case of no layers then a direct measurement of R_{ow} is possible. Although this will be different when the bottom is covered with sand instead of water, in many cases it will be close to unity if it represents a rock bottom or, in the laboratory, a steel tank, see appendix B.

The one layer case can now be solved for both R_{1w} and a_1 if this value of R_o is used as input to equations 3.4.3 and 3.4.4. In the two layer case the values of R_o and a_1 are input to equations 3.4.5/6/7 and these can be solved for R_1, R_{2w} and a_2. Likewise for the three layer case the values of R_o, a_1 and a_2 are input to give solutions for R_1, R_2, R_{3w} and a_3 and so on to the N layer case.

It is worth pointing out that in general it is possible to calculate R_{k-1} in the K layer case, from the value of $R_{(k-1)w}$ obtained in the K-1 layer case, since Z_k can be calculated from R_{kw}. This is likely to be unreliable however since the water/sediment boundary may not be fully compacted and may not be a true step function. It will be necessary measure R_o in this manner in the general case where R_o is not a good approximation to unity. Hence all the reflection coefficients are re-calculated for each case of a new layer and it is assumed that previously calculated

values of attenuation do not change as more layers are added, see discussión later.

The general solution of equation 3.4.18 is obtained by substituting

$$T_{k+1}^2 = 1 - R_{k+1}^2 \qquad \text{from equation 3.4.2}$$

and re-arranging to give,

$$R_{k+1}^2 + \left(\frac{\gamma_k}{\gamma_{k+1}^2} \cdot \frac{1}{a_{k+1} \cdot R_k}\right) \cdot R_{k+1} - 1 = 0 \qquad \text{3.4.19}$$

The solution of this quadratic is

$$R_{k+1} = -\frac{\chi}{2} \pm \sqrt{\frac{\chi^2}{4} + 1} \qquad \text{3.4.20}$$

$$\text{where } \chi = \left(\frac{f_k}{f_{k+1}}\right) \cdot \left(\frac{1}{a_{k+1}^2 \cdot R_k}\right)$$

The correct root to take depends on the sign of χ; if χ is positive then R_{k+1} must be positive and the positive root is required. If χ is negative then R_{k+1} must be negative (representing an inversion) and the negative root is required.

This result can be expressed in a series by expanding the root in a Binomial series and

$$R = 1 - \frac{\chi}{2} + \frac{\chi^2}{8} \quad \ldots\ldots \quad \text{for } \frac{\chi^2}{4} < 1$$

$$= \frac{1}{\chi^3} - \frac{1}{\chi} \quad \ldots\ldots\ldots \quad \text{for } \frac{\chi^2}{4} > 1 \qquad \text{3.4.21}$$

Clearly when χ approaches zero R approaches 1 and when χ approaches infinity R approaches zero, which is the correct physical interpretation.

3.4.4 Errors and limitations of solutions

There are two main problems with the solutions described above, first being a build up of errors as the solution of the N^{th} reflection coefficient depends on the result of the $N-1^{th}$. The second problem is that due to the limited dynamic range of any system a small return from a given reflector may be concealed within larger returns and noise.

Taking the build up of errors first in the case of equations 3.4.14/15/16/17 for the top down solution, the general result for the K^{th} layer in an N layered medium is given by,

$$R = \frac{\gamma_k}{\prod_{n=k+1}^{N} a_n^2 . T_n^2} \qquad 3.4.22$$

where the symbol $\prod$ means the extended multiplication of each term.

Now all the T_n are substituted by $1-R_n^2$ hence re-writing

$$R = \frac{\gamma_k}{\prod_{n=k+1}^{N} a_n^2 . (1 - R_n^2)} \qquad 3.4.23$$

The error in R_k for small errors in the parameters γ_k, a_n and R_n is given, by partial differentiation as

$$\delta R_k = \left(\frac{\partial R_k}{\partial \gamma_k} . \delta \gamma_k\right)^2 + \sum_{n=k+1}^{N} \left(\frac{\partial R_k}{\partial a_n} . \delta a_n\right)^2 + \sum_{n=k+1}^{N} \left(\frac{\partial R_k}{\partial R_n} . \delta R_n\right)^2$$

for uncorrelated errors.

$$\therefore \left(\frac{\delta R_k}{R_k}\right)^2 = \left(\frac{\delta \gamma_k}{\gamma_k}\right)^2 + \sum_{n=k+1}^{N} \left(\frac{2 \cdot R_n^2}{1-R_n^2}\right)^2 \cdot \left(\frac{\delta R_n}{R_n}\right)^2 + \sum_{n=k+1}^{N} \left(\frac{-2.\delta a_n}{a_n}\right)^2 \qquad 3.4.24$$

and this represents the mean square percentage error in R_k. The first term is the percentage error in the observed output from the interface k. The second term represents the accumulated errors in all the previously calculated values of reflection coefficients, for the interfaces above k. The actual value of $\delta R_n/R_n$ will get larger as n approaches k, however the accumulation effect may be reduced by the term, $\frac{2R_n^2}{1-R_n^2}$ which puts less weight on a particular error if its absolute value is small. On the other hand the effect of the error is increased if R_n approaches 1 as expected since, in this case, T_n approaches 0 and is a divisor in equation 3.4.21. The third term is the result of errors in the assumed attenuation coefficient.

The build up of errors in the case of equations 3.4.18, which are the result of dividing adjacent pairs of equations, can be derived in the same way by partial differentiation. Taking the solution working from the top downwards,

$$R_k = \frac{\gamma_k}{\gamma_{k+1}} \cdot \frac{R_{k+1}}{T_{k+1}^2} \cdot \frac{1}{a_{k+1}^2}$$

and

$$\left(\frac{\delta R_k}{R_k}\right)^2 = \left(\frac{\delta \gamma_k}{\gamma_k}\right)^2 + \left(\frac{\delta \gamma_{k+1}}{\gamma_{k+1}}\right)^2 + \left(\frac{-2\delta a_{k+1}}{a_{k+1}}\right)^2 + \left(\frac{\delta R_{k+1}}{R_{k+1}}\right)^2$$

$$+ \left(\frac{2R_{k+1}^2}{1-R_{k+1}^2}\right)^2 \cdot \left(\frac{\delta R_{k+1}}{R_{k+1}}\right)^2 \qquad \text{3.4.25}$$

for uncorrelated errors, as before.

In this case there are two contributions to the error from observed outputs from two interfaces but only one contribution from the error in attenuation coefficient for one layer. There is only one reflection coefficient contributing to the error, however this itself will have an accumulated error and the weight given to the error is never less than unity as it was in the previous case. Comparing the two expressions for errors it may be expected that the first solution will yield a better result for small R and small N, while the second solution will be better for large R and large N.

A further limit of any solution is imposed by the dynamic range of the system; a small return may not be resolved if the system is also to measure large returns unless some dynamic compression of the signal is used. However if a small return occurs in between two large returns a fixed compression law cannot be applied and a variable gain control is not suitable since relative values are required.

Using equation 3.4.19 it is possible to calculate the ratio of γ_k/γ_{k+1} which corresponds to a given

value of R_k for a set value of, $\alpha^2_{k+1}.R_k$.

Figure 3.4.2 shows a family of curves of for several values of $\alpha^2_{k+1}.R_k$ calculated from solutions to equation 3.4.19. It can be seen that a large reflector can easily obscure a small reflector below it; for example consider the case of $R_k = 0.1$ and $R_{k+1} = 0.8$. Now assuming

$$\alpha^2_{k+1} = 0.1$$

so that

$$\alpha^2_{k+1}.R_k = 0.01$$

then the ratio γ_k/γ_{k+1} will be 0.004 from figure 3.4.2. This ratio is approximately -48 dB which means that an 8 bit digital system will be stretched to its full dynamic range to represent both numbers and in practice γ_k is unlikely to be resolved especially if any noise is present.

This calculation has been carried out using the equation for the bottom up calculation but the same dynamic range limit still applies to the other solutions since the measured response is independent of the proposed method of solution.

3.5 Summary of theoretical treatment

It is worth summarising the processes that have been discussed together with the essential notation that has been used.

A signal, r(t), is transmitted at normal incidence to a planar, 'perfect' reflector and recorded as a reference pulse. The same signal is transmitted at normal incidence to the layered sediment and the reflected signals recorded and called x(t).

x(t) will be 'improved' by averaging and by deconvolving to generate the signal y(t), which will be as close as possible to the impulse response, i(t). The signal, i(t), consists of a series of impulses representing all outputs that have had an odd number of reflections, given a single impulse as the input.

The acoustic parameters will be estimated from i(t) and it is useful to break it down into components such that;

$\Gamma_{2n-1}(t)$ is that part of i(t) containing all reflections that have had 2n-1 reflections only.

so that, $$i(t) = \sum_{n=1}^{\infty} \Gamma_{2n-1}(t)$$

γ_n are the amplitudes of the individual impulses of the primaries, $\Gamma_1(t)$, that have undergone one reflection only.

so that, $$\Gamma_1(t) = \sum_{n=1}^{\infty} \gamma_n . \delta(t-t_n)$$

where t_n is the delay of γ_n etc.

For completeness the time domain signals have Fourier transforms denoted by a capital letter so that,

$$x(t) \Leftrightarrow X(\omega) \qquad \text{etc.}$$

CHAPTER 4 EXPERIMENTAL FACILITY AND EQUIPMENT

4.1 Introduction

The aim of the experimental work was to model a sub-bottom profiler, together with a layered structure of sand sediments, in the laboratory. Measurements of the reflected response could then be taken from a layered structure which was known and whose properties were well defined. The interpretation of the received signals could then be compared directly with the structure. This cannot be done with data obtained at sea because it is only possible to measure the acoustic parameters directly from core samples at isolated points.

In the laboratory it is also possible to return the transducer to a given position so that an extra layer may be laid down on top of the previous layers and a measurement repeated.

The three main constituents required of the model were,

1) sand layers of known acoustic parameters and a container for these layers.
2) a transducer with a stable mechanical positioning system.
3) suitable electronic equipment to drive the transducer and to record the received signals.

A schematic block diagram of these constituents is shown in figure 4.1.1 and their important aspects are described later in this chapter.

The physical aspects of the sands, the containers and the positioning system define the size of the experimental facility. The dimensions were not scaled from the sea going system but were derived by considering what was feasible in a laboratory tank, whilst still retaining realistic physical parameters; these aspects are discussed in section 4.2.

The transducer had to operate at a higher frequency than the sea going system in order that its wavelength would be appropriate for the size of tanks and sediment already defined. A frequency of 150 kHz would give a 1 cm wavelength in water and this was the initial aim, however the final frequency used was 165 kHz for the reasons explained in section 4.3. The beamwidth and Q factor were arranged to be approximately the same as the sea going system.

The equipment to drive the transducer and to receive the returned signals was built specifically to match the transducer characteristics and the requirements of the experimental work. However the recording and computing facility were standard items of equipment. The electronic system is described in section 4.4.

In section 4.5 an estimate of the performance that may be expected from this equipment is put forward.

4.2 Sediment Facility

4.2.1 Tanks and positioning system

Two tanks were used to set up the model, with one inside the other. The smaller tank contained the layers of sand and was placed on the bottom of the larger tank. The larger tank had a gantry system fitted to it for supporting the transducer over the smaller tank.

Note that it was possible to drain the larger tank to give physical access to the model whilst still leaving the sand in the small tank covered with water. Figure 4.2.1 shows a photograph of the smaller tank, taken from inside the larger tank, with the transducer in place.

The dimensions of the larger tank were 1.5m × 2m × 1.5m deep and those of the smaller tank 1.25m × 0.5m × 0.6m deep. The smaller tank was fitted with its length across the width of the larger tank leaving a substantial amount of room at one end of the large tank, which was necessary for preparing the sand, see later.

The width of the smaller tank was chosen so that the sides would be well away from the main beam of the transducer, when it was pointing vertically downwards. The length of the tank allowed for horizontal movement of about 1 m before the ends fouled the main beam of the transducer.

The gantry system to position the transducer was made of 3 mm thick aluminium angle, bolted to the top of the large tank. The gantry supported an optical bench and carrier which was fitted with a rack and pinion system. The carrier supported an aluminium plate which could be adjusted for small variations about the horizontal. The plate had a vertical bearing at one end and a counterweight at the other. Through the bearing ran a pole with a sliding, lockable collar and the transducer was bolted to the end of the pole. Figure 4.2.2 shows a diagram of the construction of the gantry system and figures 4.2.3 and 4.2.4 show photographs of the gantry and how it relates to the tanks and the transducer.

The optical bench and carrier allowed precise horizontal movement along the length of the smaller tank and the aluminium plate, supported by the carrier, permitted the alignment of the transducer perpendicular to the sand layers. The pole and locking collar allowed the height of the transducer, above the sand layers, to be adjusted.

The transducer could be bolted to the pole in three different ways so that it could point vertically up, down or horizontally, and the use of two collars allowed the transducer to be rotated for beam pattern measurements, whilst the transducer was horizontal.

4.2.2 The sediment

The size of the sand grains cannot be scaled down for this model because of the nature of sand. If the mean particle size is less than about 50 μm a water saturated sand becomes cohesive in nature and compacts to form a different type of medium which does not model a real sand at sea.

The main factor to consider is whether the particle size is large enough, compared to the wavelength of the insonifying sonar, to cause Rayleigh scattering. Rayleigh scattering varies as the fourth power of frequency and is significant when the wavelength and grain sizes are comparable[4,6]. The frequency of the insonifying sonar is determined by the transducer, which is described in section 4.3; this frequency is 165 kHz and has a wavelength of 9 mm in water. If the maximum size of the sand grains does not exceed 0.5 mm then Rayleigh scattering can be ignored at this frequency. Hence the acceptable limits for particle size have been set between 50 μm and 500 μm. The acoustic parameters, in particular the impedance, should be the same for this model as for the practical case at sea.

Measurements of acoustic parameters for a number of commercially graded, water saturated sands, over a range of frequencies have been made by Thomas and Pace[4]. These sands were readily available and two types were chosen for use in this model, being the 50 μm and the 250 μm size. The important acoustic parameters are,

Parameter	50 μm	250 μm
Wet density / kgm^{-3}	1750	1946
Sound velocity / ms^{-1}	1538	1660
Acoustic impedance / Rayls	2.69×10^6	3.23×10^6
Attenuation / dBm^{-1} (at 165 kHz)	78	40

where the attenuation has been derived from a regression equation, fitted to the experimental results, by Thomas and Pace[4].

A sieve analysis was carried out on these sands and compared with a sieve analysis carried out on some sand samples taken in Lyme Bay at 50° 37.9' North, 2° 58.5' West off the Dorset coast. The results are shown in figure 4.2.5 as plots of accumulative percentage weight retained by successively smaller sieve meshes. It is clear that the sea bed samples were actually graded into a narrower range than the commercial sands, however it was not possible to regrade the commercial sands to match the sea bed grading.

In order to prepare the sand before use it was necessary to remove the air from it. Natural sand at sea has been de-aerated by sedimentation and agitation over thousands of years. If sand were simply dropped into water it would inevitably trap a lot of air in the pore spaces giving an artificially low acoustic impedance.

The method chosen was to extract the air from the sand with a vacuum pump before using it. To do this a vacuum vessel with a capacity of approximately 50 kg of dry sand was used. The vessel was filled with dry sand and evacuated down to a pressure of approximately 2 kPa (≈15 torr) and held at this pressure for 20 minutes. After this time water was bled into the vessel until the sand was completely saturated. This procedure was carried out with the vacuum vessel in the empty end of the large tank, see section 4.2.1, with a flexible pipe connecting it to the vacuum pump outside the tank. The level of water in the large tank was raised so that it covered both the top of the vacuum vessel and the sides of the smaller tank such that the sand could be transferred between the two without re-exposure to air.

Extreme care had to be taken when laying a new layer on top of an existing one because it was easy to disturb the existing surface which could result in a badly defined boundary. The prepared sand was transferred from the vacuum vessel, using a hand trowel, and slowly released into suspension approximately 0.1 m above the previous layer. The smaller particles would take longer to fall out of suspension and this may have caused some fine scale layering between each trowel-full of the order of 1 mm, but this was unavoidable.

The final surface was smoothed using a flat aluminium scraper and the new layer allowed to settle

for one month before taking measurements of reflected intensity.

4.3 The Transducer

4.3.1 Transducer design considerations.

The sonar transducer was initially designed to operate at 150 kHz in order to generate a 1 cm wavelength which would be convenient with the size of the experimental facilities described in the previous section. The transducer was constructed using a ceramic disc (PZT 5a) of 50 mm diameter, 12.5 mm thick, with a thickness-mode resonance frequency of 150 kHz.

Assumming the transducer to operate as a piston in a rigid baffle, the expected beamwidth could be calculated from the normalised directivity function,

$$D(\theta) = \frac{2.J_1(k.a.SIN(\theta))}{k.a.SIN(\theta)} \qquad \text{4.3.1}$$

where a is the transducer radius,

k is the wave number and

J_1 indicates a Bessel function of order one.

Then the half power beamwidth is given by

$$\theta_B \simeq 1.62\ \lambda/2a \qquad \text{4.3.2}$$

which for $\lambda \simeq 1$ cm, $2a \simeq 5$ cms gives

$$\theta_B \simeq 11.8 \text{ degrees.}$$

This is slightly more than the ~~9 degrees~~ -3dB beamwidth of the sea going system but was as close as could be obtained with standard size ceramics.

The bandwidth of a transducer is highly dependent upon the loading imposed on the ceramic, if the ceramic is loaded directly into water there is a high mismatch of acoustic impedances giving rise to inefficient transmission into the water and a high Q factor. These effects can be alleviated by using a ¼ wave matching layer which reduces the impedance mismatch between the ceramic and the water. The bandwidth will be affected by the choice of the acoustic impedance of the material used for this matching layer. The theory of matching layers has been discussed by Kossoff[64] and the theory of multiple matching layers by Goll and Auld[65], although only a single layer is considered here.

To appreciate the changes in performance consider first the case of no matching layer. The acoustic impedance of the ceramic is 33.7×10^6 Rayls, and if it is loaded directly into water the Rayleigh relection coefficient is given by,

$$R = \frac{Z_1 - Z_o}{Z_1 + Z_o} \qquad \text{4.3.3}$$

where Z_o and Z_1 are the acoustic impedances of the ceramic and the water respectively.

$$\therefore R = -0.92$$

The transmission into water is given by

$$T^2 = 1 - R^2 \qquad \text{4.3.4}$$

$$\therefore T^2 = 0.15$$

The bandwith is given in terms of the Q factor

$$Q = \frac{\pi}{2} \cdot \frac{Z_{ceramic}}{Z_{load}} \qquad \text{4.3.5}$$

$$\therefore Q = 36$$

where Z_{load} is the acoustic impedance of the water. (1.48×10^6 Rayls.)

The insertion of a ¼ wave matching layer changes the acoustic impedance Z_{load} seen by the element and the new impedance, from transmission line theory, is

$$Z_{load} = \frac{Z^2_{\frac{1}{4}\ wave\ layer}}{Z_{water}} \qquad \text{4.3.6}$$

A suitable material for matching is perspex; although it does not give the best possible improvement for a single layer it is readily available and easy to machine accurately to the correct thickness.

The acoustic impedance of perspex is 3.16×10^6 Rayls, hence the impedance seen by the element, from equation 4.3.6, is

$$Z = \frac{(3.16 \times 10^6)^2}{1.48 \times 10^6} = 6.75 \times 10^6 \text{ Rayls.}$$

As before using equations 4.3.3/4/5 the parameters are now,

$$R = 0.66$$

$$T^2 = 0.55$$

and $Q = 8$

This Q factor is comparable with that of the sea going system and corresponds to a bandwidth of approximately 19 kHz for a centre frequency of 150 kHz.

An effect of ¼ wave plate matching is to change the resonant frequency. Kossoff[64] derives a relation by means of an electrical equivalent circuit for the element and the result he obtains is,

$$f_o = f'_o \cdot \left[1 - \frac{4\,\gamma^2}{A.Z_c.\pi^2.f'_o.c_o} \right]^{\frac{1}{2}} \qquad \text{4.3.7}$$

where f_o is the matched resonant frequency.

f'_o is the open circuit resonant frequency.

γ is the ideal transformer ratio, given by $\frac{e_{33}.A}{t}$

A is the surface area of the element face. (1.96×10^{-3} m^2).

Z_c is the acoustic impedance of the element. (33.7×10^6 Rayls)

C_o is the static capacitance given by $\frac{\epsilon_{33}.A}{t}$

e_{33} is the stress per electric field. (15.8 Cm^{-1}).

ϵ_{33} is the dielectric constant of the element ($830.\epsilon_o J^{-1}C^2m^{-1}$)

ϵ_o is the dielectric constant of free space. (8.85×10^{-12} $J^{-1}C^2m^{-1}$)

t is the thickness of the element. (12.5×10^{-3} m).

An empirical approach to the realisation of the transducer could take the following form:-

Firstly, the value of f'_o can be estimated from the circle diagram of the unmounted ceramic in air, as described by Tucker and Gazey[66]. The thickness of the matching layer should then be machined to a thickness equal to one quarter of a wavelength, measured at f_o, at the velocity in the matching layer.

However the circle diagram for the ceramic alone in air showed more than one resonance, see figure 4.3.1, which invalidates the simple theory described above. It was anticipated that one of the resonances could be made dominant by matching into the water and the initial open circuit resonance was estimated to be 162 kHz from the in air circle diagram. The matched resonant frequency was calculated to be 144 kHz and a ¼ waveplate was made up to match it. The multiple resonance condition was still apparent when the transducer was constructed, as described below, and the resonances are shown in the circle diagram for the complete transducer in water, see figure 4.3.2; there was also considerable ringing present when the transducer was tested.

Calculations showed that one of the resonances was at the same frequency as one of the radial mode resonances and it was suggested[67] that the element should be sawn through in an asymmetric manner in order that these unwanted radial mode resonances would be severely attenuated. A saw cut was made along a chord, which is illustrated in figure 4.3.3, and the element re-made into a transducer with a new waveplate. The circle diagram for this new transducer is shown in figure 4.3.4, and although this plot shows multiple resonances the extensive ringing found previously was not present. An operating frequency of 165 kHz was

chosen as being approximately central within the band of multiple resonances and the transducer was calibrated.

The physical construction of the transducer used a brass housing to form the main body of the transducer which was a cylinder of 7 cm diameter and 10 cms in length although most of this length was empty. One end was blanked off by silver soldering a brass disc over the end which was subsequently drilled and tapped to accept a standard waterproof marine plug, for the electrical connections. The other end had a flange silver soldered around the circumference which had a groove cut for an 'O' ring together with holes drilled and tapped for bolts. The ¼ wave plate was machined out to the same diameter as the flange, with holes in the same position, so that it could be bolted to the flange to form a water tight seal against the 'O' ring, see figure 4.3.5.

The element itself was glued to the centre of the ¼ wave plate such that the body of the ceramic fitted inside the cylindrical brass housing. An additional brass ring was made up to fit outside the waveplate, around the circumference, drilled for bolts so that this ring would apply an even stress to the waveplate as the bolts were tightened. A block of aluminium was bolted to the flange bolts with holes drilled and tapped, as required, to allow mounting of the transducer in a number of different orientations. Figures 4.3.6 and

4.3.7 show photographs of the transducer from two different angles.

The adhesive used to glue the ceramic to the ¼ wave plate was initially cyano-acrylate but it was found that the element tended to crack away from the waveplate and instead quick set Araldite was used. This was much stronger but had the disadvantage of tending to ooze out and creep up the sides of the ceramic as it was pressed to the waveplate. This could have partially restricted the full movement of the ceramic and affected the electrical/mechanical coupling coefficient. The Araldite also formed a thicker layer between the element and the waveplate which may have reduced the effectiveness of the matching layer.

In order to use the transducer the transmit and receive electronics had to be matched properly into the load presented by the transducer. It is possible to calculate theoretical values of impedance and at resonance the input electrical resistance of the complete transducer is given by[66],

$$R_E = \frac{R_m}{4.\gamma^2} \qquad \text{4.3.8}$$

where R_m is the mechanical impedance given by $A.Z_{load}$.

Z_{load} is defined in equation 4.3.6.

A is the surface area of the element.

γ is the transformer ratio used in equation 4.3.7.

Substituting these values,

$$R_E = 492 \text{ ohms}$$

There will be some residual capacitance at resonance due to the physical size of the element, this is given by

$$C_o = \frac{A.\epsilon_{33}}{t}$$

as defined in equation 4.3.7, and substituting the values gives,

$$C_o = 1200 \text{ pF}$$

This theoretical impedance may be expected to be in error because the theory assumes a single resonance which is not the case here and the impedance measured from the circle diagram at 165 kHz shows,

$$C_o = 1600 \text{ pF}$$

$$R_E = 1740 \text{ ohms}$$

The capacitance is comparable with the theoretical value of 1200 pF because this depends mainly on the physical size of the element. The resistance is about three times as large as the calculated value because this is dependent on the electro-mechanical coupling which does not couple to a single resonance. However the transmit and receive electronics were designed to power the load as measured from the cirlce diagram, see section 4.4

4.3.2 Transducer calibration

Beam plots were taken across two planes perpendicular to each other to check whether the saw cut had imposed some asymmetrical behaviour. These plots are shown in figure 4.3.8 which shows a satisfactory performance with sidelobes 18 dB down and a -3 dB beamwidth of 9.5 degrees.

The on axis sound pressure level was measured using a calibrated Brüel and Kjær hydrophone type 8103, and the results are shown in figure 4.3.9 as a function of frequency. These results show a source level of 37 dB re 1 Pa at 1 m per volt, at a frequency of 165 kHz.

The efficiency may be calculated knowing the measured source level and the input power. Let the equivalent plane-wave pressure amplitude near the transducer surface be P_o and let the near/far field boundary be given by the Rayleigh distance, R_o, then

$$R_o = \frac{\pi . a^2}{\lambda} \qquad \text{4.3.9}$$

where λ is the wavelength (9×10^{-3} m) and a is the transducer radius (25×10^{-3} m).

hence $R_o = 0.22$ m

The acoustic power radiated for a transducer with ka >> 1 is given by

$$\text{Acoustic power} \simeq \frac{P_o^2}{2.\rho_o c} . \pi a^2 \qquad \text{4.3.10}$$

where $k = 2\pi/\lambda$ such that $ka \simeq 17$; and $\rho_o c$ is the acoustic impedance of water (1.48×10^6 Rayls).

The electrical power input for a one volt r.m.s. signal voltage is given by

$$\text{Electrical power} = \frac{1^2}{2.R_E} \qquad \text{4.3.11}$$

Hence the efficiency is obtained by dividing equation 4.3.10 by equation 4.3.11 and,

$$\text{Efficiency} = \frac{P_o^2.\pi a^2}{2.\rho_o c} \,.\, 2.R_E \qquad \text{4.3.12}$$

The source level has been measured, above, and found to be 37 dB re 1 Pa at 1 m per volt. Hence the sound pressure amplitude at one metre, P_1 is 71 Pa per volt. Now P_1 is linked to P_o by,

$$P_1 = P_o.R_o \qquad \text{4.3.13}$$

and hence $P_o = 323$ Pa

Note that P_o is not the actual pressure at R_o but the pressure that would be obtained at R_o if the far field axial pressure were extrapolated back towards the transducer.

Substituting into equation 4.3.12 gives,

Efficiency = 24 %

The maximum pressure level within the near field is theoretically given by $2.P_o$, hence the peak pressure level obtained is 6.5 Pa per volt. The actual voltage applied to the transducer was ± 100 volts, see appendix A, hence the maximum pressure level expected would be

$\pm$ 6.5×10^{4} Pa. This is less than the ambient atmospheric pressure and so no problems with cavitation should be experienced.

A useful calibration measurement involves using the transducer to transmit a pulse and then receive a reflection from a 'perfect' reflector placed perpendicular to the transducer axis. Three possible 'perfect' reflectors were tried,

1) a water/air interface at the top of a tank of water.
2) a water/steel interface at the side of a tank.
3) a neoprene sheet glued to an aluminium plate suspended in a tank.

These each had advantages and disadvantages,

1) is the closest to being a perfect reflector but it is difficult to arrange the transducer to point upwards without introducing poles and fixing brackets into the beam.
2) is easy to set up with no obstructions in the beam but the reflection is not perfect as steel has a finite acoustic impedance (47×10^{6} Rayls), and multiple reflections can occur within the steel wall.
3) can be set up with no obstructions in the beam but the sheet must be flat over a large enough area to reflect all the power.

In each case the transducer was 0.5 m from the reflector giving a two way distance of 1 m. The Rayleigh

distance was calculated above, from equation 4.3.9, to be 0.22 m; hence this 1 m effective distance is well within the far field and this method of calibration is valid. The -3 dB beamwidth covers an area of diameter 9 cms at the reflector and in each case the reflector had linear dimensions at least ten times this before encountering an edge which may have given rise to some scattered power. A 40 μs pulse was transmitted and it was ensured that the reflection was not obscured by returns from previous pulses by choosing a low pulse repetition frequency.

The resultant measured pulse was not readily distinguishable between all three methods and the result is shown in figure 4.3.10. This pulse will be called the reference pulse and denoted by r(t).

In all three cases the amplitude of the received signal was -23 dB with respect to the transmitted signal amplitude, measured at the electrical inputs to the transducer, and this may be taken as the transmit/receive loss at 1 m.

The receive sensitivity is therefore given by -60 dB re 1v per Pa since the source level had already been measured as 37 dB re 1 Pa per volt at 1 m.

The same transmit pulse that was used to obtain the reference pulse was used to record the reflected signals, from the sediments, described later, in section 5.2.

4.4 Electronics System

4.4.1 Transmit and receive electronics

The electronic equipment was required not only to drive the transducer but to generate the transmitted pulse, to receive the returns and to provide outputs to the recording system. On the receive side the major feature was to carry out a demodulation process to obtain the in-phase and quadrature components of the received signals which were presented to the recording system. Furthermore the demodulating frequency was phase locked to the transmitted signal so that successive echoes from the same point produced the same in-phase and quadrature components. This was required so that each component could be summed over many returns and this requires that all the returns have the same phase.

Thus, the signal frequencies were reduced to the base-band, without loss of amplitude or phase information contained in the signals. The main advantage obtained is a very significant reduction in the sampling rate required, resulting in a more beneficial use of the storage and handling capacity of the computer utilised for data capture and processing.

The main feature on the transmit side was a shaped pulse generator. The shaped pulse generator gave precise control over the transmitted pulse, assuming that the pulse shape was within the bandwidth of the

transducer. Although the electro-mechanical coupling parameters of the element itself would not change, small changes in the transducer charateristics, caused by aging of the adhesive or distorion of the waveplate could occur. This control over the transmitted pulse shape gave greater confidence that repeatable results could be obtained over a long period of time.

The shaped pulse generator also acted as the control for the whole system by providing gating and trigger signals, as well as the pulse envelope itself, as shown in the block diagram in figure 4.4.1.

A function generator was run at four times the required carrier frequency which was then divided down by four (using flip-flops) to provide both "Sine" and "Cosine" signals. The Sine signal was then gated by a signal from the shaped pulse generator and taken out to the modulator which, together with the shaped pulse envelope, generated the transmitted signal. Just before each transmission the shaped pulse generator cleared the flip-flop dividers in the demodulator and gated the function generator off and on again. This system ensured that each pulse was identical, that the carrier was locked to the envelope and that the phase of the demodulating signal was locked to the carrier. The transmitted signal was amplified and transformed to match the transducer impedance.

The gain of the receive amplifier was adjusted so that the signal did not overload the demodulator. The

received signal, after filtering, was multiplied in analogue form by the Sine and Cosine terms at carrier frequency to provide two outputs which (after filtering to remove the second harmonic terms) gave the in-phase and quadrature components of the received signal which were buffered, through operational amplifiers, to the recording system. The individual components of the electronics system are described in appendix A.

4.4.2 Equipment for signal capture and processing

Consider the reference signal shown in figure 4.3.10, for example. It can be represented in the form,

$$r(t) = A(t).\mathrm{Cos}[\omega_o t + \phi(t)] \qquad \text{4.4.1}$$

Where $A(t)$ and $\phi(t)$ represent the envelope and the phase of the signal while ω_o is the carrier frequency.

In the demodulation process this signal is multiplied by $\mathrm{Cos}[\omega_o t]$ and $\mathrm{Sin}[\omega_o t]$ in two channels, the outputs of the multipliers being low-pass filtered to remove the components at $2\omega_o$. Then, apart from a constant coefficient, the filter outputs become, respectively,

$$p = A(t).\mathrm{Cos}[\phi(t)], \qquad \text{4.4.2}$$

$$\text{and } q = A(t).\mathrm{Sin}[\phi(t)]. \qquad \text{4.4.3}$$

Here, p is the in-phase component and q is the quadrature component of the narrow band signal. The

components p and q are Real functions of time but can be combined in a complex form, $\hat{r}(t)$ say, giving

$$\hat{r}(t) = p + jq \qquad 4.4.4$$

$$\text{or} \quad \hat{r}(t) = A(t).\exp(j\phi(t)) \qquad 4.4.5$$

where $\hat{r}(t)$ is called the baseband signal.

By expanding equation 4.4.1, it can be seen that

$$r(t) = p.\text{Cos}[\omega_o t] - q.\text{Sin}[\omega_o t] \qquad 4.4.6$$

The Fourier transform of r(t) has significant components around $\pm f_o$ whereas those of p and q are centred at zero frequency, with significant values at frequencies corresponding to about half the bandwidth occupied by r(t), on either side of zero. Figure 4.4.2 shows the Fourier transforms of both r(t) and $\hat{r}(t)$.

It is worth emphasising that although the baseband signal is complex the in-phase and quadrature components are both Real functions of time. The transform of the baseband signal does not have the usual Hermitian symmetry associated with transforms of Real functions and the original spectrum is related to the baseband spectrum by

$$R(\omega) = \tfrac{1}{2}\hat{R}(\omega - \omega_o) + \tfrac{1}{2}\hat{R}^*(-\omega - \omega_o) \qquad 4.4.7$$

where $R(\omega)$ and $\hat{R}(\omega)$ are the transforms of r(t) and $\hat{r}(t)$ respectively.

It can be seen from figure 4.4.2 that the highest frequency of the baseband signals and hence the required minimum sampling rate required to store these signals is much reduced.

The baseband signals were fed into a Datalab transient recorder type 905 which digitises to 8 bit resolution. Most of the measurements were recorded by sampling 256 points in a 0.512 ms range window, which is a 500 kHz sampling rate. This was more points than were required to avoid aliasing but it meant that results could be plotted directly, without interpolation, to give a visually acceptable display. Data from the transient recorder were accessed by a Hewlett Packard 9825 desktop computer using an IEEE 488 standard interface.

The storage capacity of this computer limited the number of points that it was possible to perform an FFT on to 256 points, using a radix 2, not in place algorithm. In order to allow for zero padding of the data and addittional manipulation it was necessary to reduce this sampling rate internally, so that the storage capacity was not exceeded. In this respect the demodulation process was an essential part of the system since it would not otherwise have been possible to reduce the sampling rate.

As stated above the demodulating frequency was locked to the transmit frequency and as can be seen from equation 4.4.2/3 the phase difference has been taken as zero. Since the phases of successive returns are now all the same the in-phase and quadrature components do not need to be measured at the same time from the same transmit pulse and can be measured sequentially using

the same, single channel, transient recorder. Further advantage can be taken of this phase locking by averaging a number of successive returns for each component, and typically 100 returns were averaged.

4.5 Expected Results

The expected performance, in terms of resolution, can be estimated from the description of the equipment already given.

The first improvement to the recorded signals is carried out in the deconvolution process and is illustrated in figure 4.5.1, which shows the envelope of the original transmitted signal (the reference) compared with the transform of the Hamming window. This transform is how each true impulse should be represented after the deconvolution. An improvement in the width of the envelope is shown together with the removal of the ringing portion of the transmitted signal. The window used to obtain the transform was the widest one used (44 kHz) and in practice a result as good as this will not be obtained because of noise generated in the deconvolution process.

The expected limit of time resolution can be estimated in two different ways 1) by the geometry, and 2) by the bandwidth. The geometry imposes a limit of the plane wave assumption to the spherical waves actually produced. Figure 4.5.2 illustrates the spherical wavefront meeting a plane boundary at a

distance, H, from the source. If the -3 dB beamwidth is θ then the difference, d, in the position of the actual wavefront and that of the assumed plane wave front, at this -3 dB point is given by,

$$\frac{H}{H + d} = \text{Cos}(\theta/2) = 1 - \frac{\theta^2}{8} + \ldots.$$

Taking the first two terms only,

$$d = \frac{H.\theta^2}{8}$$

Thus for a 10° beamwidth at a height of 0.5 m the difference, d, is 0.2 cm. This is a measure of the resolution limit imposed by the geometry. For comparison a sea going system with the same beamwidth at a height of 25 m would be limited to 10 cm resolution using this argument.

The bandwidth limit can be illustrated by considering the case of two returns at times t_o and t_1 with amplitudes 1 and Ω respectively. If these are deconvolved using a window, $H(\omega)$, then the output will be,

$$x(t) = h(t) * [\ \delta(t-t_o) + \Omega.\delta(t-t_1)\ ]$$

Examining the form of this in frequency domain, then

$$X(\omega) = H(\omega).\exp(-j\omega t_o).[\ 1 + \Omega.\exp(-j\omega(t_1-t_o))]$$

i.e. the transform consists of the superposition of the transform of the first return alone and a sinusoid of amplitude, Ω, and 'frequency' (t_1-t_o).

The effect of this sinusoid is shown in figure 4.5.3, which compares the Hamming window alone with the case of a sinusoid superimposed on the window. These two cases illustrate the frequency domain representation of a single return and two returns respectively, after deconvolution. The figures have been artificially generated and if the -3 dB width of the window is taken as 30 kHz then the sinusoid would represent a delay in time domain of approximately 220 μs; the ratio of the amplitudes of the two returns is 0.3 .

The conditions which are required to detect this echo can be seen to be 1) at least one cycle of the sinusoid must be within the bandwidth of the window, and 2) at least two sample points are required per cycle of the sinusoid. These conditions can be stated formally as,

1) $\omega_B.(t_1-t_o) > 2\pi$

2) $2\Delta\omega.(t_1-t_o) < 2\pi$

where $\Delta\omega$ is the spacing of points in frequency domain, and ω_B is the bandwidth of the window.
The first condition means that the resolution cannot be better than the inverse of the bandwidth; the second condition means that the length of the time record in the transform must be at least twice as long as the maximun delay between echoes.

The expected resolution can be calculated for the Hamming window proposed in section 3.2 by taking the equivalent -3 dB bandwidths of the actual windows used

in section 5.3.1. These -3 dB widths are 15, 22, 30 37 and 44 kHz and hence the resolutions expected are 67, 45, 33, 27 and 23 μs respectively. These are total times and correspond to a two way path through a layer, hence the minimum layer that can be resolved has a travel time of 12 μs from the 44 kHz window. This is equivalent to a thickness of approximately 2 cm for a velocity of 1750 ms^{-1}, and represents a greater limit on resolution than the plane wave assumption, above.

One of the fundamental properties to look for in a reflection series is an inversion of polarity that would be caused by a reflection from a softer acoustic medium; however this cannot always be done because of limitations of the width of the window that can be applied. Having divided the spectrum by the reference it is necessary to window it as decribed earlier, and using $H(\omega)$ we obtain,

$$Y(\omega) = H(\omega).\frac{X(\omega)}{R(\omega)}$$

$$\text{i.e. } y(t) = h(t) * i(t)$$

hence each spike in $i(t)$ will be convolved with $h(t)$. Considering the case where no demodulation is used then $H(\omega)$ is centred on ω_o and $h(t)$ will be an oscillating function. The width of the optimum window is determined by the bandwidth hence the "output" is similar to the original signal.

If the window bandwidth is sufficiently large, relative to the carrier frequency (i.e. small Q factor),

then the number of cycles of oscillation in h(t) are small and the central cycle is much larger than the adjacent cycles so that an inversion of polarity can easily be detected.

In order to calculate a criterion for the window width required to detect an inversion, take the simple case of a rectangular window centred on f_o, the transform is given by[66],

$$2f_o \cdot \frac{SIN(2\pi Wt)}{2\pi Wt} \cdot COS(2\pi f_o t) \qquad \text{4.5.1}$$

where the width of the rectangular window is 2W.

Figure 4.5.4 shows artificially generated outputs from the deconvolution process for the case of three different rectangular windows applied in frequency domain. As an example the rectangular window is taken as 30 kHz in each case and the values of carrier frequency are 45, 100 and 150 kHz, respectively. These correspond to cases where the polarity can easily be detected, can just be detected and cannot be detected, respectively.

The envelope of this function reaches a peak at t=0 and this coincides with a peak of one of the cycles of the Cosine function. An adjacent peak of the Cosine function will be smaller than the central one and it is possible to state an arbitary criterion for the detection of an inversion by stating that this adjacent peak should be less than or equal to one half of the amplitude of the central peak, see figure 4.5.4.

Now the period of the Cosine function is $1/f_o$ and the point at which the envelope falls to one half of its peak value is given by $2Wt = 0.6$. Putting $t = 1/f_o$ gives,

$$2W = 0.6\ f_o \qquad \text{4.5.2}$$

i.e. the window must be at least as wide as $0.6\ f_o$ to detect an inversion. [If f_o = 165 kHz then, window width > 99 kHz.]

This calculation has not considered signal to noise ratio hence for this criterion to be valid a bandwidth of 99 kHz must must be completely free of any noise. Whilst it is attractive to consider a much wider window than the bandwidth the deconvolution process is defeated by erroneous frequency components generated by division at frequencies where the signal to noise ratio is small.

The factor of one half stated in the criterion is arbitary and if the signal were free of noise then a larger fraction may still enable an inversion to be detected; the criterion chosen depends on the signal to noise ratio.

It is worth repeating this calculation for the Hamming window proposed in section 3.2. In this case the envelope of the transform of the window is given by[se],

$$0.54q(t) + 0.23q(t + 1/2W) + 0.23q(t - 1/2W) \qquad \text{4.5.3}$$

where $$q(t) = \frac{SIN(2\pi Wt)}{\pi t}$$

Figure 4.5.5 shows artificially generated outputs from the deconvolution process for the case of three different Hamming windows applied in frequency domain. As an example the Hamming window is taken as 30 kHz to the -3 dB points in each case and the values of carrier frequency are 45, 67 and 150 kHz, respectively, as before. These correspond to cases where the polarity can easily be detected, can just be detected and cannot be detected, respectively.

This envelope falls to one half of its peak value at a point given by $2Wt = 0.9$. If this window was also applied at f_o then the envelope will be multiplied by the same Cosine function as before with period $1/f_o$ and the criterion for inversion detection with this window is

$$2W = 0.9\ f_o \qquad \text{4.5.4}$$

i.e. the window must be at least as wide as $0.9\ f_o$, and if f_o = 165 kHz then, window width $\geq$ 148 kHz.

This is the total width of the window and as pointed out earlier this window has an effective -3 dB bandwidth of $0.38 \times 148 = 56$ kHz. This bandwidth represents a Q factor of about 3, for an operating frequency of 165 kHz, and although some sonar transmitters are physically capable of producing this sort of pulse, transducers based on a ceramic element, such as the one built for this work, are not generally able to even with ¼ wave plate matching. The transducer had a theoretical Q factor of about 8 and

hence it will not be possible to detect inversions of polarity in this work.

CHAPTER 5 EXPERIMENTAL WORK AND RESULTS.

5.1 Introduction.

This introduction will explain how the measurements have been made and illustrate the method of obtaining the in-phase and quadrature components of the signals, as well showing the advantages gained.

All the measurements were taken by using the shortest pulse available (nominally 40 μs.), and using the lowest p.r.f. (which gave 33 ms between pulses). The amplitude of the transmit pulse was set at 200 volts peak to peak, measured at the electrical inputs to the transducer.

Firstly the reference pulse, r(t), was recorded by reflecting the pulse from a 'perfect' reflector 0.5 m away, as described in section 4.3. A recording was made before any deconvolution or filtering had taken place, at the electrical connections to the transducer, for illustrative purposes. The recording was made using the transient recorder which was set to sample 1024 points in a sweep of 0.512 ms. This gave a sampling frequency of 2 MHz, which is equivalent to about 12 points per cycle of the carrier, and this recording of the reference pulse was shown earlier in figure 4.3.10. The peak to peak level of the signal measured from figure 5.1.1 is 13.8 volts which gives a two way transmit/receive loss, at 0.5 m, of -23 dB.

The gain of the receiver was turned down so that the demodulators were not overloaded and the two analogue channels coould be observed on an oscilloscope as in-phase and quadrature components. Since the phase of the transmit pulse was locked to the phase of the demodulating frequency the phase of the two channels was the same for each pulse and a stable trace could be obtained on the oscilloscope by triggering from the transmit instant. The transient recorder could be triggered in the same way so that successive recordings could be added in order to improve the signal to noise ratio. The transient recorder was a single channel device and this method allowed first the in-phase components to be summed and stored in the computer and then the quadrature components since their phases would remain the same, and it was not neccessary to capture both channels at the same instant from the same transmit pulse. Each channel was summed over 100 records.

The demodulated signals were initially sampled at a rate of 256 points in a sweep of 0.512 ms sweep, which is a sampling rate of 500 kHz, in order to provide enough points to be plotted clearly. The in-phase and quadrature components of the reference are shown in figure 5.1.1 and in this case where it is seen that both components were predominately negative. For comparison the in-phase and quadrature components of a signal reflected from a sand layer are shown in figure 5.1.2, which shows that the components may be both positive and

negative; indeed if the transducer were to be moved backwards or forwards the components will cycle around by 360° every time the total path changes by one wavelength of the demodulation frequency.

The amplitude of the reference, calculated from the square root of the sum of the squares of the two components, has already been shown in figure 4.5.1; since it is not expected to be able to reveal polarity inversions, it will be the amplitudes of the signals that will be used for the main measurements.

The power spectrum of the baseband signal has been calculated by writing the baseband signal as a complex number, with the in-phase component as the Real part and the quadrature component as the Imaginary part; the power spectrum of the original signal has been artificially reconstructed from the baseband spectrum, using equation 4.4.7, for illustrative purposes only, and these spectrums have already been shown in figure 4.4.2. It can be seen that the significant components of the baseband signal are centred around the zero frequency point while those of the original signal are centred around $\pm f_o$. Also the baseband spectrum has the same shape around the zero frequency point that the original spectrum had around f_o, i.e. the original spectrum has been shifted to the left and filtered.

The baseband spectrum is no longer symmetric around d.c. as expected since it has been transformed from a complex function of t. Also note that there is a large

negative dip in the baseband spectrum at - 87 kHz, this dip will be referred to later in the disussion of noise in the deconvolution.

The baseband spectrum shows that an absolute minimum sampling frequency of about 125 kHz is required to recover the baseband signal as compared with about 500 kHz in the case of the original signal. In practice there was no difference in the results obtained by sampling at this absolute minimum frequency or at a higher frequency, as expected , and the signal processing calculations were carried out using the lower sampling rate and only re-sampled to 256 points for the purposes of producing outputs on the plotter.

The following sections describe, specifically, the measurements that were taken on the sediments and the signal processing calculations that were performed.

5.2 Measurements taken with the model

A set of signal returns for one layer of sediment and then for two and three layers were captured. Each set consisted of the signals obtained at 10 positions at 10 cms intervals horizontally across the sediment layers. The signals were corrected for a 1/R spreading loss, as described in section 3.1.1, and also corrected for the receiver gain before storage in the computer.

The first layer to be set up was of 250 μm sand, described in section 4.2.2, and was laid down in two

sections of approximately 5 cms deep each. A set of measurements were taken after the first section was laid and recorded by photographing an oscilloscope trace. The purpose of this was to establish how well separated the two main returns were. It was decided to add the second section to ensure that this layer was well resolved. This set of photographs, shown in figure 5.2.1, also gave confidence that this method of laying down layers gave a hoizontally homogeneous medium. The photographs show good consistency in the observed returns however there was some difference between adjacent measurements but repeated attempts at smoothing the surface failed to improve the consistency any further.

A second layer of 50 μm sand was laid on top of the first layer, taking care not to disturb the flat surface of the first layer. This second layer was 3 cm deep making a total of 13 cm of sediment. A second set of measurements were taken with this two layer model. The positioning equipment described in section 4.2.1 permitted the transducer to be repositioned accurately.

It was decided that the second layer could be resolved and a third was laid on top. The third layer was of 250 μm sand, which is the same as the first, and was 5 cms deep. A third set of measurements was taken with this three layer model taking the same precautions as for the first.

The reflected signals for the cases of 1, 2 and 3 layers have been reproduced in figure 5.2.2 directly from the electrical signals at the transducer outputs, before any processing. The recordings were taken at a horizontal position in the centre of the tank, although the results at other horizontal positions showed the same level of consistency as the photographs in figure 5.2.1.

All the measurements were taken with the transducer at 0.5 m from the top of the sand layers and it was checked for vertical alignment at each measurement point. The gantry was checked and adjusted so that it was parallel with the bottom of the tank. The geometry of the arrangement ensured that any reflections, from the sides of the tank would be well down in the sidelobes of the beam pattern of the transducer and not resolveable with an 8 bit digital system.

The depth of sand in each layer was measured by filling the small tank completely with water whilst the large tank was empty, standing a wooden rule on top of the sand layer and reading off the water depth. Measurements at several points over the surface checked the horizontal accuracy of the layer and core samples taken when the final three layer measurements were recorded confirmed these measurements were accurate to within 2 mm.

5.3 Deterministic Deconvolution

5.3.1 Deterministic deconvolution results

The recorded signals returned from the sediment for the cases of one, two and three layers were all deconvolved with the reference signal using the method decribed in section 3.2, for five differrent Hamming window widths. The window widths used in the computer were an integer number of increments in frequency domain, but these have been expressed as an equivalent - 3 dB bandwidth, which is 38 % of the total window width as pointed out in section 3.2.2. The five window widths used were 15, 22, 30, 37 and 44 kHz.

The results at different horizontal positions were so similar, for a given number of layers, that it is not worth presenting them separately and only the results from one horizontal position are shown in each case. This is the position in the centre of the tank and was the same for each different window.

The results have been calculated at baseband, in the computer, and instead of showing the Real and Imaginary components separately only the amplitude is shown. The amplitudes have been scaled to make the results consistent for different window widths and the scaling factor used is given by,

$$1.08\ W/N$$

Where W is the number of points in the half window width

and N is the number of points used in the inverse transform.

This factor is the peak amplitude of the transform of the window alone[66] and hence represents the amplitude of the deconvolution of the reference by itself. The resulting scaled amplitudes can be considered therefore to be relative to that of the reference.

The results for one, two and three layers are shown in figures 5.3.1, 5.3.2 and 5.3.3 respectively together with the envelope of the original signal in each case for comparison. These figures have been split into two parts over two pages in order to reproduce the results at a reasonable size.

It is possible to estimate a series of impulses from the deconvolved outputs. The amplitude of each impulse can be measured directly off the 'y' axis scale, since the plots have been normalised, but a judgement must be made between peaks that are true returns and peaks that are noise produced in the deconvolution process; this is largely a subjective judgement. In this case the judgement is made with the prior knowledge of what layers are actually present and in this way valid data are input to the parameter determination methods.

The widest window will resolve the true returns best with respect to time but suffer most from noise produced in the deconvolution process, the narrower windows produce the most accurate amplitude

measurements, assuming the returns are resolved. The amplitude of each return for different window widths have been tabulated in each case and are shown in figure 5.3.4.

5.3.2 Calculation of acoustic parameters

The acoustic parameters of the sand layers will be calculated using the 'bottom up' method described in section 3.4 by solving equation 3.4.19 given the input data tabulated in figure 5.3.4. These tabulated results obtained from different windows should all be the same after normalising; however, the results show some variation occurring at the wider windows where noise becomes significant. Having identified the true returns from results of wide windows, the amplitudes can be measured with most accuracy from the results with narrow windows - assuming the returns are separated. Thus the results used for the calculations will be from the narrowest window that resolves all the returns. The notation used is that defined in figure 3.4.1.

It has already been stated that the 'no layer' case, corresponding to a reflection from the bottom of the steel tank, yields a value of R_o of unity, see appendix B. This value of R_o is then carried forward, a priori, to the one layer case.

<u>One layer case</u>

From equation 3.4.13,

$$R_{1w} = \gamma_1 \qquad \text{5.3.1}$$

$$R_o = \frac{\gamma_o}{a_1^2 . T_{1w}^2} \qquad \text{5.3.2}$$

where $\gamma_1 = 0.402$

$\gamma_o = 0.286$ from figure 5.3.4

and $R_o = 1$ from the 'no layer' case.

Substituting these values,

$R_{1w} = 0.402,$

giving $T_{1w}^2 = 1 - 0.402^2 = 0.838$

$$a_1^2 = \frac{0.286}{(1 - 0.402^2)} = 0.34$$

Two layer case.

From equation 3.4.13,

$$R_{2w} = \gamma_2 \qquad \text{5.3.3}$$

$$R_1 = \frac{\gamma_1}{a_2^2 . T_{2w}^2} \qquad \text{5.3.4}$$

$$R_o = \frac{\gamma_o}{a_2^2 . a_1^2 . T_{2w}^2 . T_1^2} \qquad \text{5.3.5}$$

where $\gamma_2 = 0.314$

$\gamma_1 = 0.077$

$\gamma_o = 0.162$ from figure 5.3.4

and $R_o = 1$ from the 'no layer' case

$a_1^2 = 0.34$ from the one layer case.

Substituting these values into equation 3.4.19 for the bottom layer,

$$R_1 = -\frac{X}{2} \pm \sqrt{\frac{X^2}{4} + 1}$$

where $\chi = \left(\frac{\gamma_o}{\gamma_1}\right).\left(\frac{1}{a_1^2 \ .R_o}\right)$

then, $\chi = \frac{(0.162)}{(0.077)}.\frac{1}{(0.34).(1)} = 6.19$

As $|R_1| < 1$ the solution is

$$R_1 = 0.156$$

For the top layer it is only necessary to substitute directly into equations 5.3.3 and 5.3.4,

hence $R_{2w} = 0.314$

$$a_2^2 = \frac{0.077}{(1 - 0.314^2).(0.156)}$$

$$\therefore a_2^2 = 0.55$$

Three layer case

From equation 3.4.13,

$$R_{3w} = \gamma_3 \qquad \text{5.3.6}$$

$$R_2 = \frac{\gamma_2}{a_3^2.T_{3w}^2} \qquad \text{5.3.7}$$

$$R_1 = \frac{\gamma_1}{a_3^2.a_2^2.T_{3w}^2.T_2^2} \qquad \text{5.3.8}$$

$$R_o = \frac{\gamma_o}{a_3^2.a_2^2.a_1^2.T_{3w}^2.T_2^2.T_1^2} \qquad \text{5.3.9}$$

where $\gamma_3 = 0.39$

$\gamma_2 = 0.083$

$\gamma_1 = 0.039$

$\gamma_o = 0.095$ from figure 5.3.4,

and $R_o = 1$ from the 'no layer' case

$a_1^2 = 0.34$ from the one layer case.

$a_2^2 = 0.55$ from the one layer case.

Substituting these values into equation 3.4.19 for the bottom layer,

$$R_1 = -\frac{\chi}{2} \pm \sqrt{\frac{\chi^2}{4} + 1}$$

where $\chi = \left(\frac{\gamma_o}{\gamma_1}\right).\left(\frac{1}{a_1^2 . R_o}\right)$

then, $\chi = \frac{(0.095)}{(0.039)} . \frac{1}{(0.34).(1)} = 7.16$

As $|R_1| < 1$ the solution is

$$\underline{R_1 = 0.137}$$

Next, substituting these values into equation 3.4.19 for the middle layer,

$$R_2 = -\frac{\chi}{2} \pm \sqrt{\frac{\chi^2}{4} + 1}$$

where $\chi = \left(\frac{\gamma_1}{\gamma_2}\right).\left(\frac{1}{a_2^2 . R_1}\right)$

then, $\chi = \frac{(0.039)}{(0.083)} . \frac{1}{(0.55).(0.137)} = 6.24$

As $|R_2| < 1$ the solution is

$$\underline{R_2 = 0.16}$$

The next layer is the top layer and does not require equation 3.4.19, hence substituting directly into equations 5.3.6 and 5.3.7,

hence $\underline{R_{3w} = 0.39}$

and,

$$a_3^2 = \frac{0.083}{(1 - 0.39^2).(0.16)}$$

$$\therefore \quad a_3^2 = 0.65$$

These results are tabulated in figure 5.3.2 which shows which result has been calculated from each case and also shows which values have been used from the results of the previous cases.

The acoustic impedances of each layer have been calculated by re-arranging the equation for the Rayleigh reflection coefficient to give,

$$\frac{Z_2}{Z_1} = \frac{1 - R}{1 + R}$$

where R is the reflection coefficient,

Z_1, Z_2 are the impedances of the media on each side of the boundary.

and taking the acoustic impedance of the water to be 1.48×10^6 Rayls.

The attenuation measured for each layer has been converted to a coefficient, measured in dBm^{-1}, given the layer thicknesses, which were measured when the layers were put down, of 10, 3 and 5 cms for the bottom, middle and top layers respectively. Hence the values of impedance were calculated afresh for each new layer while the attenuations were only calculated once. These values of impedance and attenuation are tabulated in figure 5.3.6 together with the values measured by Thomas and Pace[4] for comparison.

5.4 Acousticore Displays

The deconvolved data had been reduced to amplitude only representation since it had been previously established, in section 4.5, that it would not be possible to detect polarity inversions. This presents two problems 1) the output of the acouticore algorithm will be in error at a true negative return and this will propogate through to the end of the integration, 2) the noise components are now all made positive and this will cause the noise to integrate up to impose a positive ramp on the acousticore output which may swamp the useful information.

The first problem is present whatever method is used although the error will not always propogate; the second problem is particular to this integration method and the following results will illustrate the problem.

The acousticore method was applied directly to the results from the deconvolved outputs. These outputs had been already corrected for a 1/R spreading loss but not for any attenuation within the layers. Since the acousticore method assumes lossless layers the outputs will be in error.

All the outputs have the first step at time t=0 since the deconvolved outputs have been shifted likewise. The time before t=0 corresponds to the water, hence $Z_n=Z_\omega$. The first step is genuinely positive and should be correctly represented and the acousticore output should rise to $3.23/1.48 \simeq 2.18$, for

the one and three layer cases, and 2.69/1.48 ≈ 1.82, for the two layer case, respectively.

These results are shown in figure 5.4.1 for the case of the 44 kHz window results, which should give the best resolution, for the case of one , two and three layers.

The effect of additive noise is shown in all three cases as a positive ramp imposed on the useful information. The effect completely dominates the 3 layer case where the deconvolution noise is worst. For comparison the plot of the 2 layer case is repeated in figure 5.4.2 together with the result from the 30 kHz window, which shows a much less pronounced ramp. The actual impedances shown will, of course, be incorrect apart from the first because the acousticore method has assumed lossless layers. Rather than applying a correction for attenuation to the deconvolved results here, it will be more useful to use the same measured values for the primary outputs, already used for the inputs to the algebraic solution, and tabulated in figure 5.3.4.

These results as stated before are based on knowing where the interfaces are and measuring the amplitudes of the returns at that point, then all returns in between are assumed to be noise and set to zero, thus generating the primary outputs.

Integrating these primary outputs numerically reduces simply to adding the amplitudes of the returns

at each interface, since they have already been normalised in the deconvolution process. A correction for attenuation can be applied using the results of the algebraic solution for the attenuation in each layer. Figure 5.4.3 shows the primary outputs reproduced from figure 5.3.4 together with the corrected outputs which would have been obtained if there were no attenuation. The second return in the three layer case has also been set to negative which represents what it would have been if the deconvolution process was ideal; this will test the ability of the acousticore process to calculate non monotonic imedance changes.

The results of integrating these outputs are shown in figure 5.4.4. together with the deduced acoustic impedances calculated from equation 3.3.10.

Comparing with the results in figure 5.3.5 from the algebraic solution it is apparent that these results show equally as good agreement with the results of Thomas and Pace[4], in spite of the 'modest' impedance change and the 'continuous' impedance profile assumptions. It must be emphasised though that,

1. The sign of γ_2 in the three layer case was put to negative using 'a priori' knowledge; this was required because the deconvolution technique could not distinguish polarity reversals and is not a fault of the acousticore technique. The acousticore

technique has coped with this negative input and thus monotonic changes are not essential.

2. It was necessary to adjust the values of y(t) to what they would have been if there were no attenuation, using the results of the algebraic solution. This is a drawback of the acousticore technique, if the algebraic results not been available then it would have been necessary to adjust y(t) based on an estimate.

CHAPTER 6 DISCUSSION AND CONCLUSIONS

6.1 Deconvolution noise

The deconvolution process can generate noise by generating erroneous frequency components at frequencies where the signal to noise ratio is small. To illustrate this more clearly the result of dividing the Fourier transform of a signal returned from the sand by the Fourier transform of the reference pulse is shown in figure 6.2.1. The signals were reduced to baseband first and the power spectrum of the reference is shown for comparison. The range of the frequency axis has been artificially extended well beyond the significant components.

The figure shows that the result of the division is reasonably well behaved around the zero frequency point, where the signal to noise ratio is high, but away from that point the result is more erratic and generally has a larger amplitude than the result near the zero frequency point. This erratic behaviour represents the erroneous frequency components which are dominated by some very large spikes. Whether they affect the deconvolved signal or not depends on whether the window employed encompasses them.

The outputs from the deconvolution show a sinusoid breaking through into the deconvolved results as the window is widened - the effect is most noticeable in the three layer case. This sinusoid can be referred to as

noise (in the sense of an unwanted signal), but it is possible to identify the exact origin of this noise component. The frequency of the sinusoid can be estimated by counting the number of cycles in a 100 μs range. This is easiest done in the three layer case with the 44 kHz window where it shows up best but it should be noted that the effect is apparent for all cases and that the sinusoid is at the same frequency for each case, see figures 5.3.1/2/3.

The frequency is estimated to be 85 kHz and this corresponds to one of the large spikes in figure 6.2.1, which in turn corresponds to the large negative dip in the power spectrum of the reference, referred to earlier in section 5.1. Since the reference is the divisor a large value is obtained at this point and the exact amplitude depends on the magnitude of the numerator, which is the transform of the signal from the sand layers. This noise component is more significant in the three layer case than the two layer case and more so in the two than the one, because the transform contains a sinusoid for each reflection, see section 4.5. The more reflections the more sinusoids and the greater the chance that they will interfere to produce a large magnitude to coincide with the negative dip in the reference of the power spectrum.

6.2 Effects of Deconvolution

The deconvolution operation has generated broad

peaks and low noise levels in the case of narrow windows and high noise levels with sharp peaks and good resolution in the case of wide windows; hence there is a trade off between noise and resolution.

The deconvolved outputs and the original unprocessed signals appear superficially to be similar, because the maximum width of the window used is determined by the signal bandwidth, for the reasons given above. However the transform of the window is symmetrical but the original wavelet is not symmetrical because of ringing in the transducer, see figure 4.5.1. Hence the non-symmetric wavelet is replaced by the symmetrical window transform, and any ringing is removed.

The ability to remove any ringing portion of the wavelet is demonstrated in the case of one layer, see figure 5.3.1. The unprocessed signal shows a small peak in between the two main peaks at approximately 0.12 μs. The deconvolved signal, with a 15 kHz window, has effectively removed this contribution showing that the original signal was part of the ringing of the first return and not a new return. A similar ringing can be seen to have been removed in the two layer case however in both cases the effect is less noticeable at the wider window widths due to exessive noise swamping the information. The effect with the three layer case is unfortunately not shown at all and none of the deconvolved signals for any window show much improvement

over the original unprocessed signal, because the information is swamped by noise.

6.3 Multiple Reflections

Multiple reflections within a layer can give rise to extra outputs that do not represent a new interface. Consider, first, only multiple reflections that have taken place within the top layer; in the case of one layer a multiple reflection is apparently shown at 0.3 μs in the unprocessed signal, see figure 5.3.1. This has not been removed by the deconvolving process and so must be a true signal. If this has undergone a downwards reflection at the top of layer one and a second upward reflection from the bottom of layer one before being transmitted through the top of layer one then its amplitude will be given by,

$$a_1^2 . R_1 . R_o . \gamma_o$$

where the same notation is used that was defined in figure 3.4.1.

Evaluating this from the results of figures 5.3.5 and 5.3.6 the amplitude should be 0.039. The amplitude measured from figure 5.3.1, for the 15 kHz window deconvolution, is 0.033. This close agreement means that this contribution to the signal may safely be regarded as a multiple reflection. The delay of this multiple is at twice the delay of the return γ_o compared with γ_1 which is the correct delay for this reflection.

The two layer case apparently shows a multiple at 0.1 ms, which is most clearly shown in the result with the 22 kHz window, see figure 5.3.2. A similar calculation of the expected amplitude of the first multiple would be given by,

$$a_2^2 . R_2 . R_1 . \gamma_1$$

where the same notation is used that was defined in figure 3.4.1.

This evaluates to an amplitude of 0.0015, which is much less than the observed output of approximately 0.02; indeed, comparing it with the scale of the amplitude axis, it should not even have been resolved by an 8 bit digital recording.. The observed output is therefore assumed to have been generated by noise.

In the three layer case the first multiple from γ_2 will interfere partly with the third output, γ_1. However, the amplitude of the multiple in this case is given by

$$a_3^2 . R_3 . R_2 . \gamma_2$$

where the same notation is used that was defined in figure 3.4.1.

This evaluates to 0.004 and, comparing it with the scale of the amplitude axis, it will just toggle the two least significant bits of an 8 bit digital number, but it will be completely swamped by the return, γ_1, which it overlaps. Similar calculations for all other possible multiple reflections show that none will be

resolved with this 8 bit system, hence the only multiple reflections that may be expected to be seen have been successfully identified.

6.4 Resolution

An improvement in resolution has been obtained of about 2:1 in the case of the 44 kHz window which can be seen by comparing the width of the peaks from the deconvolved outputs with the width of the original signal in figures 5.3.1/2/3. This has been acheived at the expense of some loss of signal to noise ratio, however the method has made it possible to choose a combination of resolution and signal to noise ratio for a particular application.

The resolution limit was estimated earlier, in section 4.5, as 1/B where B is the bandwidth. For the windows used here the corresponding resolutions expected are 67, 45, 33, 27 and 23 μs respectively for windows of 15, 22, 30, 37 and 44 kHz bandwidth.

It can be seen that this resolution is obtained by examining the results of figures 5.3.1, 5.3.2 and 5.3.3 and in particular the resolution of the top layer in the two layer case in figure 5.3.2. This case shows that the second return is obscured with the 15 kHz window, just visible with the 22 kHz window and well resolved by the 30 kHz window. Since the two way travel time of this 3 cms layer is 40 μs then this 1/B criterion is shown to be applicable here.

Since it is the bandwidth which limits the resolution more severely than the beamwidth, see section 4.5, then any improvement in the resolution can only be obtained by increasing the bandwidth and no further improvement will be gained by reducing the beamwidth alone. In particular a Q factor of three or less is needed if polarity is to be determined by this method.

6.5 Reflector Identification

It is necessary to identify the reflection coefficient series first before any computation for acoustic parameters can be made. The deconvolution process has already gone part of the way towards this, but only an 'ideal' deconvolution can result in a series of impulses corresponding to the true reflection coefficient series. Hence it is necessary to make a judgement between what constitutes a reflection from an interface and what is a noise component.

This can be done by an operator who makes a subjective estimate of the local average value of the signal and uses this to assess whether a particular return is significantly larger than the average to be part of the reflection coefficient series. It is possible to automate this but the criterion for estimating the local average will vary depending on the nature of the signal and the application. An automatic technique will be more reliable with higher signal to noise ratios, and hence better deconvolved signals.

In this work with a small number of layers and a high signal to noise ratio the reflectors can easily be identified by eye without the need for any further calculations; it was checked that they did indeed occur at the correct time delays for the known layers present. Having identified the reflectors the amplitudes can be read off the y - axis scale, assuming the amplitudes have been normalised.

6.6 Acoustic Parameters

The results obtained for the calculations of acoustic parameters using equation 3.4.19 are in agreement with the values taken from Thomas and Pace[4], to within about 10%. The values of reflection coefficient, and hence impedance, were each calculated afresh for the case of each new layer. The attenuation in each layer was only calculated once whilst that layer was the top layer. This was done on the assumption that the attenuation would not change significantly with increasing overburden pressure.

The effects of increasing overburden pressure on attenuation were discussed by Hamilton[25]. Although he reports that very little data are available the gradients of attenuation in sand are better known than those in silt-clays. In sands, such as those used in this experimental work, attenuation decreases with the -1/6 power of overburden pressure. Hence with the shallow depths considered here, no significant effect

should be observed. The situation with silt-clays, such as may be found deposited in estuaries, is completely different. The attenuation appears to increase with depth, because of porosity reduction, down to the first few hundred metres but the data do not justify calculating a gradient. It appears that the gradient is small enough to be ignored but Hamilton's data is more concerned with depths of some thousands of metres and does not show detail for the first few metres.

If it is required to monitor the attenuation of sub-bottom layers then equation 3.4.19 can be solved for each attenuation afresh for each new layer and for one new reflection coefficient. However, as pointed out in section 3.4.2, this value of reflection coefficient will have been calculated for the top water/sediment interface and when it is passed on to the case of the next layer it will have to be modified, depending on the difference in acoustic impedance of the new layer and the water. Useful information may be obtained about the state of compaction of silty sub-bottom layers using this method, although the rate of change of attenuation may not be enough to give very accurate results.

6.7 Acousticore Method

The acousticore process was applied in two ways, firstly as an algorithm with the deconvolved signal as the input; and secondly by using the estimated impulse

response measured from the deconvolved signals, tabulated in figure 5.3.4, and integrating numerically by hand.

The first method is seen to have suffered severely from the lack of polarity determination; the problem is manifested in two ways, 1) the impedance of the middle layer in the three layer case generates an increasing step in the output impedance profile when it should show a decrease, and 2) the noise components, being all positive, integrate to impose a large slope on the results instead of integrating to zero as they should. This problem is caused because the received signals did not have sufficient bandwidth for the deconvolution process to determine their polarity. If the polarity were determined the acousticore method would require attenuation information to generate the correct results since the method itself assumes lossless layers

The second method has used data with polarity determined which would represent the output from an 'ideal' deconvolution. The data was modified using the attenuations calculated previously in order to represent lossless layers and the method has generated correct results to within 10%. Hence, in principle, it has been established that the parameters can be extracted to an accuracy of about 10 % by using the primary outputs only, given the attenuation in each layer and a deconvolution result which determines the polarity of the returns.

6.8 Application to Sea Situation

The dominant problem with applying this work to a sea situation is background noise from the sea environment. As an example consider a sea going system with an operating frequency of 12 kHz and a bandwidth of 4 kHz. Now, ambient noise varies depending on the location and conditions, but a figure of 95 dB re 1 μPa per root Hz at 12 kHz represents an upper value of ambient noise, measured at coastal locations in high winds up to 40 kts[7]. Hence in this 4 kHz band a noise level of 130 dB re 1 μPa is obtained. If such a system radiates 1 kW of acoustic power with a directivity index ≈ 26 dB (for an 8° beamwidth); then the source level generated, in the direction of the beam, will be ≈ 45 dB re 1 Wm^{-2} at 1 m or 226 dB re 1 μPa at 1 m. This is 96 dB above the calculated noise level and hence a total signal attenuation (due to all sources) of 90 dB would result in a signal to noise ratio of 6 dB.

The main sources of attenuation to consider are spreading loss, absorption within the sediment, partial transmission losses and reflection losses at each interface. For a towing height of 10 m and a penetration of 10 m there will be a spreading loss of approximately 26 dB. Attenuation is very variable and may be within the range 0.3 to 8 dBm^{-1} at 12 kHz[25], however taking a value of 2 dBm^{-1} there will be an absorption loss of 40 dB for a two way path through this 10 m depth. A single reflection from an interface with

a reflection coefficient of 0.25 would result in a 12 dB loss, and two way transmission through ten such interfaces would give a further 6 dB loss. Hence in this example a total loss of 84 dB has been accounted for and a resulting signal to noise ratio of 12 dB would be obtained. This may be considered a good signal return, however if the attenuation had been taken as 3 dBm^{-1} instead, then the signal to noise ratio would have been -8 dB and effective penetration to 10 m would not have been achieved.

In practice the noise may not be isotropic, especially if its source is either wave motion at the sea surface or engine noise of the towing ship. If the main beam of the transducer is directed downwards then this noise can only enter the system through sidelobes of the beam pattern or after a reflection from the sea bottom; in either case the noise level will be less than that used for the example above.

Further gains in signal to noise ratio may be obtained by transmitting longer pulses. A tone burst would be about 0.25 ms long with a 4 kHz bandwidth, but for a towing height of 10 m it would be possible to transmit pulses of 4 ms, without problems, giving a processing gain of up to 12 dB.

6.9 Summary

A successful laboratory echo sounder has been built together with an efficient means of capturing the

reflected signals. A sediment facility has been developed which has enabled realistic sea sediments to be investigated using the echo sounder at normal incidence. Three sediment structures were investigated using first one layer, then two layers and then three layers of sediment and the signals captured by the system have been used to investigate some signal processing methods.

A deconvolution process has been demonstrated and shown to give an improved resolution at the expense of signal to noise ratio. An improvement of up to two to one could be achieved with the bandwidth available, before noise dominated the output.

The deconvolved output has been used to calculate the parameters of each buried layer in the three cases, using two different methods:

1) A parameter method based on calculations using equations derived from the amplitudes of successive primary returns has been put forward and has successfully calculated both attenuation and reflection coefficients to an accuracy of about 10%. In order to calculate both parameters together it was necessary to 're-survey' the sediment each time a new layer was added so that results from a previous survey could be used for the next one and so on. It was also necessary to pick out the reflectors by eye, however this method could be most useful in harbours or estuaries where it is

possible to monitor the build up of sediments at regular intervals.

2) The acousticore method has been used but did not prove very useful because the deconvolution process did not give a sufficiently good input to the algorithm. It was shown numerically however that the acousticore method can achieve results accurate to within 10% using the primary inputs only, if the data are corrected for attenuation and the data also contain polarity information. This method did not require the sediment to be re-surveyed each time a new layer was added.

Neither of these methods gave the correct result for the impedance of the middle layer in the three layer case without 'a priori' information. This layer had a lower impedance than the layer on top which would have produced a polariy inversion and the deconvolution process was not able to detect this, because the input signals had insufficient bandwidth.

The parametric source described in chapter 2 would enable the polarity to be detected, and an area of future work could be to use a parametric source in order to detect inversions of polarity using the deconvolution process.

Further useful work would combine both the parameter calculation method and the acousticore method to provide a method which calculates both impedance and attenuation, together, without the need to re-survey an area each time a new layer is added.

APPENDIX A

A.1 Shaped Pulse Generator

This unit controlled the pulse length and pulse repetition frequency (p.r.f.) as well as generating the pulse envelope itself. The envelope itself was derived by using a 20 bit shift register. A single high level was clocked round and each output was taken through a separate potentiometer to be summed in an operational amplifier. Each potentiometer was adjusted so that the required voltage could be tapped off the relevant high level and the envelope set up. The pulse length then required 20 clocks and was therefore adjustable by varying the frequency of this clock. An astable mulivibrator was used for this clock and the pulse length could be varied from 40 μs to 300 μs.

The p.r.f. was controlled with a '555' timer chip. The p.r.f. could be varied from periods of 1 to 33 ms and this timer initiated a high level into the shift register. Simple TTL circuitry ensured that only one high level was present in the shift register at any time and also that the shift register clock was locked to the p.r.f. so that there was no jitter in the p.r.f. generated. The trigger to the recording equipment was taken from the first output of the shift register and a gate pulse was derived from the start of the first output to the end of the last output using a flip-flop.

The pulse envelope was filtered and bufferred out through an op-amp. A ciruit diagram is shown in figure A.1.1.

A.2 Modulator

This unit multiplied the carrier with the envelope to generate the desired signal for transmission. The modulation was done with an LM 1496 chip and the circuit is shown in figure A.2.1. The inputs were kept at a constant level and the output was set at 1 volt peak to peak throughout the work. Two balanced outputs were available but only one was used in this instance and any d.c. level decoupled by a capacitor in the amplifier. The data sheet for the device specified 60 dB rejection of the carrier for no modulator input, however in practice only about 45 db rejection was achieved. This was not considered enough since this would break through into the receive side. To overcome the problem the carrier was actually gated before presenting it to the modulator input. Even with some breakthrough in the gating device the rejection was now nearly 100 dB and this was considered adequate.

A.3 Transmitting Amplifier

This unit was mainly for current gain although some voltage gain was incorporated as well. The amplifier had a conventional common emitter input stage and used a complementary pair of output drivers as shown in figure

A.3.1. The input impedance was about 10 kΩ so that it did not load the modulator output, and the output impedance was approximately 1 Ω. The voltage gain was varied with a potentiometer between the input and output stages and a maximum gain of about 28 dB was available giving 25 volts peak to peak output.

A.4 Demodulator

The demodulation process was carried out on the analogue signal in two channels. A block diagram of the process is shown in figure A.4.1 which can be described in two parts; 1) generation of the Sine and Cosine components, and 2) the demodulation process.

The Sine and Cosine generation was controlled by a synchronisation pulse and a gating signal from the shaped pulse generator, and an input square wave, at a frequency of $4f_o$, from the function generator. The input signal from the function generator was divided down using flip-flops to obtain two outputs, 90° out of phase with each other, at a frequency of f_o. The synchronisation pulse occurred at the instant before transmission and was used to clear the flip-flops so that they would always start a the same phase relative to each transmit pulse. The outputs, at f_o and $f_o + 90°$, were fed through Op amps to low pass filters. These Op amps were also used to adjust the d.c. level applied to the filters during the synchronisation time. If this were not done then the d.c. level in the filter

would fall during the synchronisation time and the filter outputs would need several cycles to settle at the end of the synchronisation time - by maintaining the d.c. level this settling time was minimised.

The outputs from the RC filter now represent the Sine and Cosine components respectively and one of the channels was gated out through a CMOS (4016) analogue gate to the transmit side using the gating signal provided by the shaped pulse generator.

Hence both the carrier for the transmit side and for the demodulation were at the same frequency and with the same relative phase for every transmit pulse. Figure A.3.2 shows a circuit diagram of the generation of these Sine and Cosine outputs.

The demodulators were identical with the modulator used to generate the transmit pulse (LM 1496) except for changes in resistor values effecting the input impedance. These devices had two balanced outputs and these were summed in differential operational amplifiers to generate a signal centred on d.c., the modulators were adjusted for minimum breakthrough.

This signal needed to be filtered and each channel had a two stage low pass Sallen and Key active filter. This gave a total of 24 dB per octave roll off and effectively removed all the signal components at $2f_o$ to below -48 dB on the desired signals. These filter outputs were then made available on B.N.C. connectors for the Datalab transient recorder. Figure A.3.3 shows

the circuit diagram of the demodulation and filter components.

A.5 Receive Amplifier

The low ranges involved in this work meant that the returned signals actually generated voltages of the order of a volt at the transducer outputs. Hence there was no requirement for amplification but it was necessary to amplify the signals and it was necessary to reduce the signal amplitudes to prevent them overloading the demodulating circuits. The receiver was a switched attenuator as shown in figure A.5.1, and merely buffered the transducer outputs from the demodulating circuits. Two back to back diodes were incorporated across the inputs and these shorted out the high voltage transmit signal but did not effect the smaller received signals. A suitable resistor network limited the current that they took so that the transmit amplifier was not shorted but the receiver was protected; the voltage lost on receive was minimised by the high input impedance of the '531 operational amplifiers.

A.6 Matching Transformer

The matching transformer was required for two reasons; 1) to amplify the output voltage from the power amplifier, 2) to balance out the static capacitance of the the transducer element.

The first reason is concerned with driving the transducer with a reasonable amount of power. The resistance of the element was 1890 ohms and if a power of 10 watts is required (say) then the necessary r.m.s. voltage is given by,

$$\text{Power} = V^2/R$$

and therefore V = 137 volts r.m.s.

This a peak to peak voltage of 388 volts and, given that the maximun output voltage of the power amplifier was 25 volts peak to peak, the ratio of the number of turns required on the transformer is 25:388 in order to input 10 watts to the transducer using full power.

In practise the applied voltage was set at 200 volts peak to peak by turning down the power amplifier gain and this would represent a power of about 2.5 watts.

The secondary turning on the transformer did not balance out the static capacitance of the element on its own and an additional inductor was included so that the impedance seen by the amplifier was purely resistive.

Two back to back diodes were placed in series with the transformer outputs and the purpose of these was to pass the high voltage transmit signal but to block the small received signals, and prevent them from being shorted out by the transformer.

APPENDIX B

B.1 Reflection coefficient of steel tank.

The reflection coefficient from the botttom of the steel tank may be calculated by treating it as three layers consisting of sand/steel/water. The bottom layer is taken to be water because the small tank was supported on wooden blocks such that the small tank was approximately 0.1 m above the bottom of the large tank.

The reflected signal, f_r, is linked to the incident signal, f_i, by the relationship[1,2],

$$\frac{f_r}{f_i} = \frac{R_{12} + R_{23}.\exp(-2jk_2L)}{1 + R_{12}.R_{23}.\exp(-2jk_2L)}$$

where acoustic impedance of sand, Z_1 = 3.23×10^6 Rayls

acoustic impedance of steel, Z_2 = 46×10^6 Rayls

acoustic impedance of water, Z_3 = 1.5×10^6 Rayls

thickness of steel layer, L = 3.2 mm

wavenumber in steel layer, k = 36 mm

and R_{12} and R_{23} are the Rayleigh reflection coefficients at each interface given by,

$$R_{12} = \frac{Z_2 - Z_1}{Z_2 + Z_1}$$

and $$R_{23} = \frac{Z_3 - Z_2}{Z_3 + Z_2}$$

Substituting in these numbers gives,

$$\frac{f_r}{f_i} = 0.95 + j0.22$$

i.e. the reflected signal has an amplitude of 0.98 and a phase of 13° with respect to the incident signal.

REFERENCES

1. Biot M.A., 'Theory of propogation of elastic waves in a fluid-saturated porous solid. I. Low frequency range.' J.Acoust.Soc.Am., 28(2), 168-178, (1956)

2. Biot M.A., 'Theory of propogation of elastic waves in a fluid-saturated porous solid. II. Higher frequency range.' J.Acoust.Soc.Am., 28(2), 179-191, (1956)

3. Yew C.H. and Jogi P.N., 'Study of wave motions in fluid saturated porous rocks.' J.Acoust.Soc.Am., 60(1), 2-8, (July 1976)

4. Thomas P.R. and Pace N.G., 'Broadband measurements of acoustic attenuation in water saturated sands.' Ultrasonics, 13-17, (Jan 1980).

5. Hampton L.D., 'Acoustic properties of sediments.' J.Acoust.Soc.Am., 42(4), 882-890, (June 1967).

6. Nolle A.W., Hoyer W.A., Mifsud J.F., Runyan W.R. and Ward M.B., 'Acoustical properties of water filled sands.' J.Acoust.Soc.Am., 35(9), 1394-1408, (Sept 1963).

7. McCann C. and McCann D.M., 'The attenuation of compressional waves in marine sediments.' Geophysics, 34(6), 882-892, (Dec 1969).

8. Ferrero M.A. and Sacerdote G.G., Acustica 1, 137,(1951).

9. Urick R.J., J.Appl.Phys. 18, 983, (1947)

10. Stoll R.D., 'Theoretical aspects of sound transmission in sediments.' J.Acoust.Soc.Am., 68(5), 1341-1350, (Nov 1980).

11. Barnard G.R., Bardin J.L. and Hempkins W.B., 'Underwater sound reflection from layered media.' J.Acoust.Soc.Am., 36(11), 2119-2123, (Nov 1964).

12. Brekhovskikh, 'Waves in layered media.' Academic Press Inc., New York, (1960).

13. Hilterman F.J., 'Three dimensional seismic modelling.' Geophysics, 35(6), 1020-1037, (Dec 1970).

14. Hilterman F.J., 'Amplitudes of seismic waves - a quick look.' Geophysics, 40(5), 745-762, (Oct 1975).

15. Woods J.P., 'A seismic model using sound waves in air.' Geophysics, 40(4), 593-607, (Aug 1975).

16. Smith S.G., 'A reflection profile modelling system.' Geophs.J.R.astr.Soc. 49, 723-737, (1977).

17 Rutherford S.R. and Hawker K.E., 'Effects of density gradients on bottom loss for a class of marine sediments,' J.Acoust.Soc.Am., 63(3), 750-757, (Mar 1978).

18. Hawker K.E., 'Influence of Stonely waves on plane-wave reflection coefficients: characteristics of bottom reflection loss.' J.Acoust.Soc.Am., 64(2), 548-555, (Aug 1978).

19. Hawker K.E., Williams W.E. and Foreman T.L., 'A study of the acoustical effects of sub-bottom absorption profiles.' J.Acoust.Soc.Am., 65(2), (Feb 1979).

20. Fryer G.J., 'Reflectivity of the ocean bottom at low frequency.' J.Acoust.Soc.Am., 63(1), (Jan 1978).

21. Mithchell S.K. and Lemmon J.J., 'A ray theory model of acoustic interaction with the ocean bottom.' J.Acoust.Soc.Am., 66(3), (Sept 1979).

22. Cron B.F., and Nuttal A.H., 'Phase distortion of a pulse caused by bottom reflection.' J.Acoust.Soc.Am., 37(3), 486-492, (Mar 1965).

23. Nuttal A.H. and Cron B.F., 'Signal waveform distortion caused by reflection off lossy-layered bottoms.' J.Acoust.Soc.Am., 40(5), 1094-1107, (Mar 1966).

24. Schreiber B.C., 'Sound velocity in deep sea sediments.' J.Geophys.Res., 73(4), 1259-1268, (Feb 1968).

25. Hamilton E.L., 'Geoacoustic modelling of the sea floor.' J.Acoust.Soc.Am., 68(5), 1313-1340, (Nov 1980).

26. Hamilton E.L., 'Sound velocity gradients in marine sediments.' J.Acoust.Soc.Am., 65(4), 909-922, (Apr 1979).

27. Hamilton E.L., 'Prediction of in-situ acoustic and elastic properties of marine sediments.' Geophysics, 36(2), 266-284, (Apr 1971).

28. Tucholke B.E. and Shirley D.J., 'Comparison of laboratory and in-situ compressional wave velocity measurements on sediment cores from the Western North Atlantic.' J.Geophys.Res., 84(B2), 687-695, (Feb 1979).

29 Houtz R., Ewing J. and Le Pichon X., 'Velocity of deep sea sediments from sonobouy data.' J.Geophys.Res., 73(8), 2615-2641, (Apr 1968).

30. Hamilton E.L., Bachman R.T., Curray J.R. and Moore D.G., 'Sediment velocites from sonobouys: Bengal Fan, Sunda Trench, Andaman Basin and Nicobar Fan.' J.Geophys.Res., 82(20), 3003-3012, (July 1970).

31. Hamilton E.L., Moore D.G., Buffington E.C., Sherrer P.L. and Curray J.R., 'Sediment velocities from sonobouys: Bay of Bengal, Bering Sea, Japan Sea and North Pacific.' J.Geophys.Res., 79(17), 2653-2668, (June 1974).

32. Houtz R.E., 'Comparison of velocity-depth characteristics in Western Atlantic and Norwegian Sea sediments.' J.Acoust.Soc.Am., 68(5), 1409-1414, (Nov 1980).

33. Jones J.L., Leslie C.B. and Barton L.E., 'Acoustic characteristics of underwater bottoms.' J.Acoust.Soc.Am., 36(1), 154-157, (Jan 1964).

34. Hamilton E.L., 'Reflection coefficients and bottom losses at normal incidence computed from Pacific sediment properties.' Geophysics, 35(6), 995-1004, (Dec 1970).

35. Hamilton E.L., 'Compressional-wave attenuation in marine sediments.' Geophysics, 37(4), 620-646, (Aug 1972).

36. Hamilton E.L., 'Sound velocity-density relations in sea-floor sediments and rocks.' J.Acoust.Soc.Am., 63(2), 366-377, (Feb 1978).

37. Tucholke B.E., 'Acoustic environment of the Hatteras and Nares Abyssal plains, western North Atlantic Ocean, determined from velocities and physical properties of sediment cores.' J.Acoust.Soc.Am., 68(5), 1376-1390, (Nov 1980).

38. Seismograph Service (England) Ltd., 'Seismic data processing facilities and techniques,' Internal report, (1982).

39. Tyce R.C., 'Near-bottom observations of 4 kHz acoustic reflectivity and attenuation.' Geophysics, 41(4), 673-699, (Aug 1976).

40. Tyce R.C., Mayer L.A. and Speiss F.N., 'Near-bottom seismic profiling: High lateral variability, anomalous amplitudes and estimates of attenuation.' J.Acoust.Soc.Am., 68(5), 1391-1402, (Nov 1980).

41. Marchisio G.B. and Hodgkiss W.S., 'Deconvolution applied to a near-bottom seismic profiler.' J.Acoust.Soc.Am., 72(5), 1478-1491, (Nov 1982).

42. Hutchins R.W., McKeown D.L. and King L.H., 'A deep tow high resolution seismic system for Continental shelf mapping.' Geoscience Canada, 3(2), 95-100, (May 1976).

43. Hutchins R.W., 'Removal of tow fish motion noise from high resolution seismic profiles.' Presented at SEG-US Navy symposium on 'Acoustic imaging and on board data recording and processing equipment.' Held at National Space Technology laboratories, Bay St. Louis, Mississippi (Aug 1978).

44. Simpkin P.G., 'Near and far field characteristics of the Huntec boomer sound source.' Internal report, Huntec '70 Ltd., 25, Howden Road, Ontario (Jan 1970).

45. Parrot D.R., Dodds D.J., King L.H. and Simpkin P.G., 'Measurement and evaluation of the acoustic reflectivity of the sea floor.' Can.J.Earth Sci., 17, 722-737, (1980).

46. Dodds D.J., 'Attenuation estimates from high resolution sub-bottom profiler echoes.' Bottom-Interacting Ocean Acoustics, Plenum press, New York and London, 173-191, (1980).

47. Pettersen P., Hovem J.M., Lovik A. and Knudsen T., 'A new sub-bottom profiling sonar using a non-linear sound source.' The Radio and Electronic Engineer, 47(3), 105-111, (Mar 1977).

48. Ulrych T.J., 'Application of homomorphic deconvolution to seismology.' Geophysics, 36(4) 650-660, (Aug 1971).

49. Harris F.J., 'On the use of windows for harmonic analysis with the discrete Fourier transform.' Proc. IEEE, 66(1), 51-83, (Jan 1978).

50. Bogert B.P., Healey M.J.R. and Tukey J.W., 'The quefrency analysis of time series for echoes: Cepstrum, psuedo-autocovariance, cross-cepstrum and saphe cracking.' Proc. Sym. on Time Series Analysis, Rosenblatt M.(Editor), New York, John Wiley and Sons, 209-243, (1963).

51 Oppenheim A.V., Schafer R.W. and Stockam Jr. T.G., 'Non-linear filtering of multiplied and convolved signals.' Proc. IEEE, 65(8), 1264-1291, (Aug 1968).

52. Arya V.K. and Holden H.D., 'Deconvolution of seismic data - an overview.' IEEE Transactions on Geoscience Electronics, GE-16(2), 95-98, (Apr 1978).

53. Stoffa P.L., Buhl P. and Bryan G.M., 'The application of homomorphic deconvolution to shallow water marine seismology - part I: Models.' Geophysics, 39(4), 401-416, (Aug 1974).

54. Stoffa P.L., Buhl P. and Bryan G.M., 'The application of homomorphic deconvolution to shallow water marine seismology - part II: Real data.' Geophysics, 39(4), 417-426, (Aug 1974).

55. Stoffa P.L., Buhl P. and Bryan G.M., 'Cepstrum aliasing and the calculation of the Hilbert transform.' Geophysics, 39(4), 543-544, (Aug 1974).

56. Otis R.M. and Smith R.B., 'Homomorphic deconvolution by log spectral averaging.' Geophysics, 42(6), 1146-1157, (Oct 1979).

57. Oppenheim A.V. and Schafer R.W., 'Digital signal processing.' Prentice Hall-Inc, Englewood Cliffs, New Jersey, (1975).

58. Leeman S., 'The impediography equations.' International Symposium on Acoustical Imaging, 8th, Miami, (1978).

59. Wright H.A., and Miles P.R., '"Acousticore" - a new concept in acoustic prospecting for minerals and preconstruction surveying.' Bolt, Beranek and Newman Inc, Cambridge, Massachusetts 02138, (Sep 1973).

60. Wright H.A., 'Impulse-response function corresponding to reflection from a region of continuous impedance change.' J.Acost.Soc.Am., 53(5), 1356-1359, (1973).

61. Hamilton E.L., Shumway G., Menard H.W. and Shipek C.J., 'Acoustic and other physical properties of shallow water sediments off San Diego.' J.Acoust.Soc.Am., 28(1), (1956).

62. Shumway G., 'Sound velocity versus temperature in water saturated sediments.' Geophysics, 23(3), (1958).

63. Algada Ltd., 68, Mousehole Lane, Bitterne Park, Southampton, SO2 4EZ.

64 Kossoff G., 'The effects of backing and matching on the performance piezolectric ceramic transducers.' IEEE Trans. Sonics Ultrasonics, SU-13, 20-30, (Mar 1966).

65. Goll J.H. and Auld B.A., 'Multilayer impedance matching for broadbanding of water loaded piezoelectric transducers and high Q electric resonators.' IEEE Trans. Sonics Ultrasonics, SU-22(1), 52-53, (Jan 1975).

66. Tucker and Gazey, 'Applied underwater acoustics.' Pergamon Press, (1966).

67. Berktay H.O., Private communication, (Sep 1980).

68. Brigham E.O., 'The fast Fourier transform.' Prentice-Hall Inc, Englewood Cliffs, New Jersey, (1974).

69. Papoulis A., 'The Fourier integral and it's applications.' McGraw-Hill, (1962).

70. Mendel J.M. and Habibi-Ashrafi F., 'A survey of approaches to solving inverse problems for lossless layered media systems.' IEEE Transactions on Geoscience and Remote Sensing, GE-18(4), (Oct 1980).

71 Urick R.J., 'Principles of Underwater Sound for Engineers.' McGraw-Hill, New York.

72 Officer C.B., 'Introduction to the theory of sound transmission.' McGraw-Hill, New York.

73 Robinson E.A., 'Predictive decomposition of time series with application to seismic exploration.' Geophysics, 32(3), 418-484, (June 1967).

74 Konrad W.L., 'Applications of the parametric acoustic source.' Proc. Conf. on "Underwater applications of non-linear acoustics", Univ of Bath, (Sept 1979).

75 Bryan G.M., 'The hydrophone-pinger experiment.' J.Acoust.Soc.Am., 68(5), 1403-1408, (Nov 1980).

76 Walsh G.M., 'Practical application of the finite amplitude technique to narrow beam depth measurement.' Brit.Acoust.Soc., Proc. Sym. on "Non-linear acoustics.', Univ. Birmingham, (April 1970).

74 Berktay H.O., Smith B.V., Braithwaite M. and Whitehouse M., 'Sub-bottom profilers using parametric sources.' Proc. Conf. on "Underwater applications of non-linear acoustics", Univ of Bath, (Sept 1979).

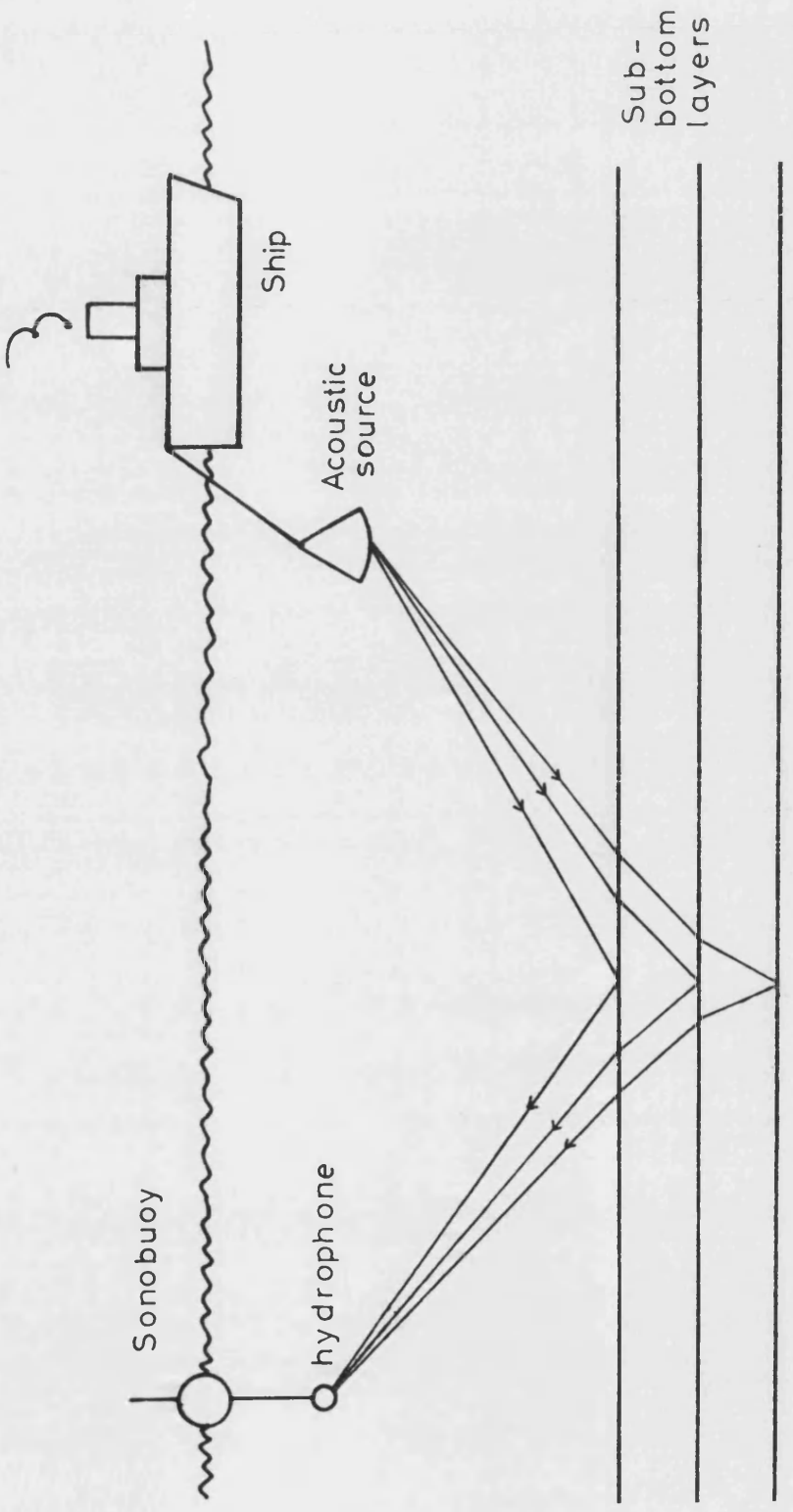

COLLECTION OF ACOUSTIC
DATA USING SONOBUOYS

Figure 2.4.1

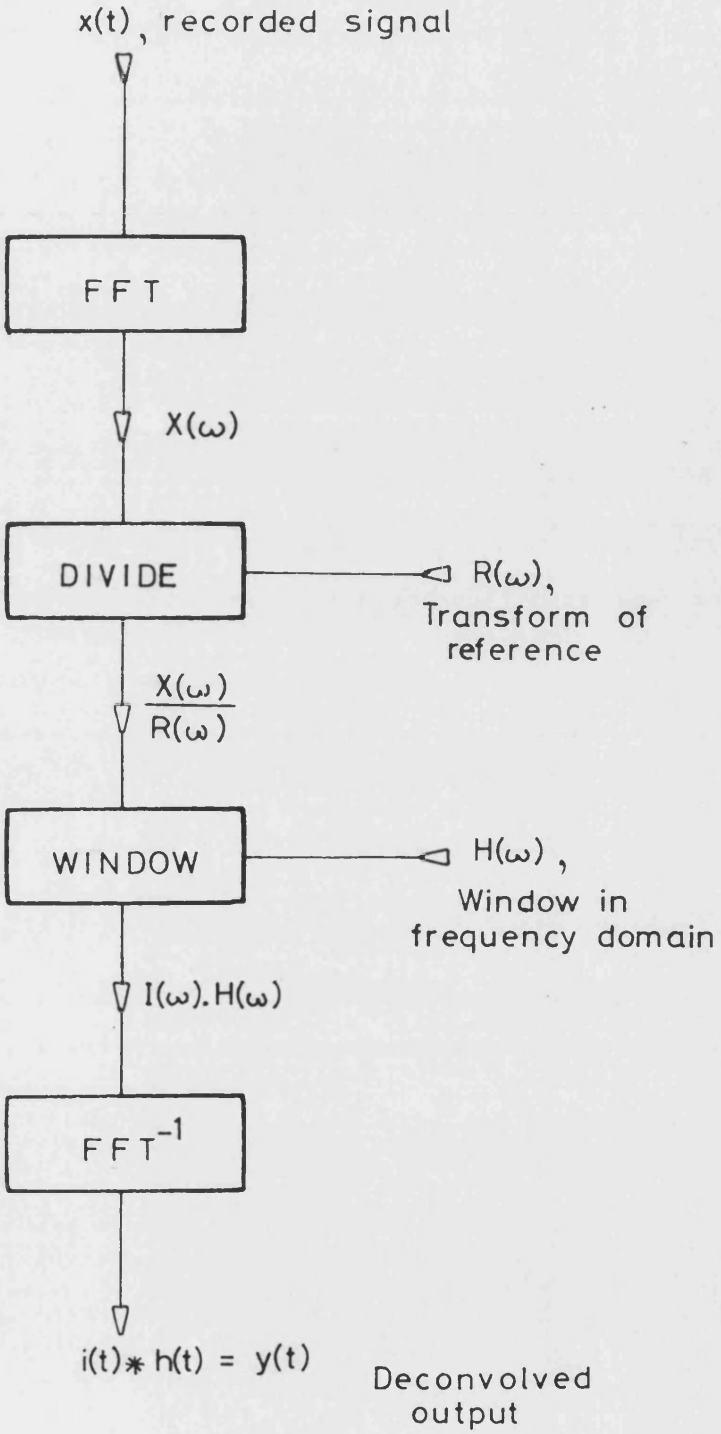

SCHEMATIC BLOCK DIAGRAM
OF DECONVOLUTION PROCESS

Figure 3.2.1

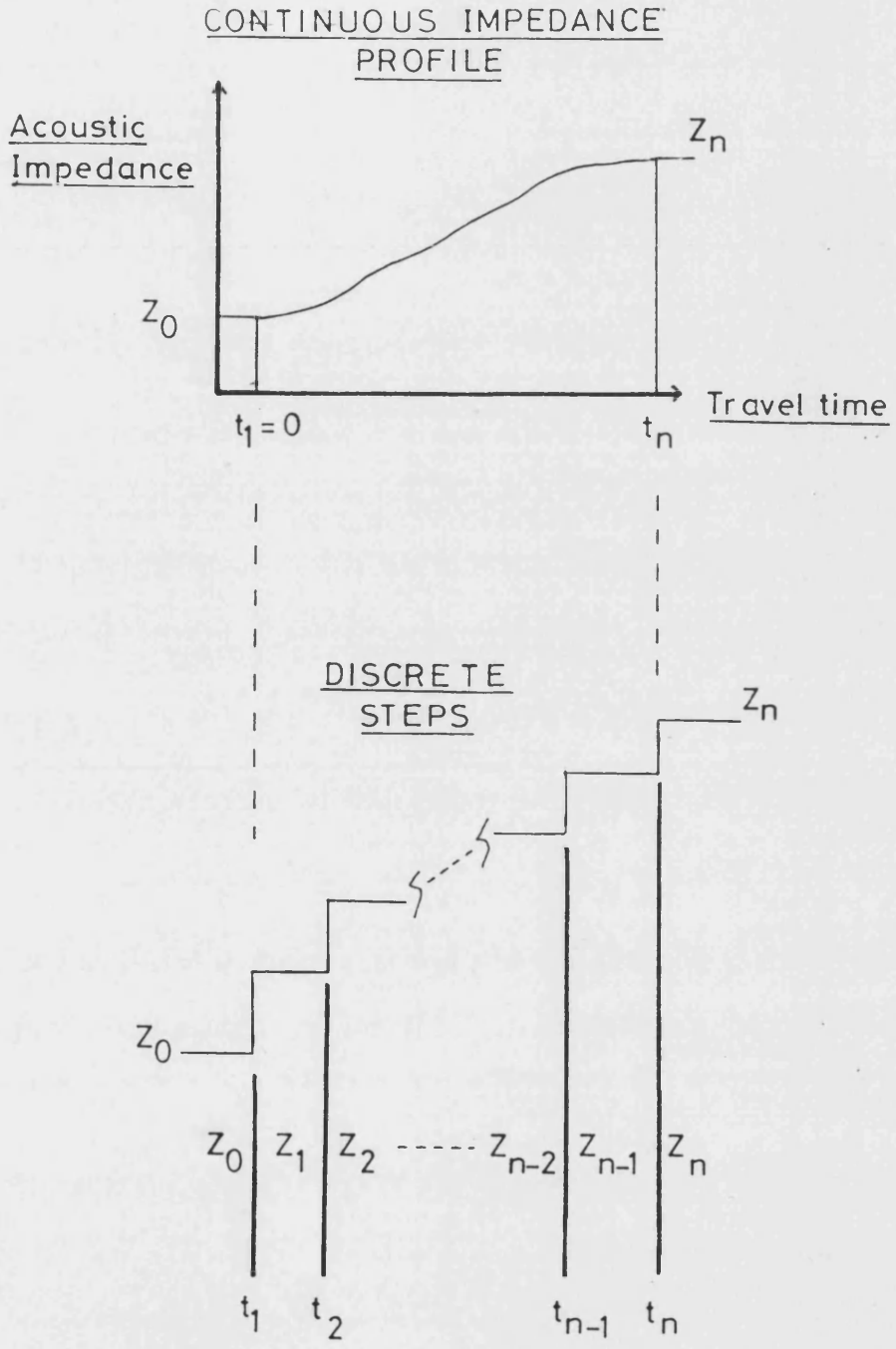

ACOUSTICORE MODEL

Figure 3.3.1

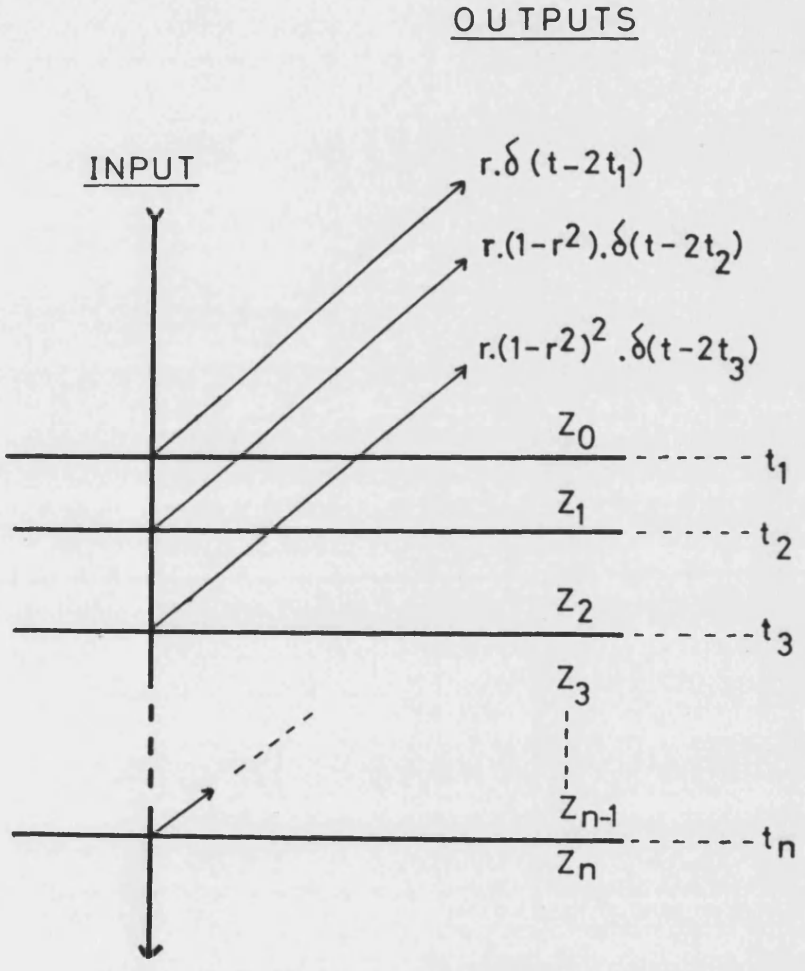

NOTE
Outputs are shown displaced from the horizontal for clarity

SINGLY REFLECTED OUTPUTS FROM ACOUSTICORE MODEL

Figure 3.3.2

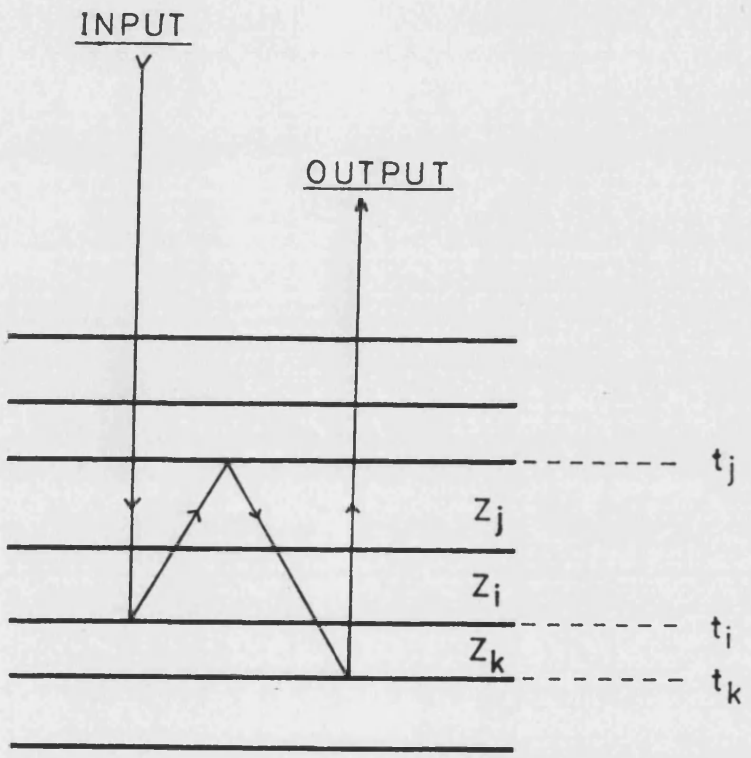

Triple reflection from layers i,j and k

[ray path displaced from vertical for clarity only]

TRIPLY REFLECTED OUTPUTS FROM ACOUSTIÇORE MODEL

Figure 3.3.3

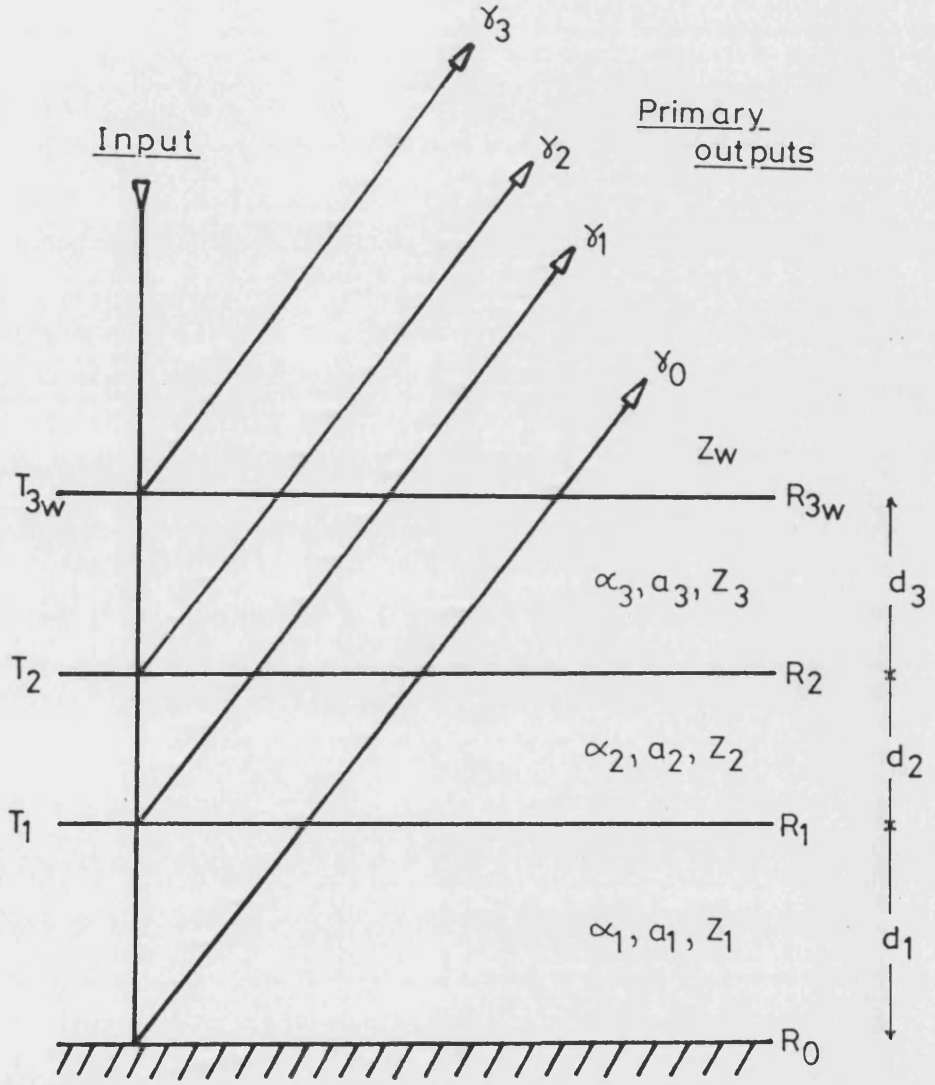

DEFINITION OF NOTATION

Figure 3.4.1

DYNAMIC RANGE LIMIT

Figure 3.4.2

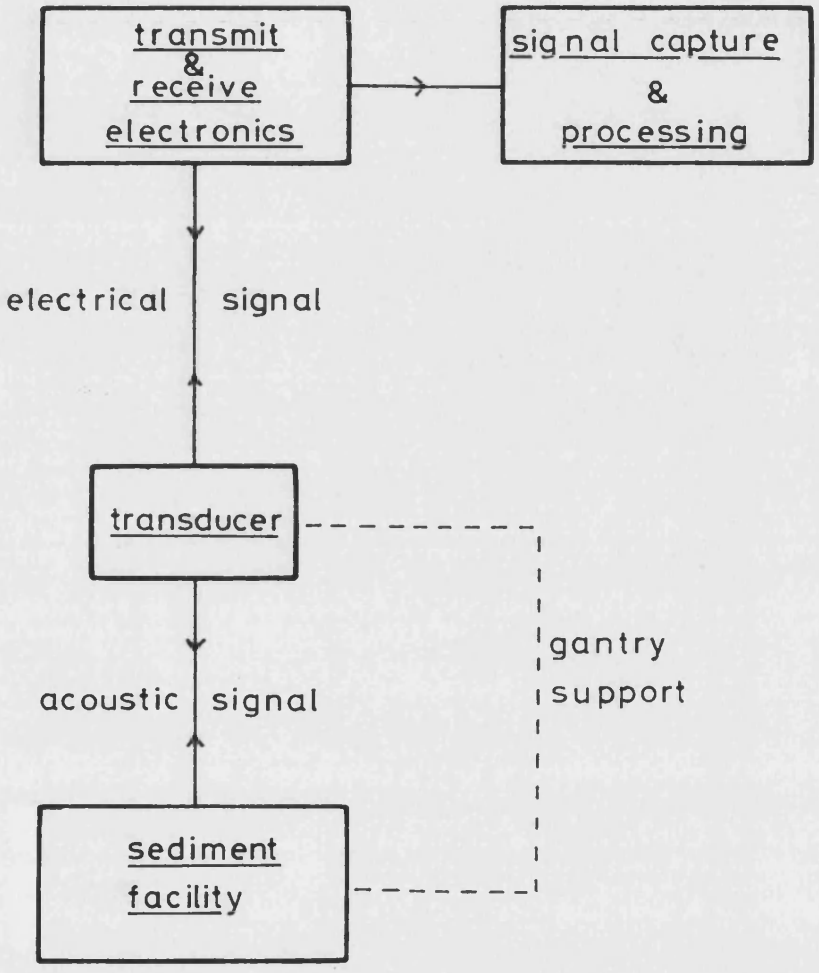

SCHEMATIC BLOCK DIAGRAM OF THE EQUIPMENT

Figure 4.1.1

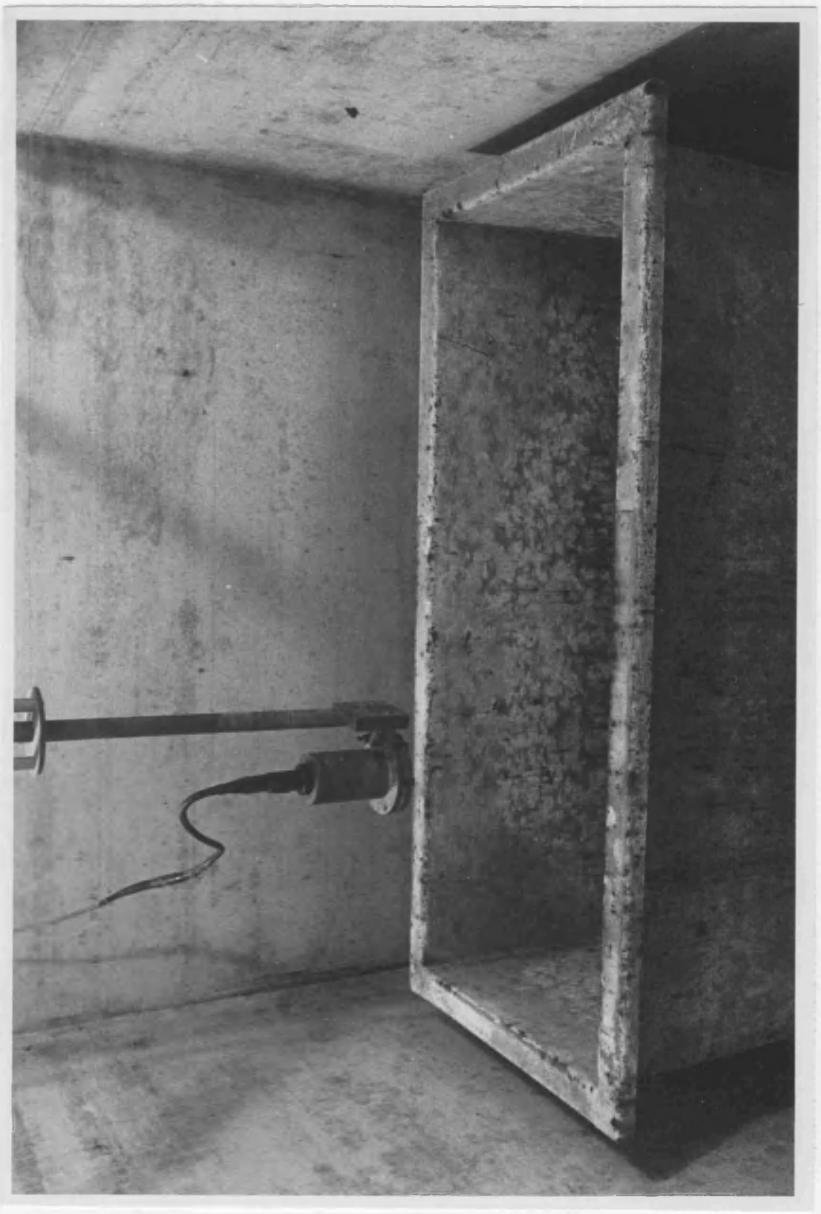

SMALL TANK INSIDE LARGE TANK

Figure 4.2.1

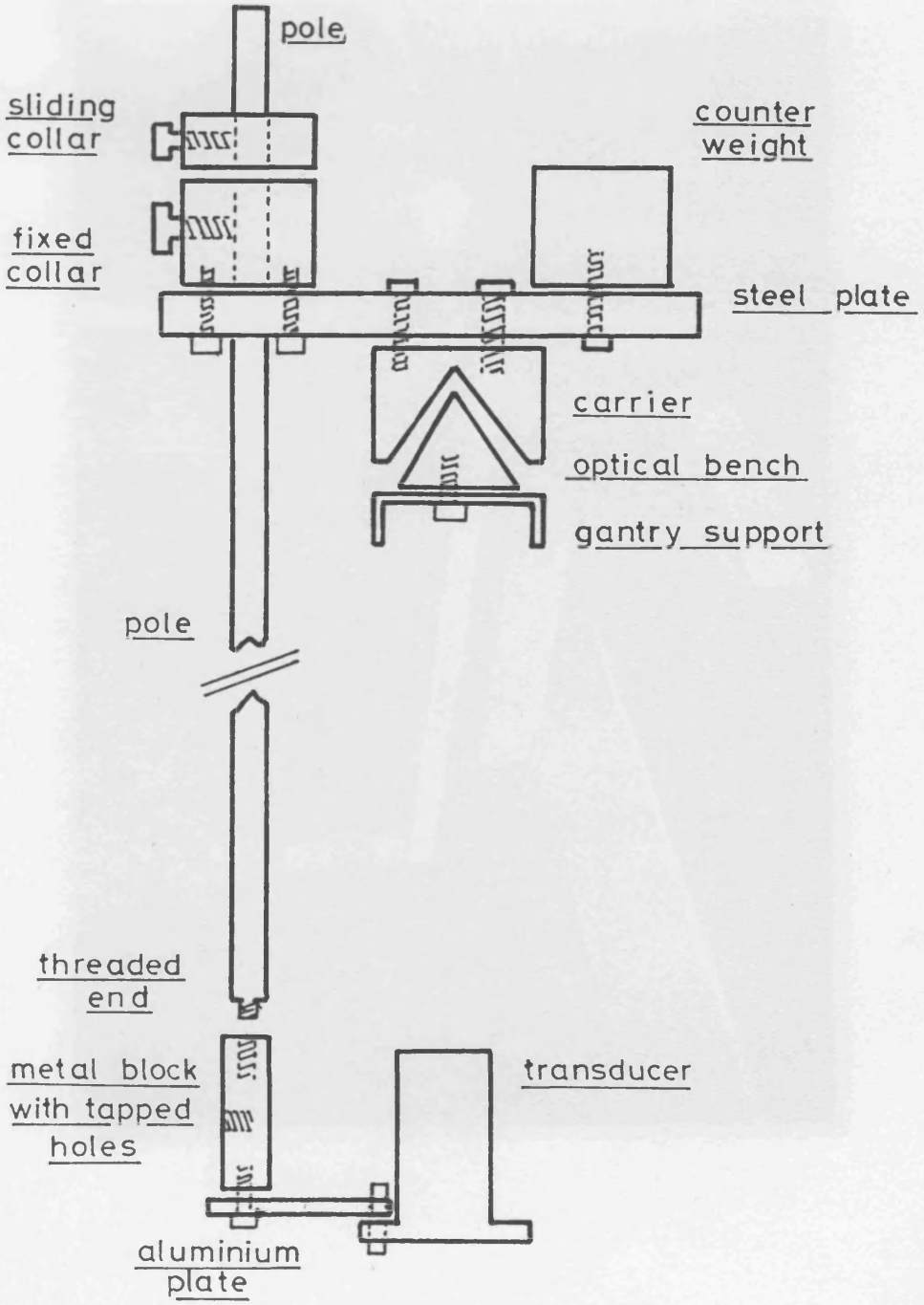

TRANSDUCER SUPPORT ASSEMBLY

Figure 4.2.2

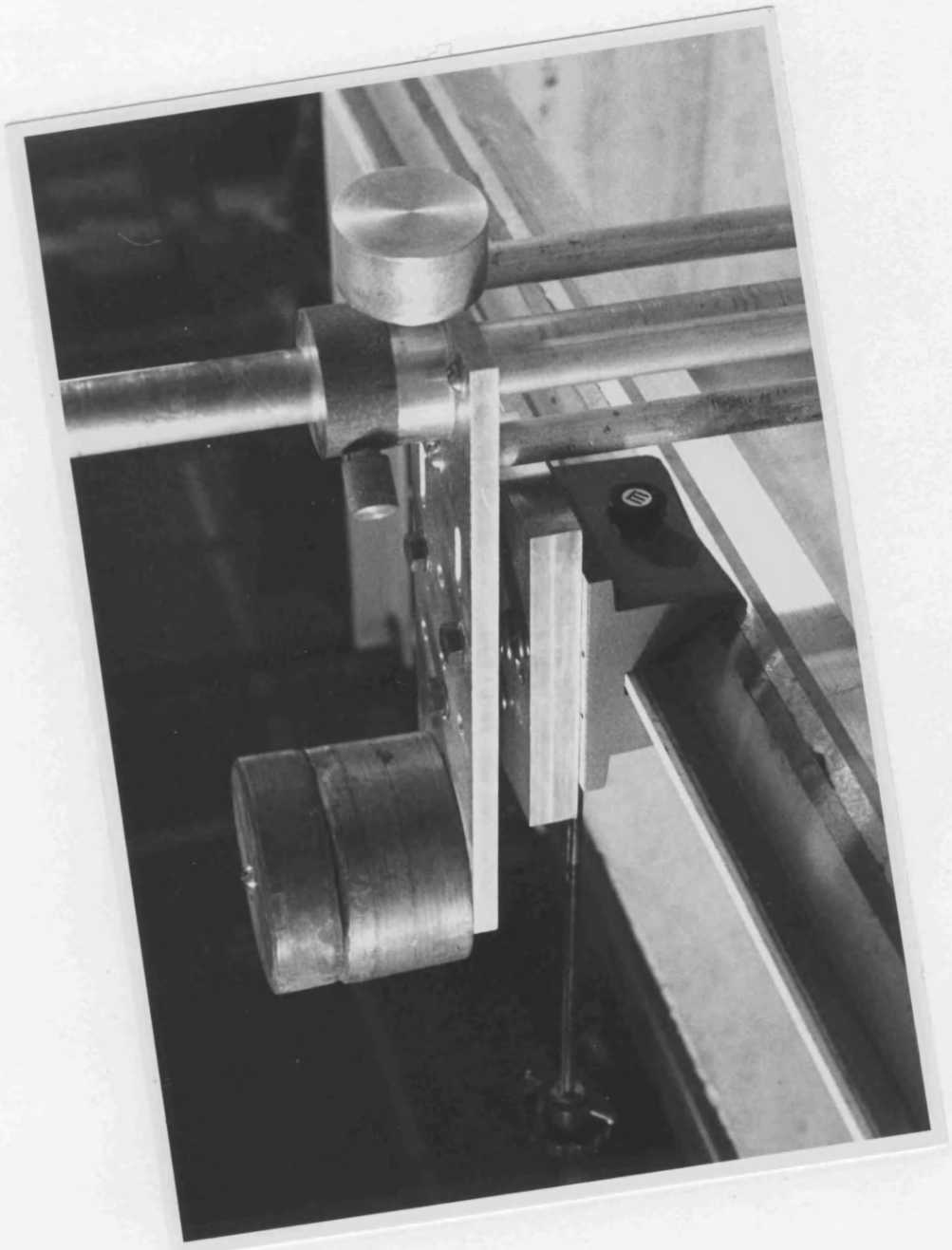

CLOSE UP OF GANTRY SYSTEM Figure 4.2.3

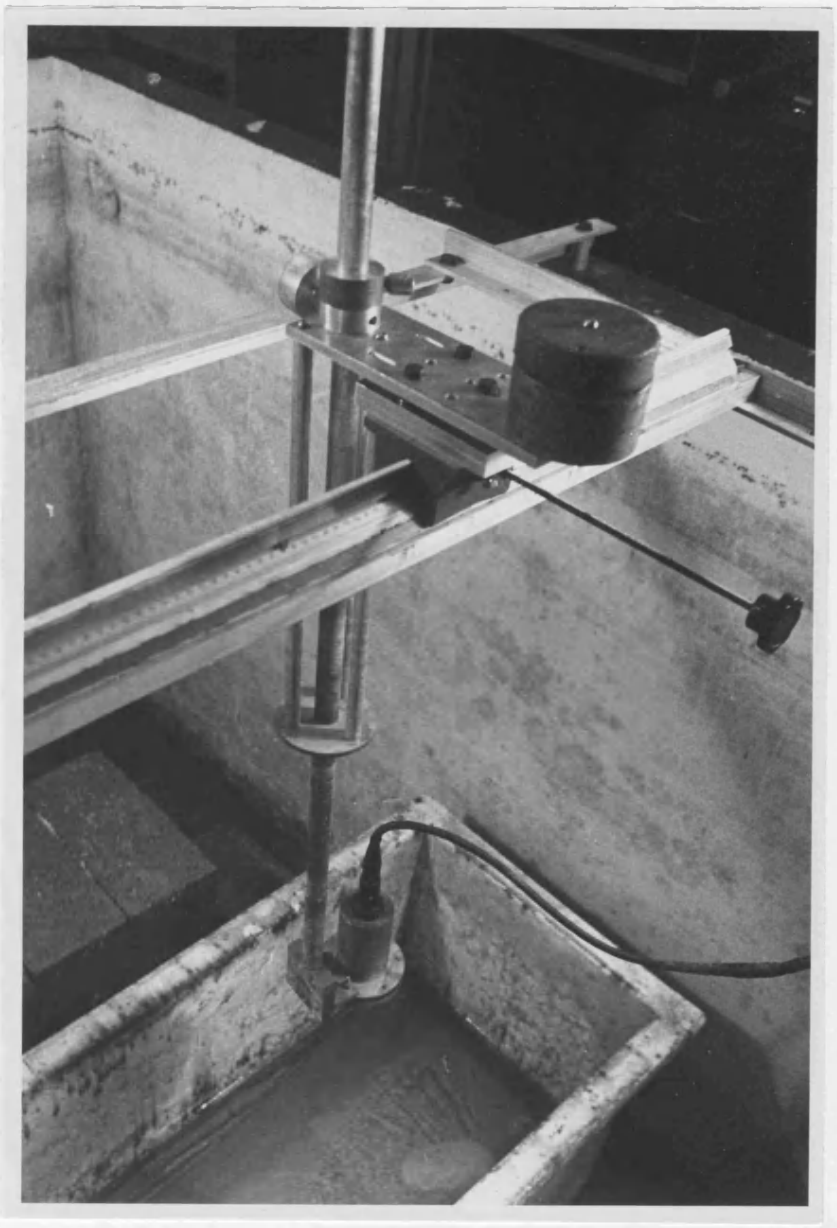

GANTRY SYSTEM
RELATIVE TO THE TANKS

Figure 4.2.4

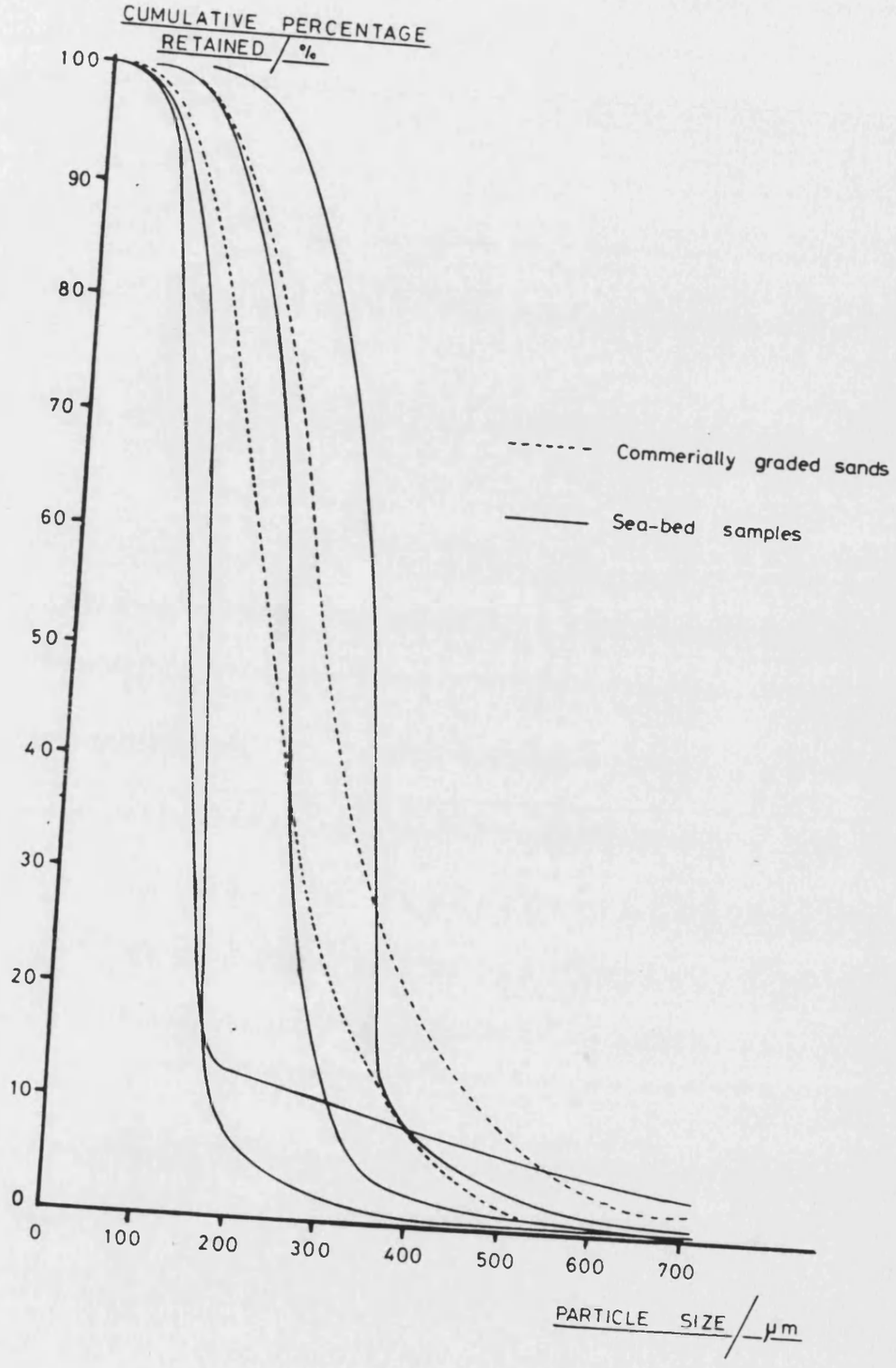

SEIVE ANALYSIS RESULTS

Figure 4.2.5

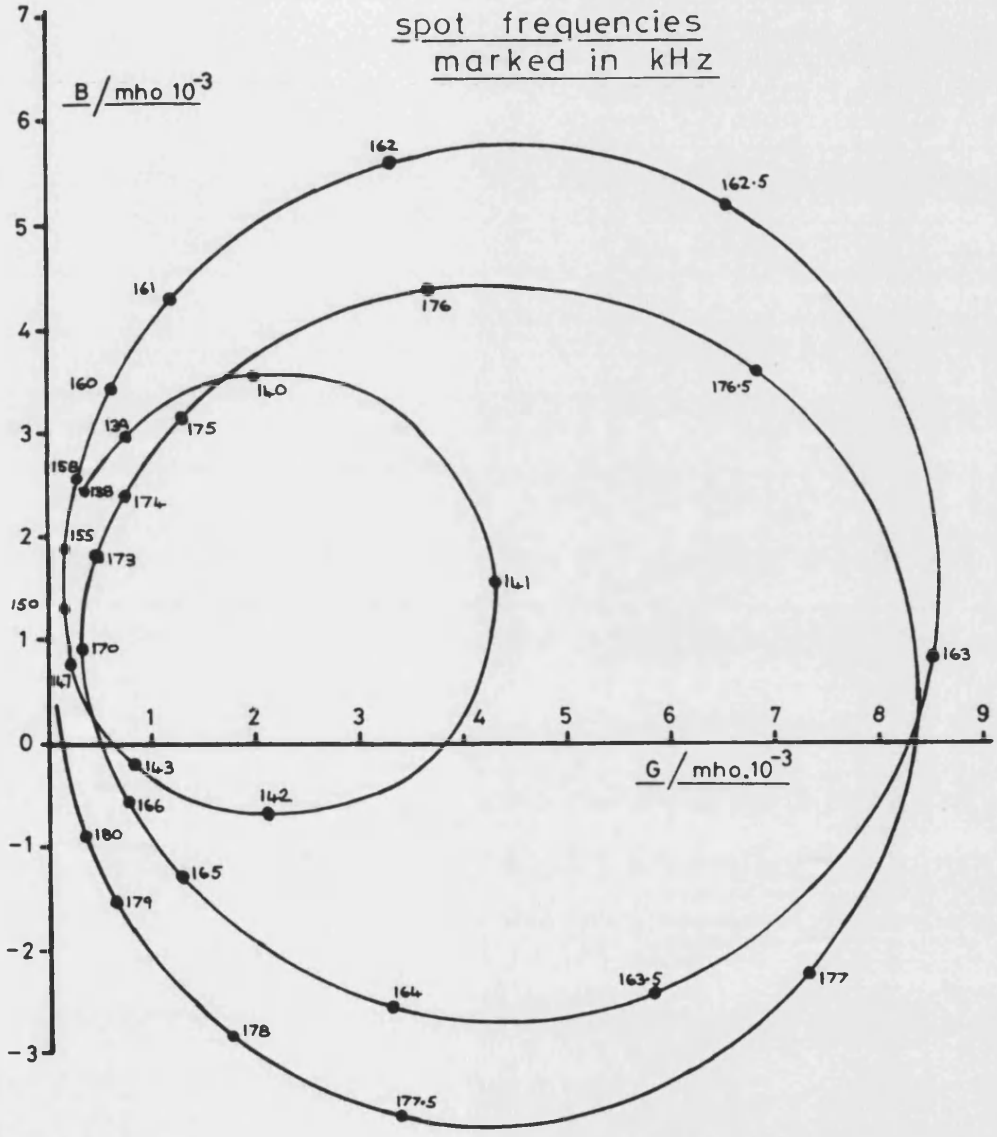

CIRCLE DIAGRAM OF
CERAMIC IN AIR

Figure 4.3.1

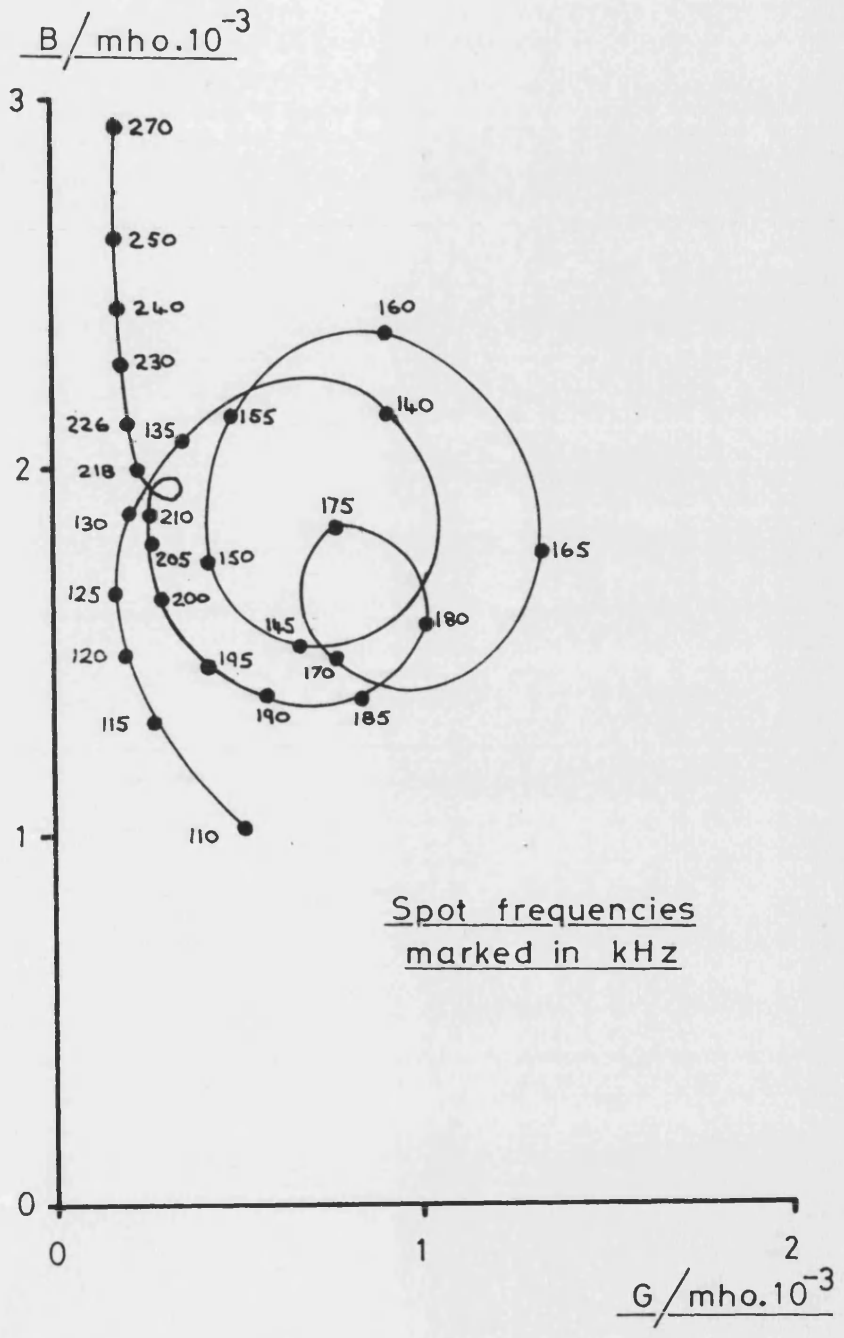

CIRCLE DIAGRAM OF COMPLETE TRANSDUCER IN WATER

Figure 4.3.2

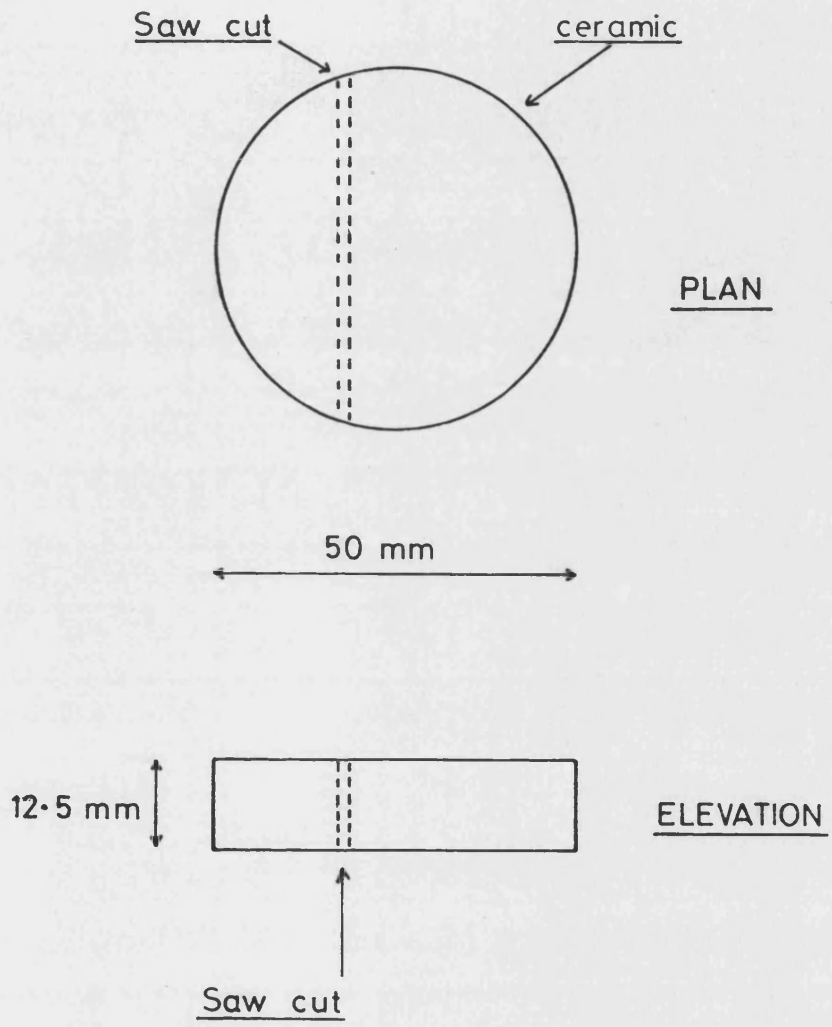

POSITION OF SAW CUT
IN CERAMIC

Figure 4.3.3

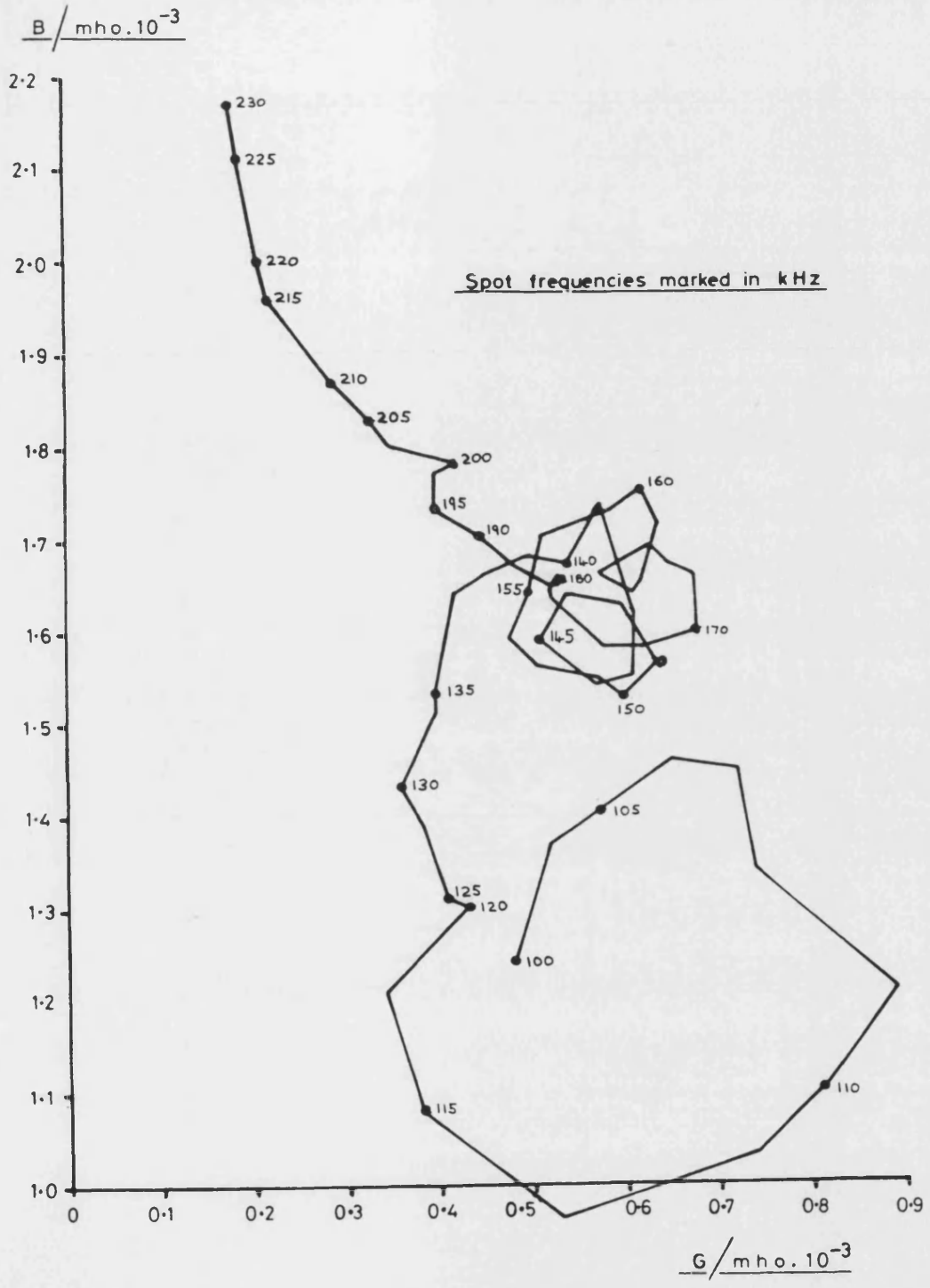

CIRCLE DIAGRAM OF TRANSDUCER WITH SAWN CERAMIC IN WATER

Figure 4.3.4

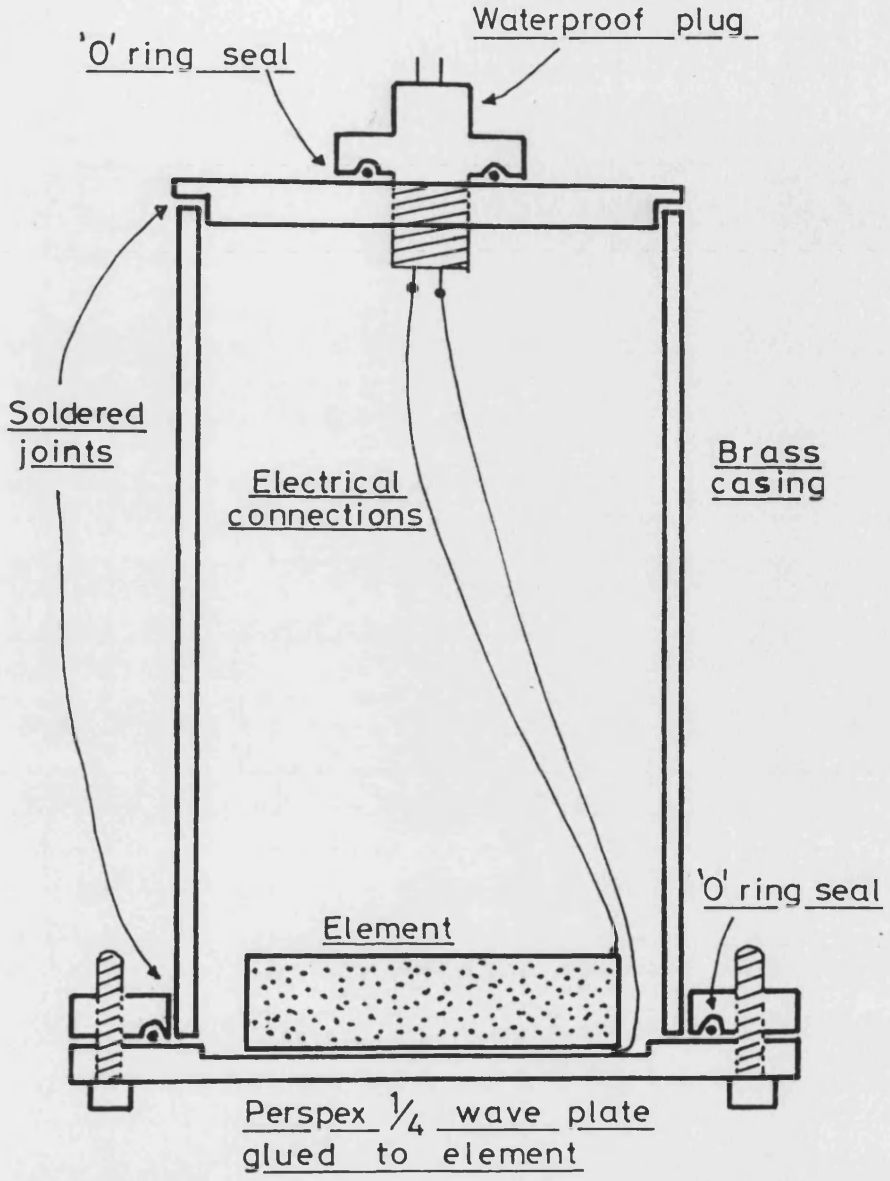

TRANSDUCER CONSTRUCTION

Figure 4.3.5

TRANSDUCER - SIDE VIEW

Figure 4.3.6

TRANSDUCER – FRONT VIEW

Figure 4.3.7

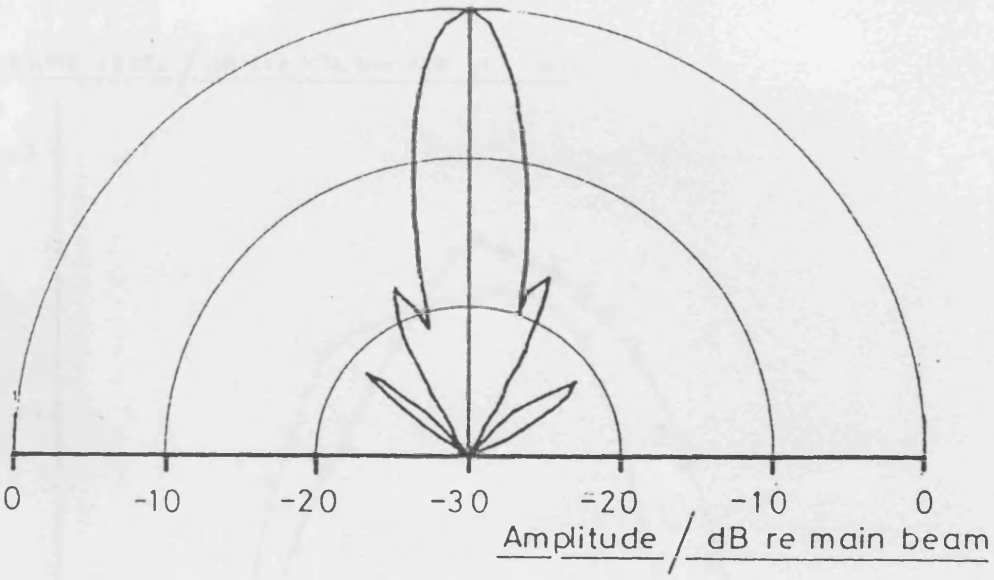

VERTICAL SECTION

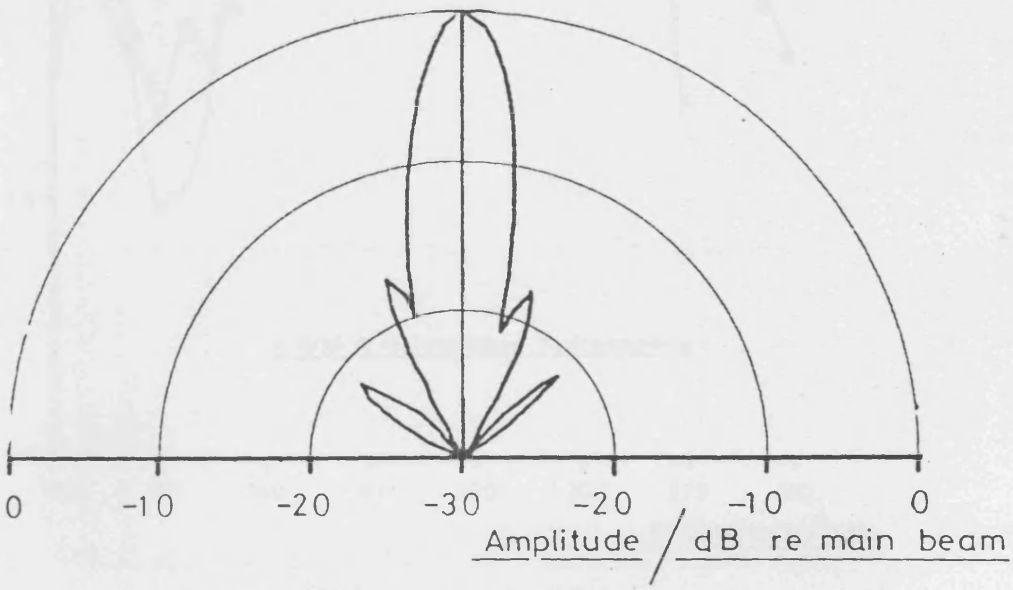

HORIZONTAL SECTION

BEAM PLOT OF TRANSDUCER

Figure 4.3.8

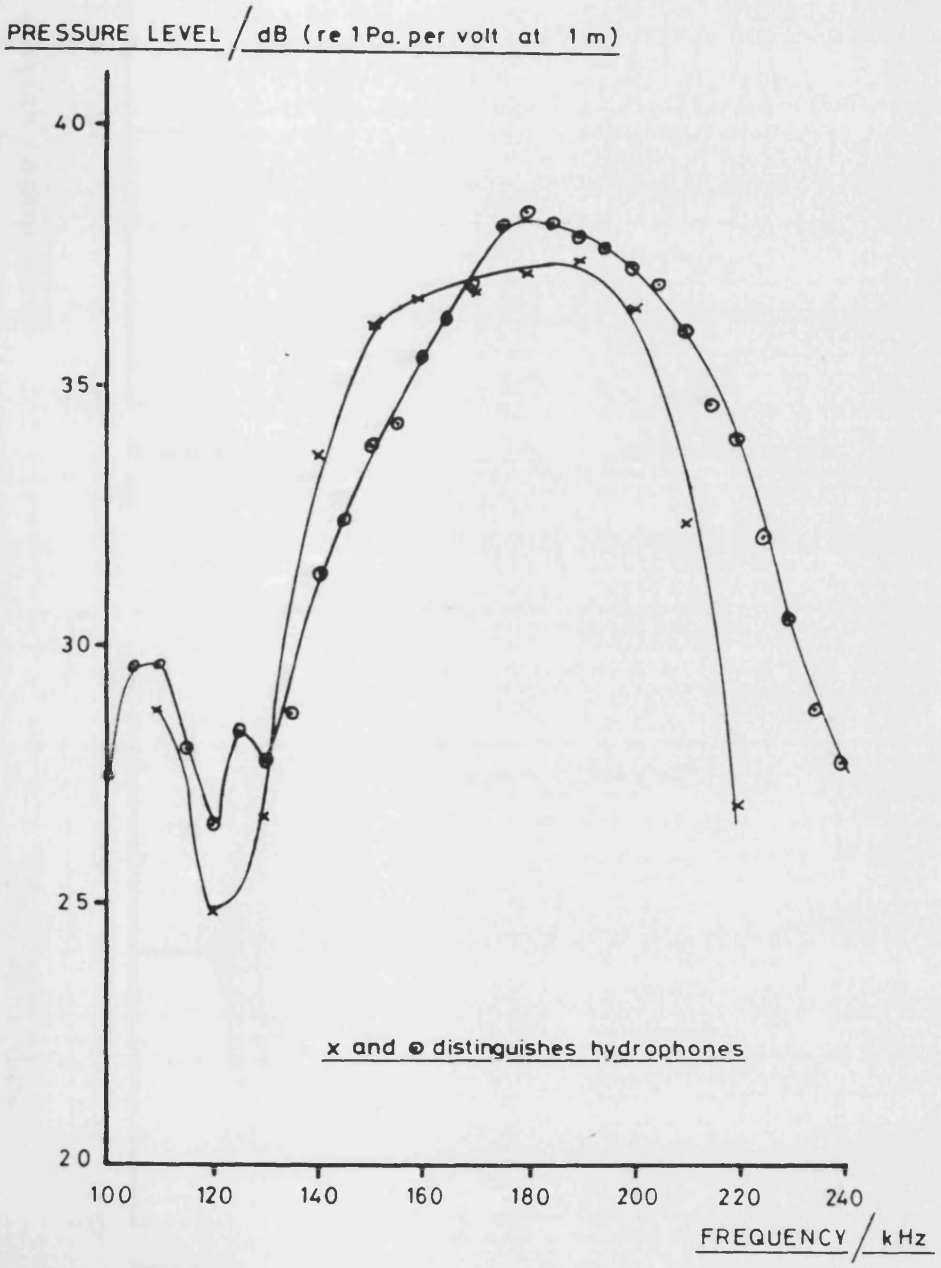

ON – AXIS SOUND PRESSURE LEVEL VERSUS FREQUENCY

Figure 4.3.9

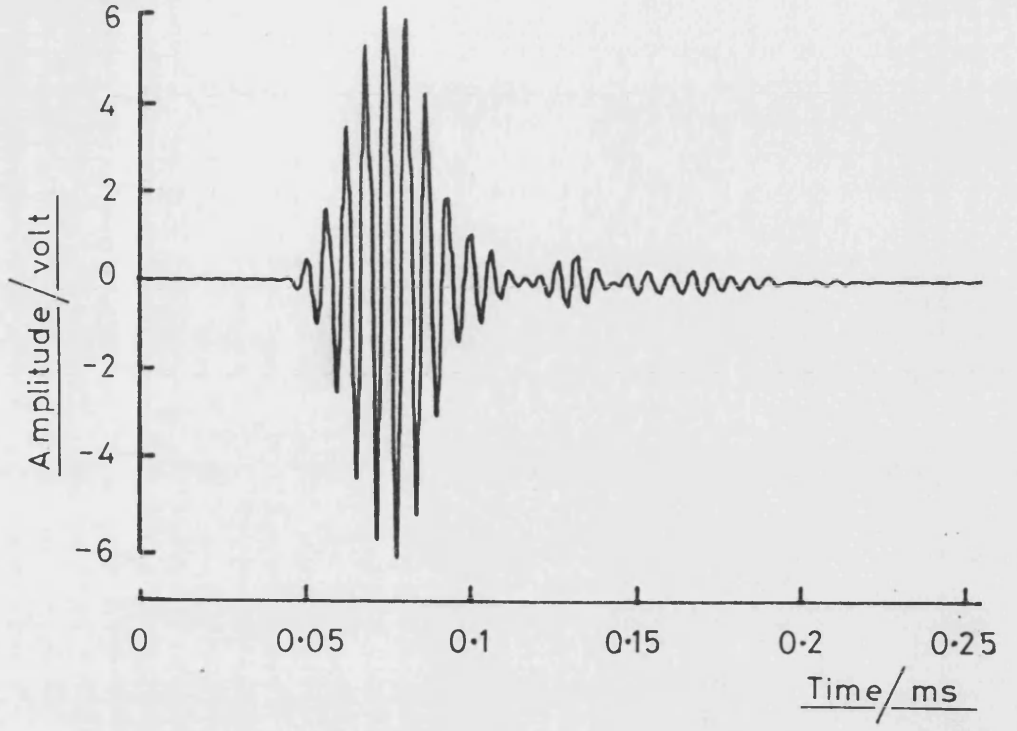

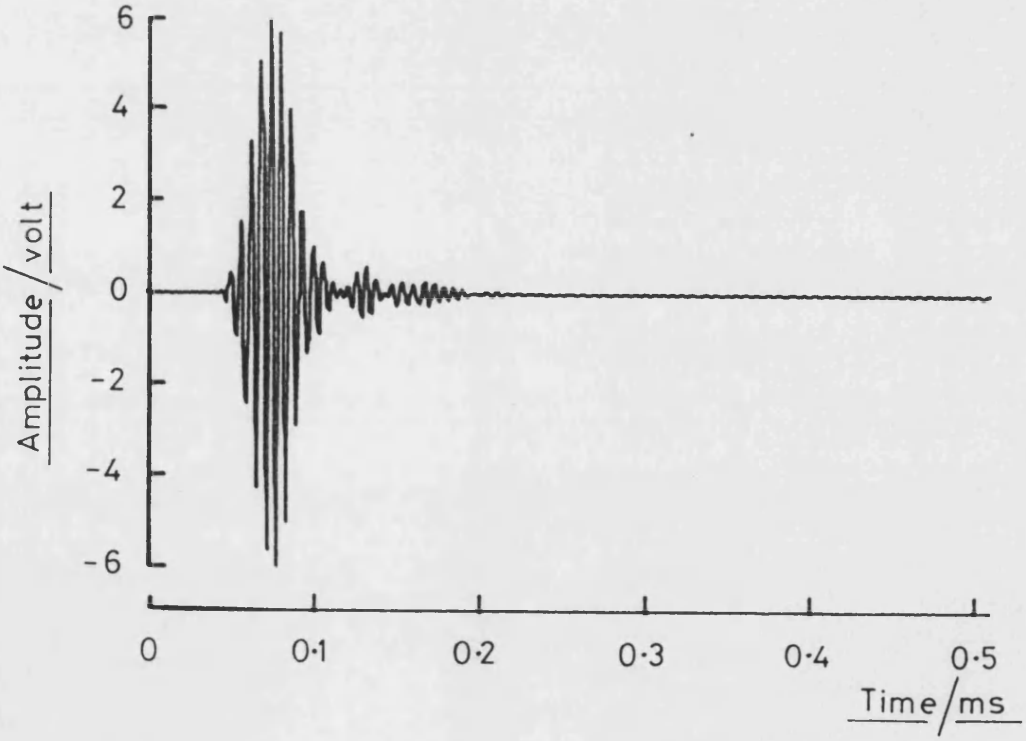

(two different time scales)

THE REFERENCE PULSE

Figure 4.3.10

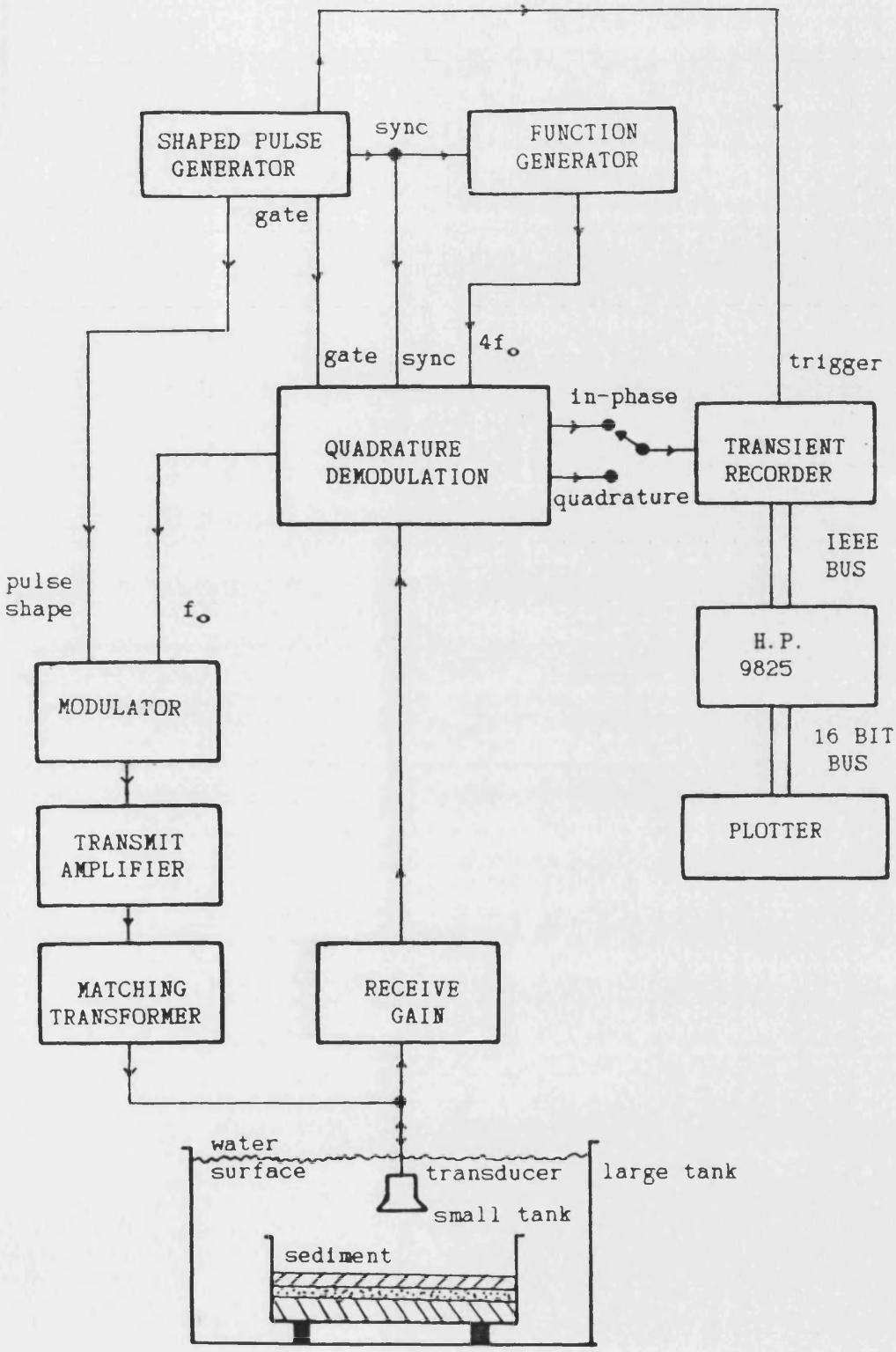

SYSTEM BLOCK DIAGRAM

Figure 4.4.1

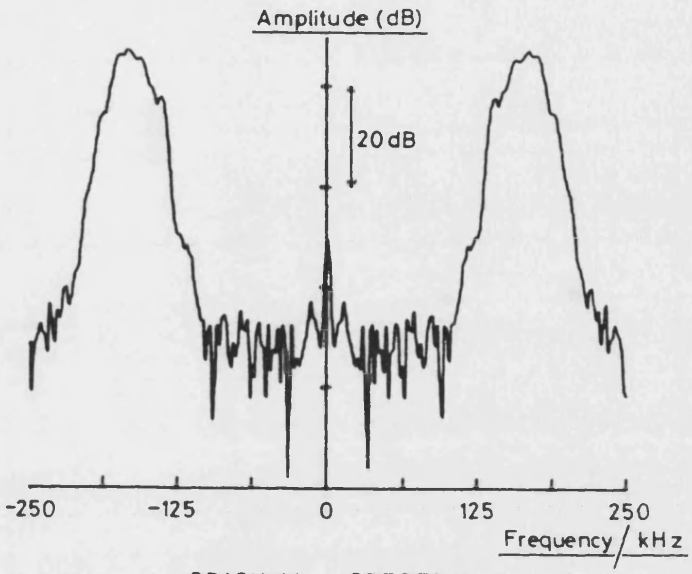

ORIGINAL SPECTRUM
(artificially re-constructed)

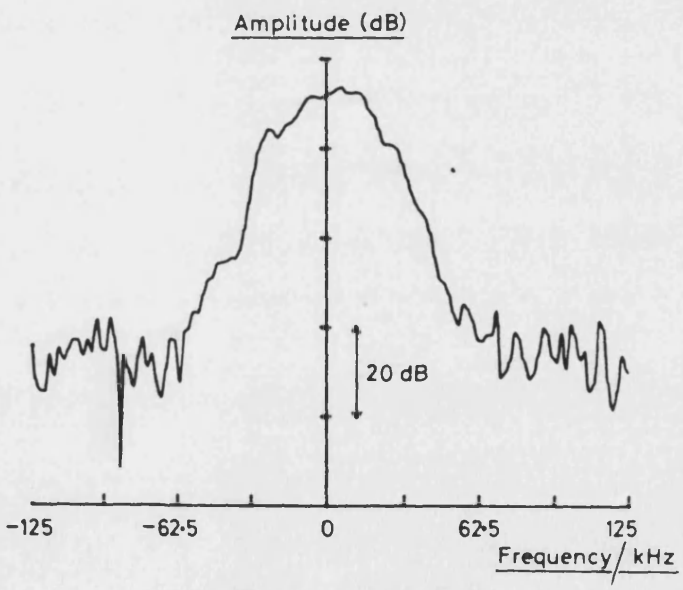

BASEBAND SPECTRUM

AMPLITUDE SPECTRUM OF BASEBAND AND ORIGINAL REFERENCE

Figure 4.4.2

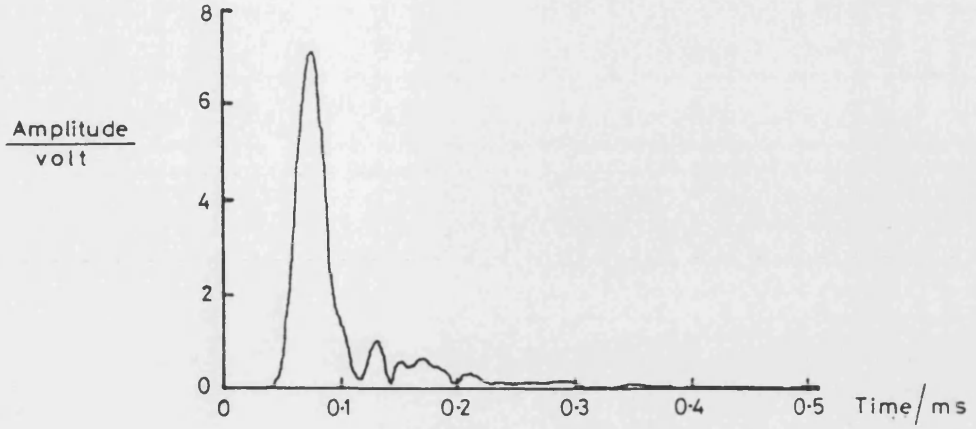

AMPLITUDE OF REFERENCE PULSE

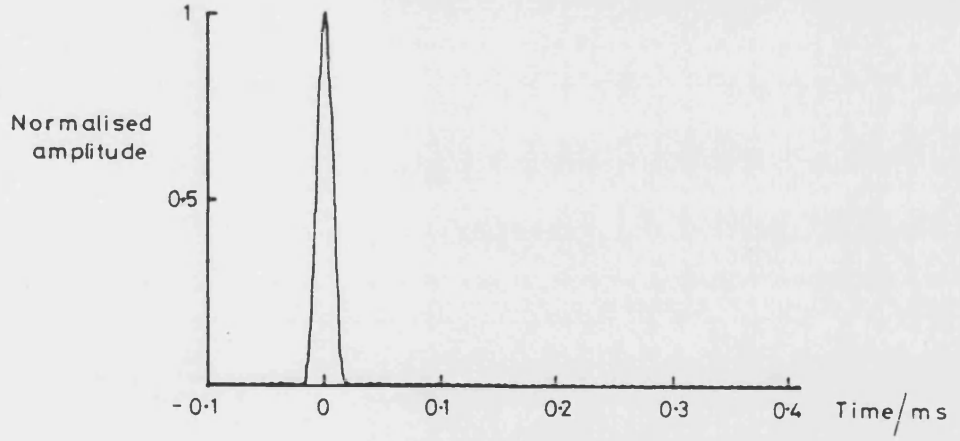

TRANSFORM OF HAMMING WINDOW
(Width = 44 kHz to -3dB pts)

COMPARISON OF REFERENCE PULSE WITH TRANSFORM OF WINDOW

Figure 4.5.1

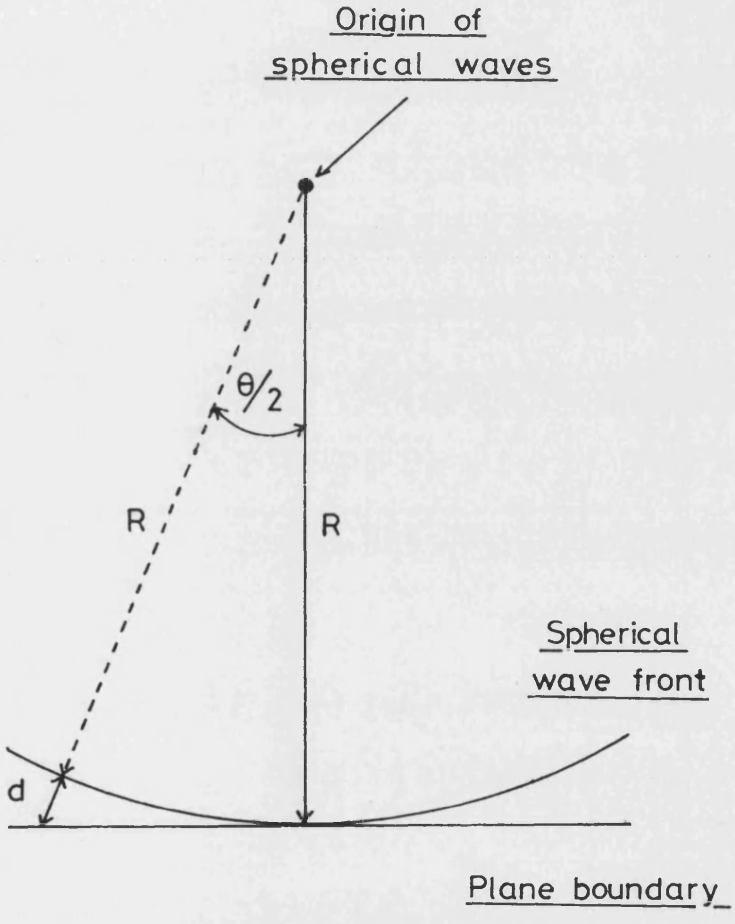

TIME RESOLUTION LIMIT
WITH SPHERICAL-WAVES

Figure 4.5.2

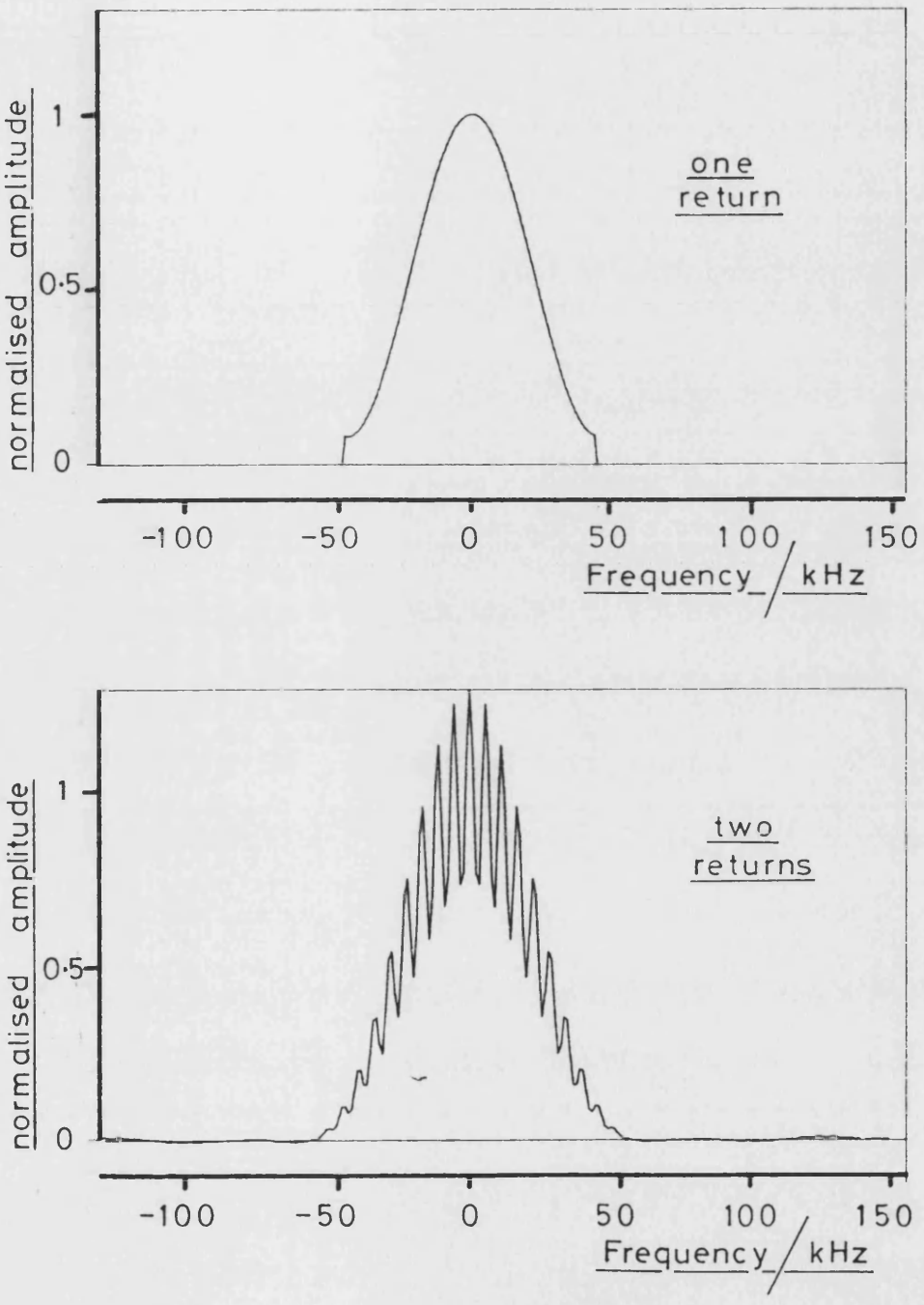

TRANSFORMS OF ONE RETURN
AND TWO RETURNS

Figure 4.5.3

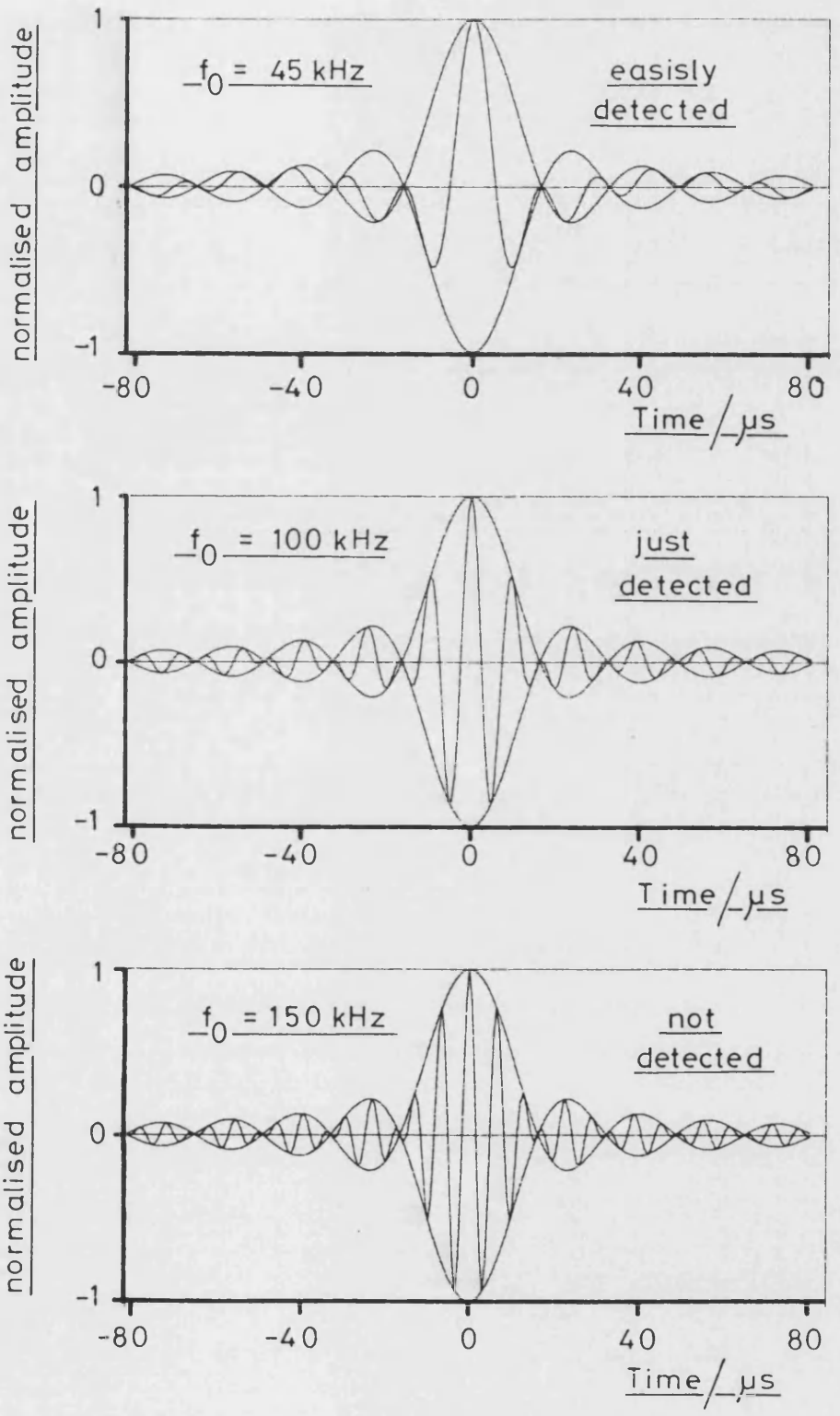

INVERSION DETECTION WITH
30 kHz RECTANGULAR WINDOW

Figure 4.5.4

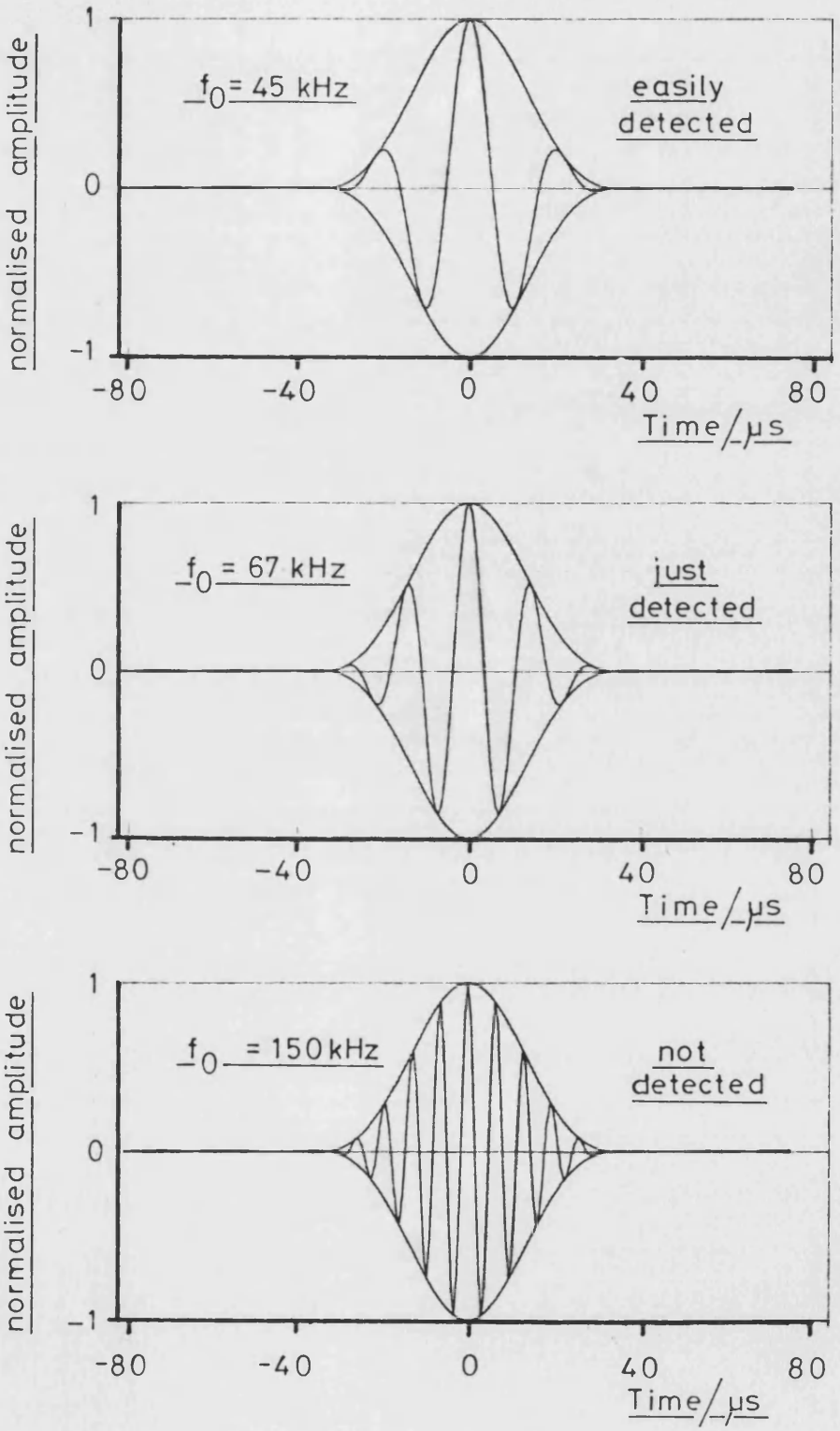

INVERSION DETECTION WITH
30 kHz HAMMING WINDOW

Figure 4.5.5

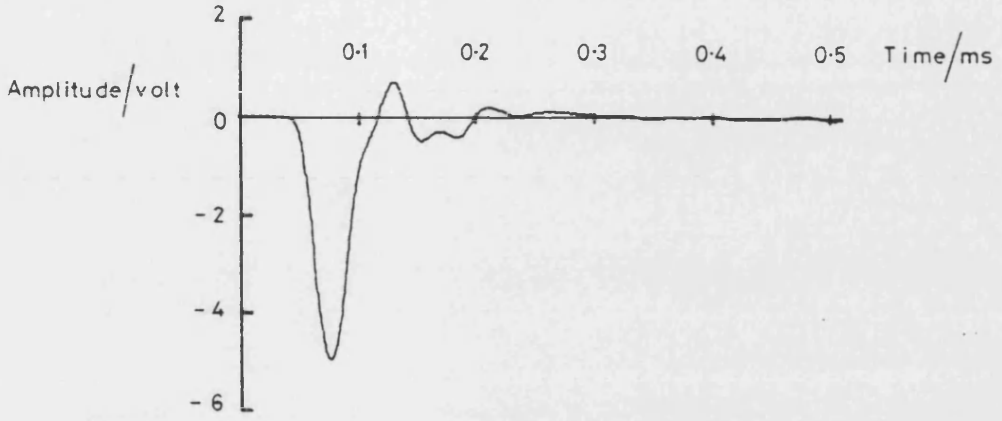

IN-PHASE COMPONENT

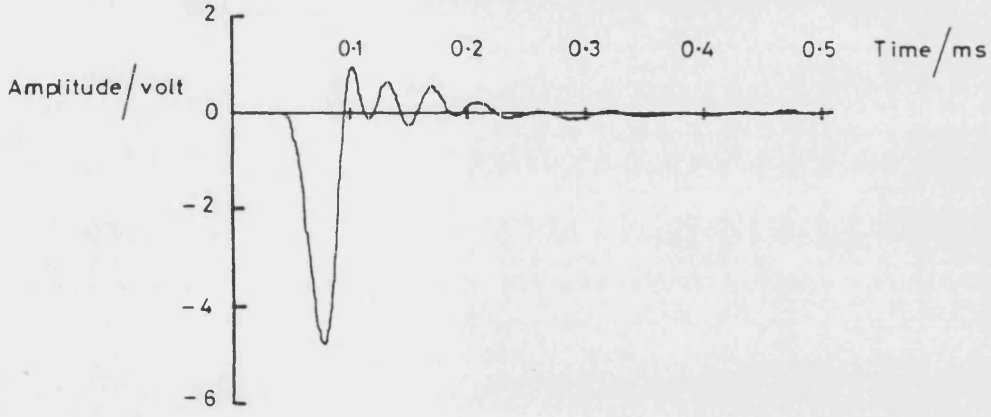

QUADRATURE COMPONENT

DEMODULATED COMPONENTS
OF REFERENCE PULSE

Figure 5.1.1

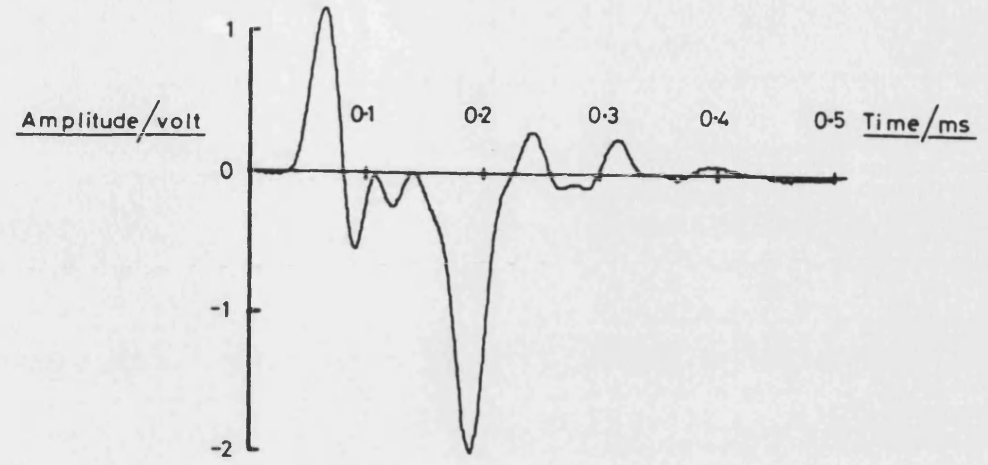

IN-PHASE COMPONENT

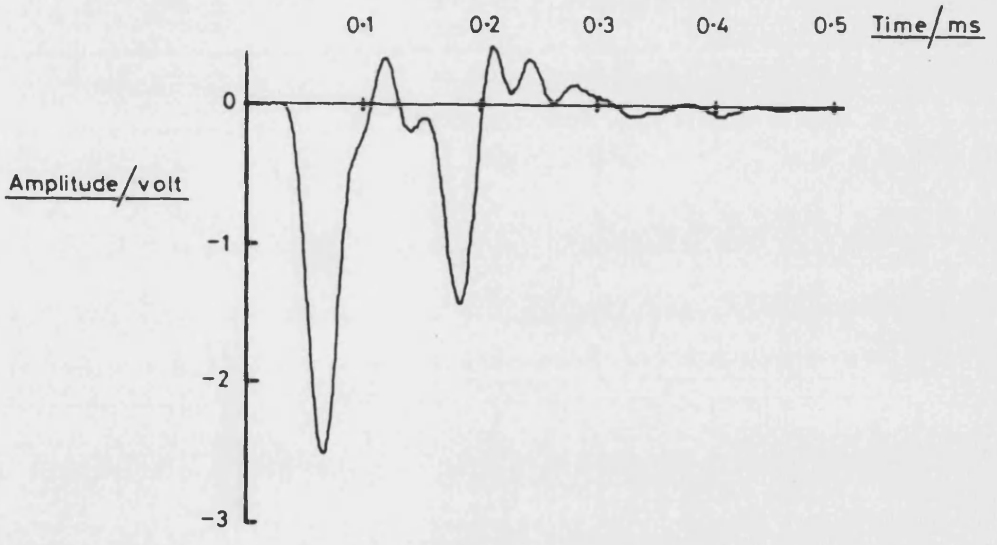

QUADRATURE COMPONENT

DEMODULATED COMPONENTS OF SIGNAL FROM SAND LAYER

Figure 5.1.2

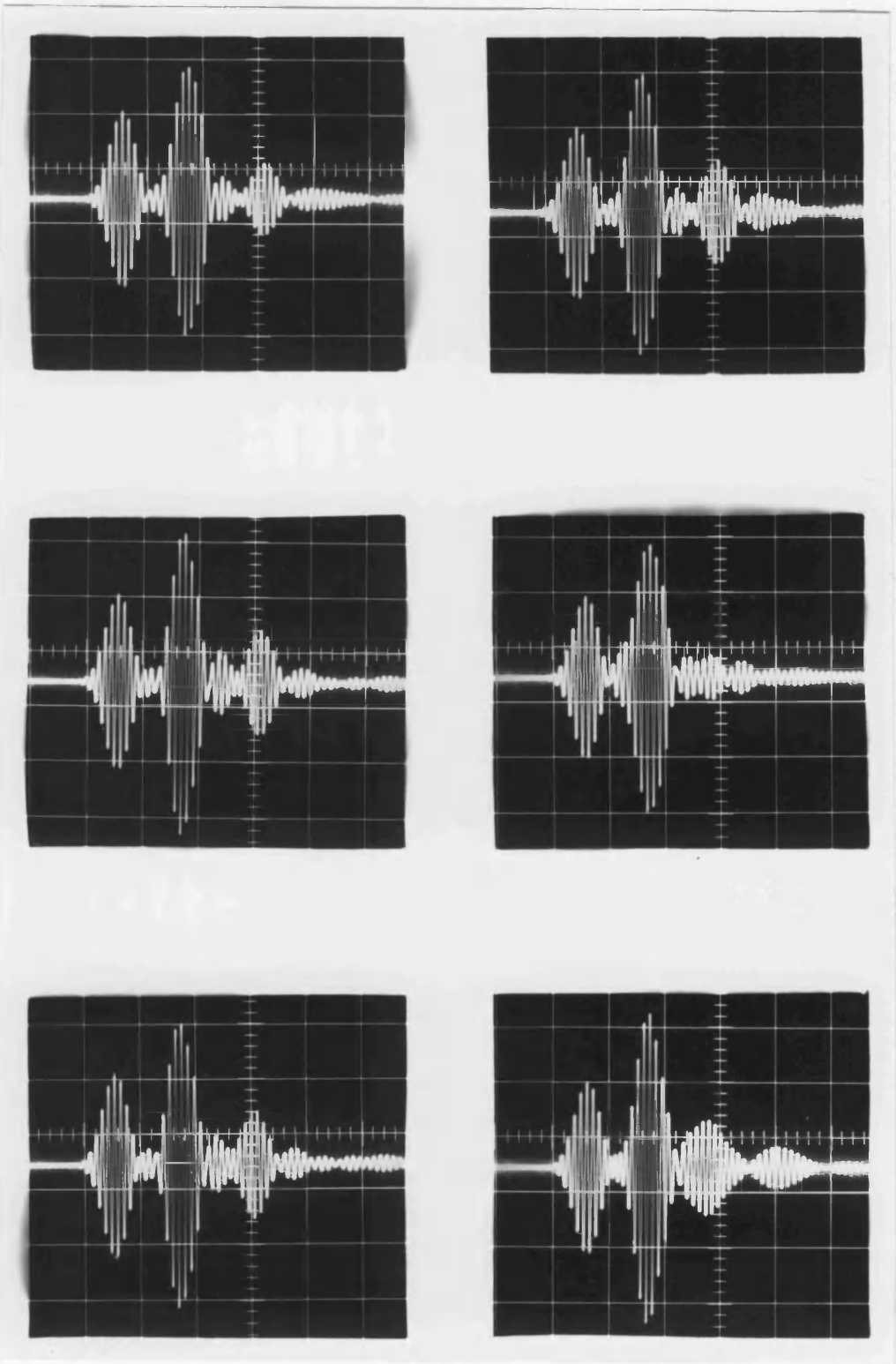

50 μs per division

RETURNED ECHOES FROM
5 cm SAND LAYER

Figure 5.2.1

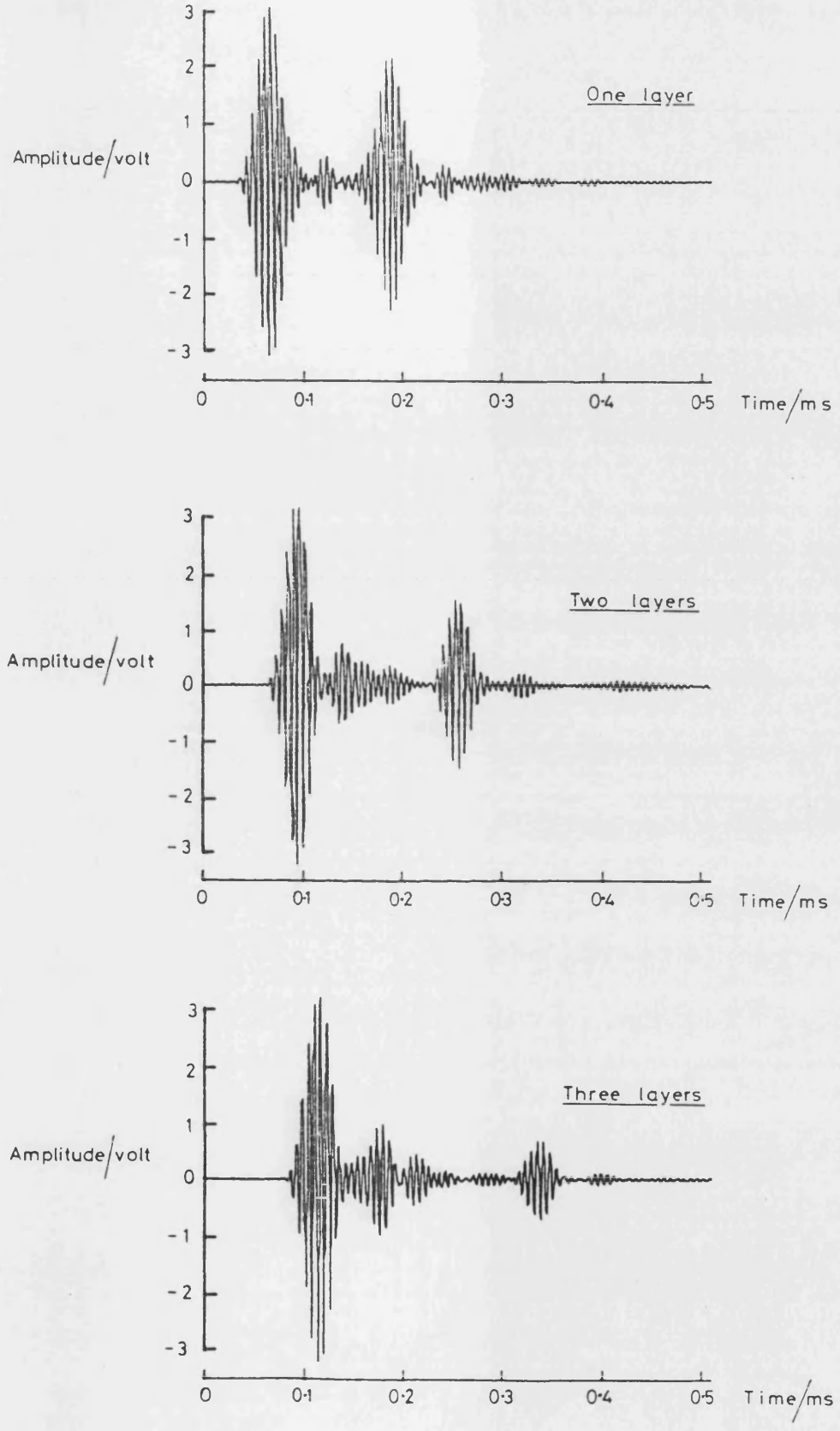

REFLECTED SIGNALS

Figure 5.2.2

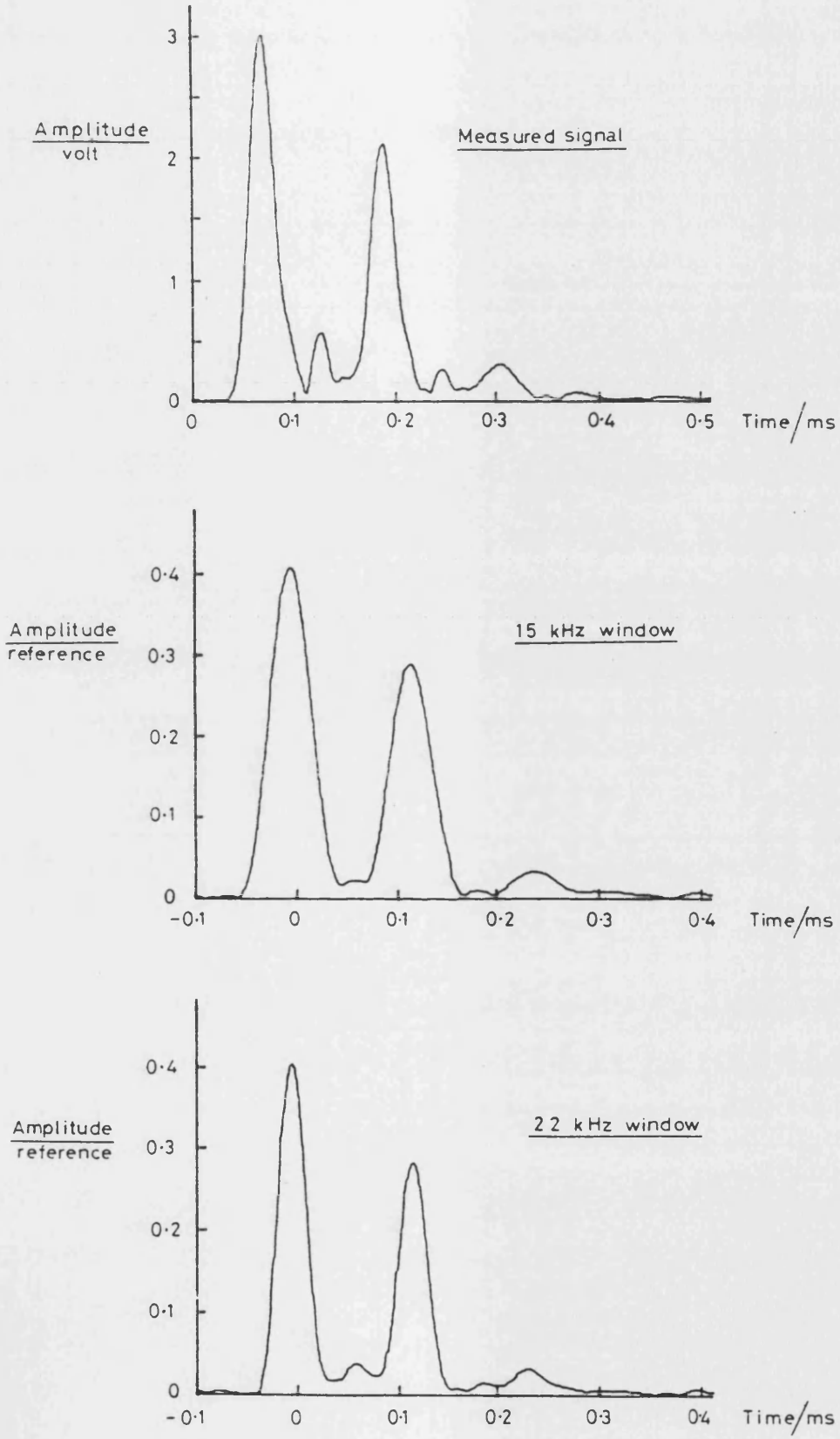

ONE LAYER DECONVOLUTIONS

(part 1 of 2)

Figure 5.3.1(a)

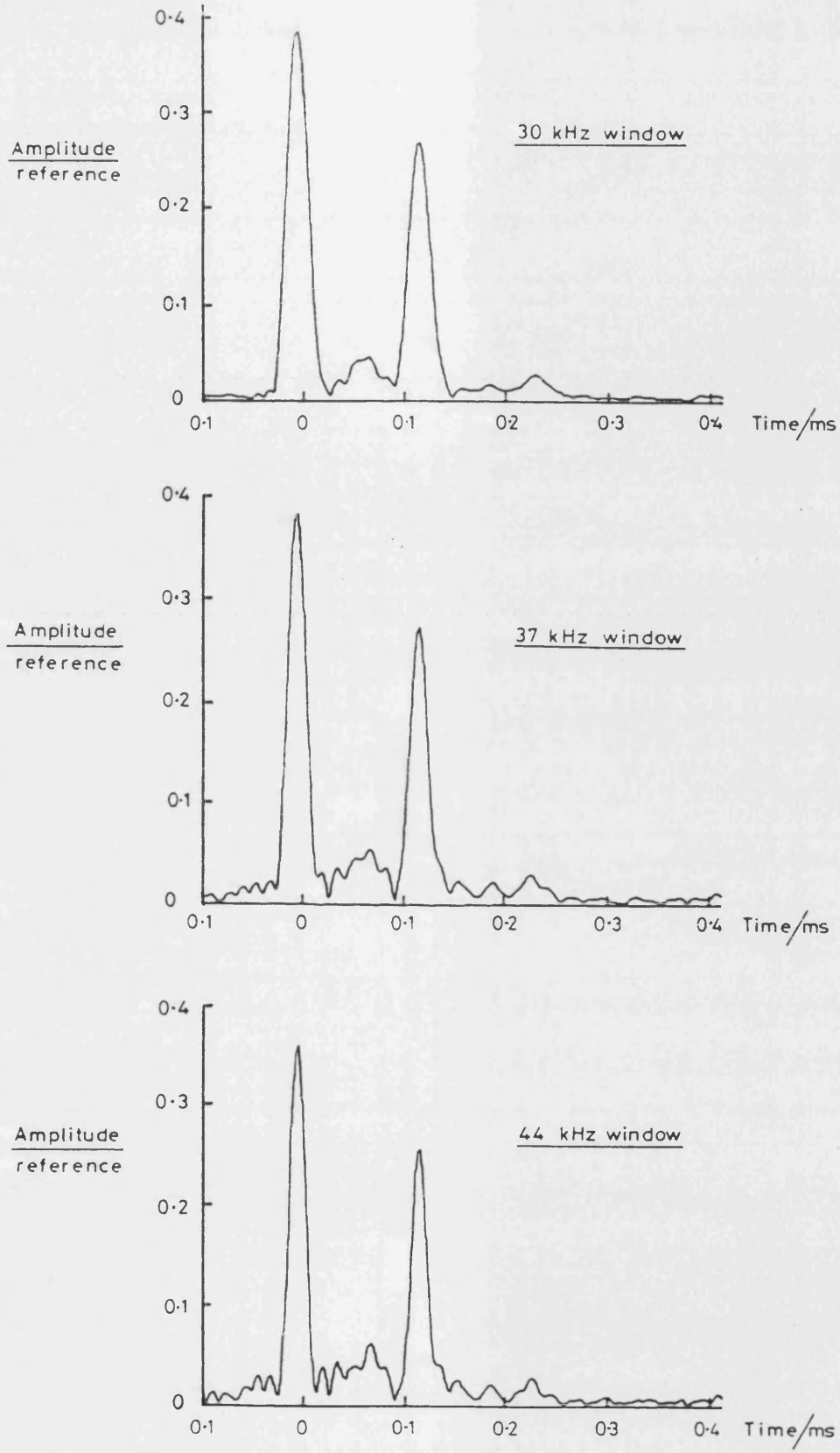

ONE LAYER DECONVOLUTIONS

(part 2 of 2)

Figure 5.3.1 (b)

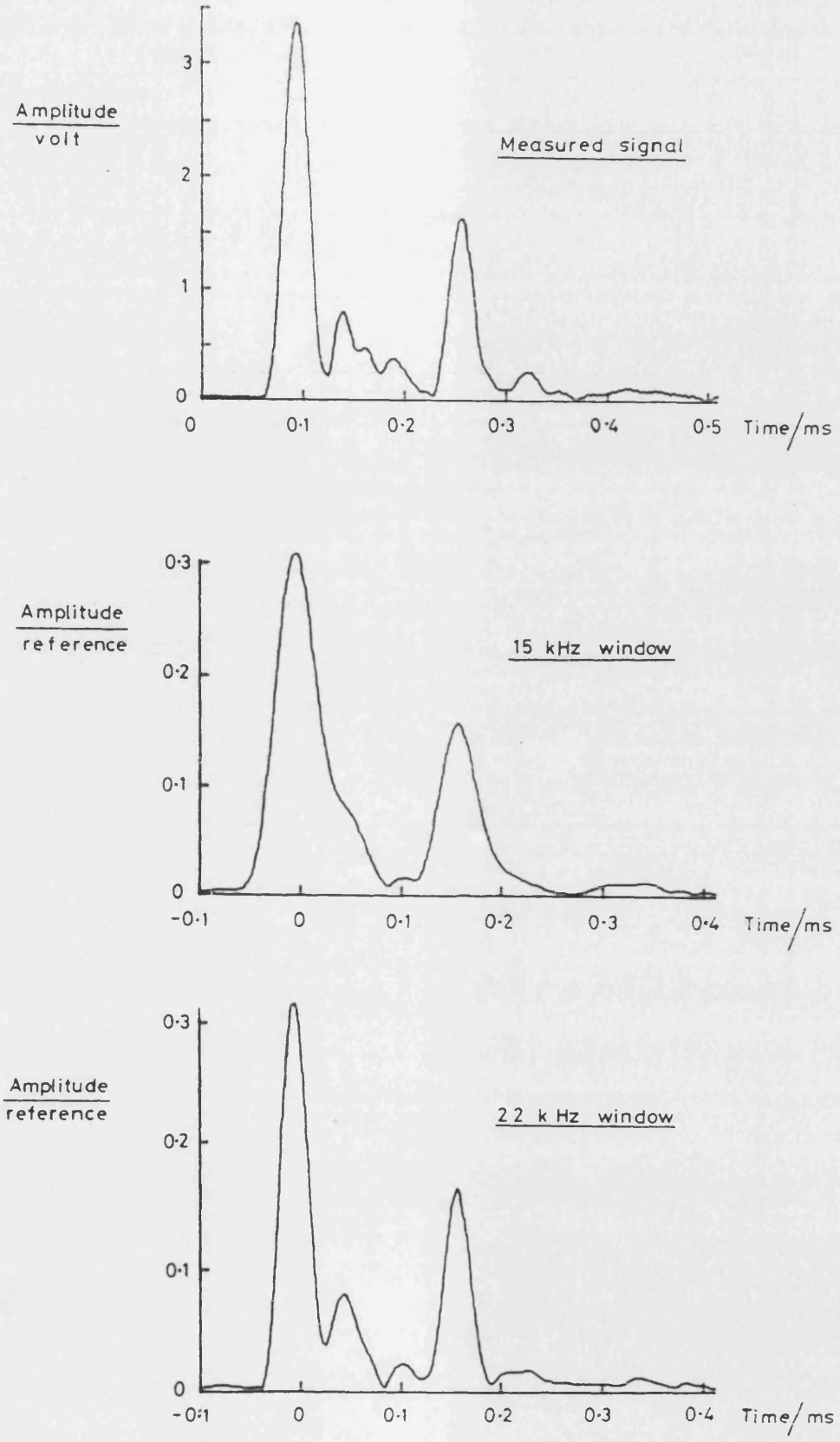

TWO LAYER DECONVOLUTIONS
(part 1 of 2)

Figure 5.3.2(a)

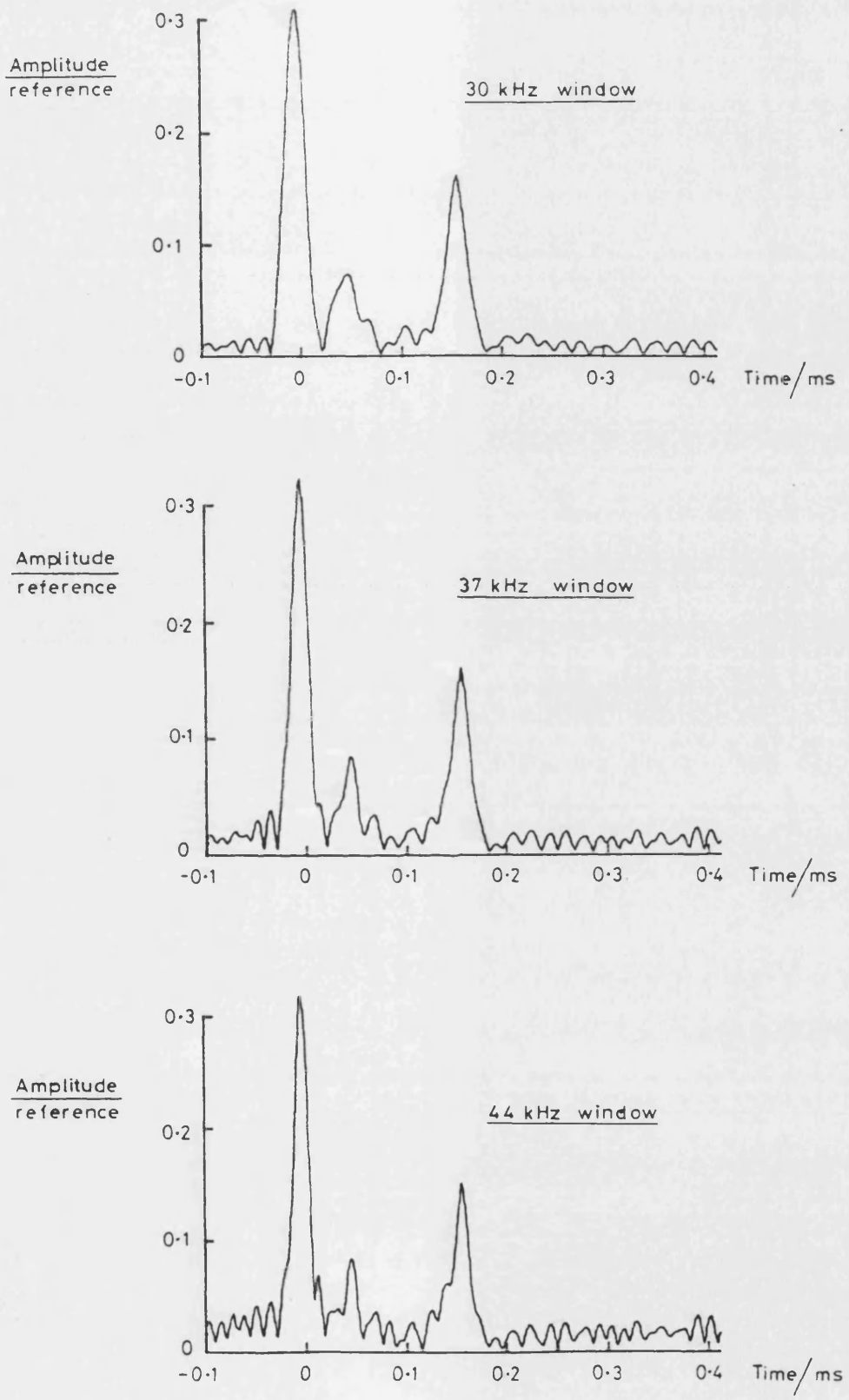

TWO LAYER DECONVOLUTIONS

(part 2 of 2)

Figure 5.3.2(b)

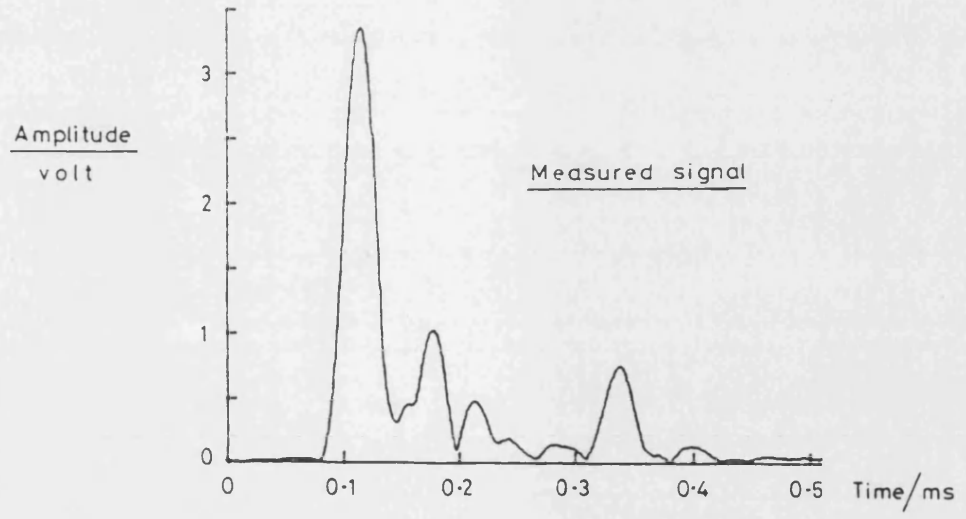

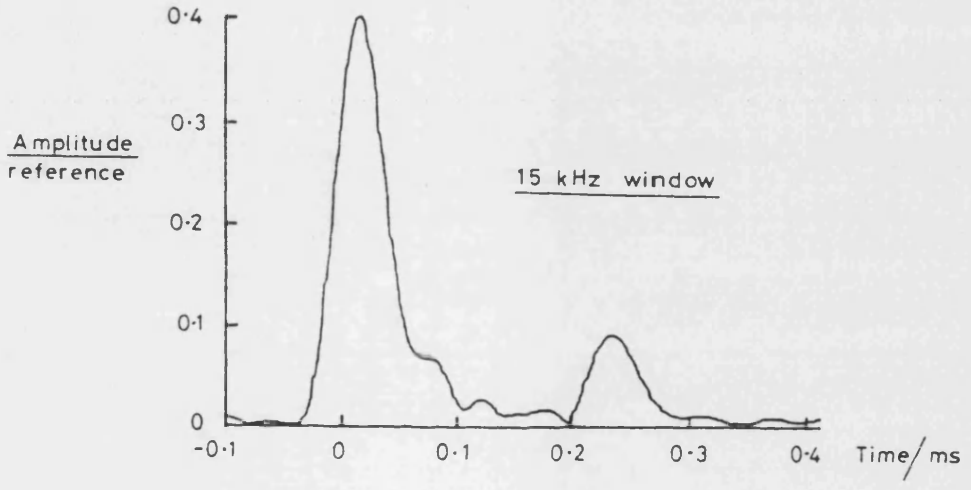

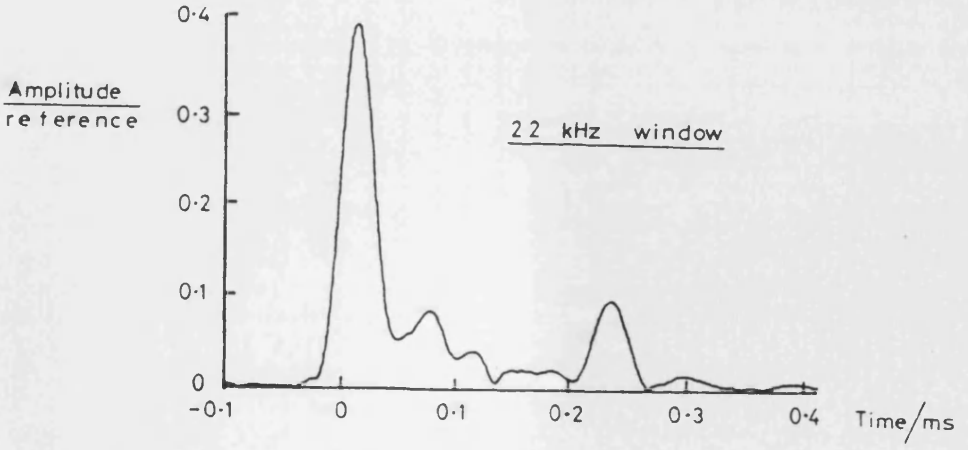

THREE LAYER DECONVOLUTIONS
(part 1 of 2)

Figure 5.3.3(a)

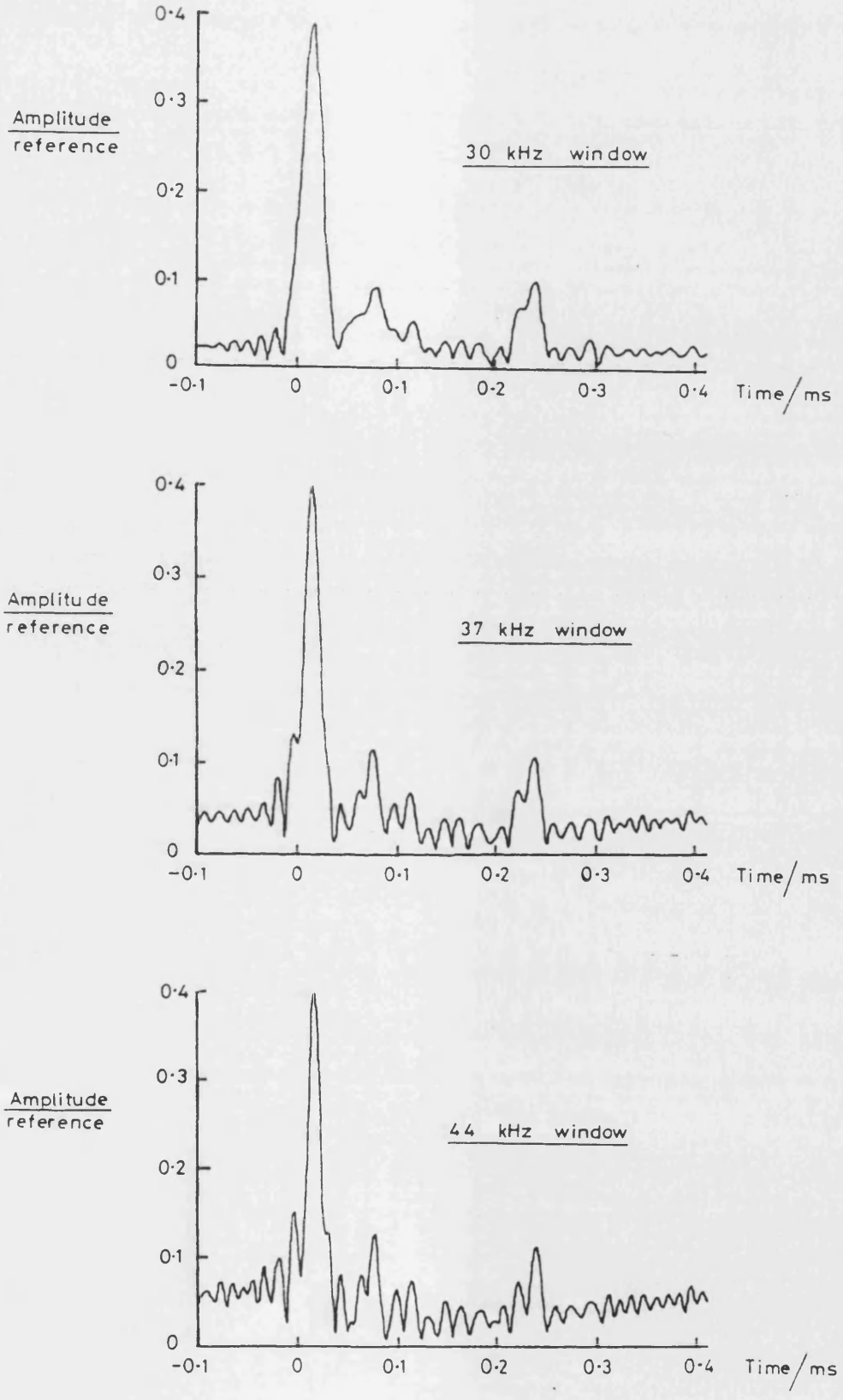

THREE LAYER DECONVOLUTIONS

(part 2 of 2)

Figure 5.3.3(b)

Primary return	Window width / kHz.				
	15	22	30	37	44
One Layer					
γ_1	0.402	0.404	0.388	0.376	0.357
γ_0	0.286	0.285	0.268	0.288	0.254
Two Layers					
γ_2	0.312	0.314	0.312	0.320	0.325
γ_1	*.***	0.077	0.074	0.084	0.085
γ_0	0.0158	0.162	0.164	0.161	0.154
Three Layers					
γ_3	0.396	0.390	0.386	0.391	0.400
γ_2	*.***	0.083	0.090	0.114	0.125
γ_1	0.026	0.039	0.050	0.089	0.075
γ_0	0.090	0.095	0.100	0.104	0.110

*.*** means the return is not resolveable.

DECONVOLVED AMPLITUDES

Figure 5.3.4

Reflection coefficient	Number of layers in each case			
	0	1	2	3
R_3	/	/	/	0.319
R_2	/	/	0.314	0.16
R_1	/	0.402	0.156	0.137
R_o	1 →	1 →	1 →	1
Attenuation in layer				
a_3^2	/	/	/	0.65
a_2^2	/	/	0.55 →	0.55
a_1^2	/	0.34 →	0.34 →	0.34

REFLECTION COEFFICIENTS
AND
ATTENUATIONS IN EACH LAYER

Figure 5.3.5

Acoustic impedance $\times 10^6$ Rayls	Number of layers in each case			Value calculated from Thomas and Pace[4]
	1	2	3	
Z_3	/	/	3.37	3.23
Z_2	/	2.83	2.44	2.69
Z_1	3.46	3.87	3.21	3.23
Attenuation coefficient (dBm^{-1})				
α_3	/	/	37	40
α_2	/	86	/	78
α_1	45	/	/	40

DERIVED ACOUSTIC IMPEDANCES AND ATTENUATION COEFFICIENTS

Figure 5.3.6

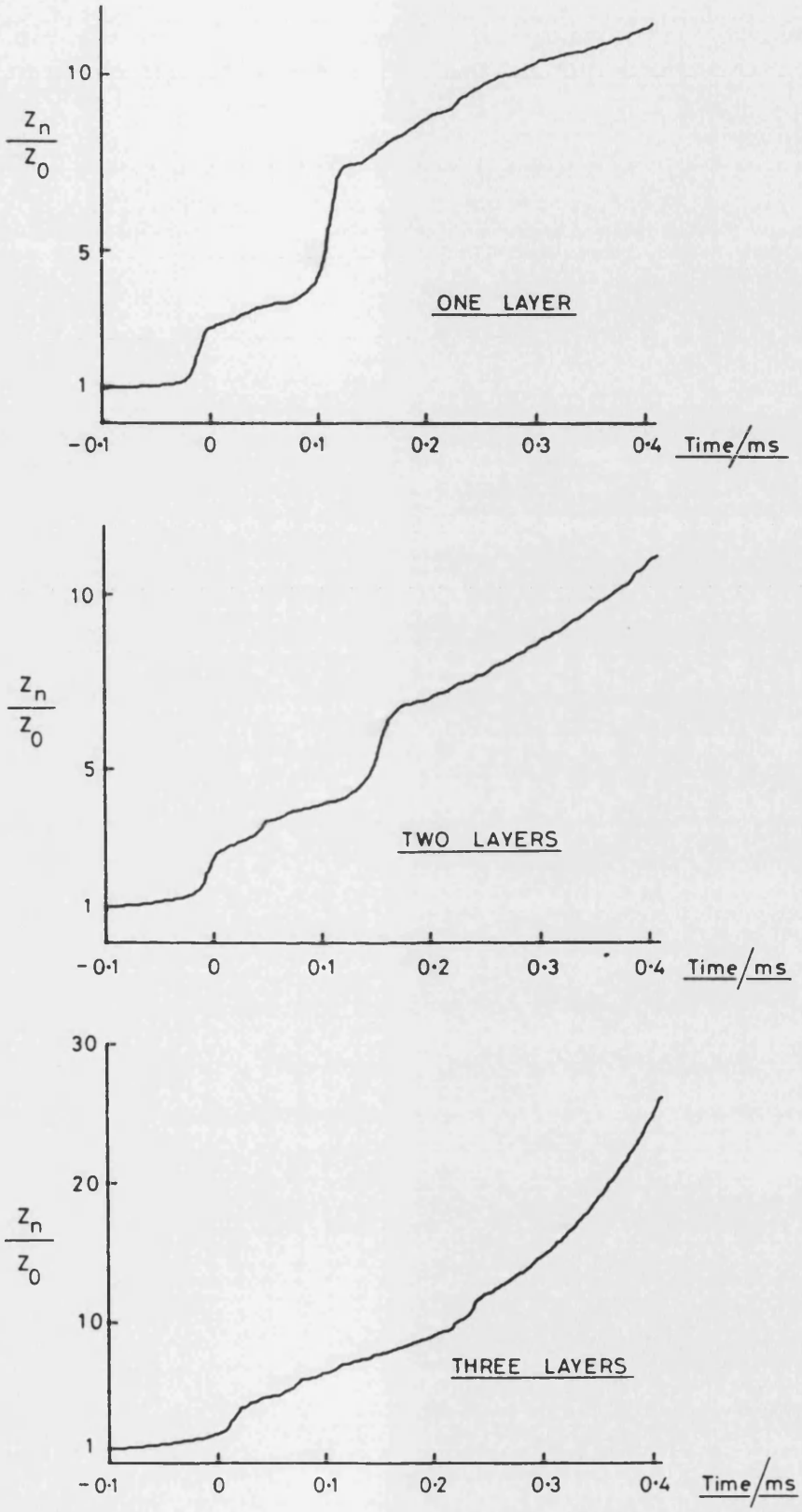

ACOUSTICORE RESULTS WITH
44 kHz WINDOW

Figure 5.4.1

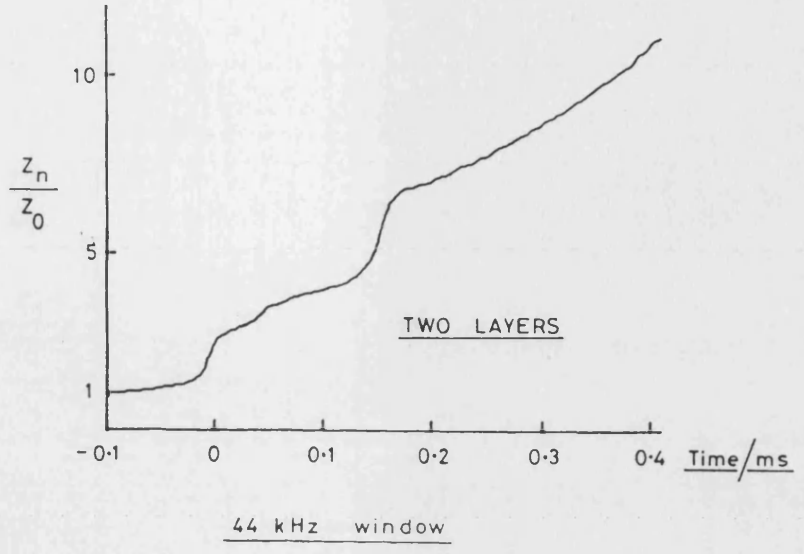

44 kHz window

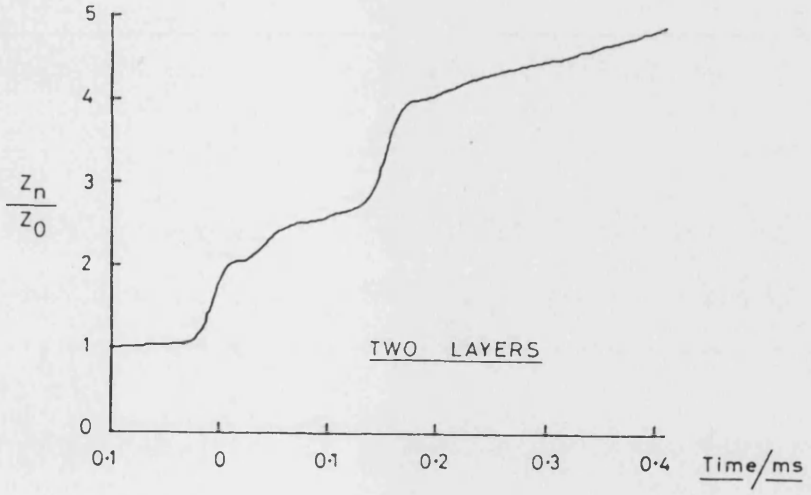

30 kHz window

ACOUSTICORE RESULTS WITH TWO DIFFERENT WINDOWS

Figure 5.4.2

Primary output	Deconvolved amplitude corresponding to primary output	Corrected for attenuation in each layer
1 layer		
γ_1	0.404	0.404
γ_0	0.285	0.84
2 layers		
γ_2	0.314	0.314
γ_1	0.077	0.14
γ_0	0.162	0.87
3 layers		
γ_3	0.390	0.390
γ_2	-0.083	-0.13
γ_1	0.039	0.11
γ_0	0.095	0.78

IMPULSE RESPONSES
CORRECTED FOR ATTENUATION

Figure 5.4.3

Interface number	Result of integration down to each interface	Deduced acoustic impedance of lower interface
1 layer		
1	0.404	3.32
0	1.244	17.8
2 layer		
2	0.314	2.77
1	0.454	3.67
0	1.324	20.9
3 layer		
3	0.39	3.23
2	0.26	2.49
1	0.37	3.10
0	1.15	14.8

NUMERICAL INTEGRATION RESULTS
AND
DEDUCED ACOUSTIC IMPEDANCES

Figure 5.4.4

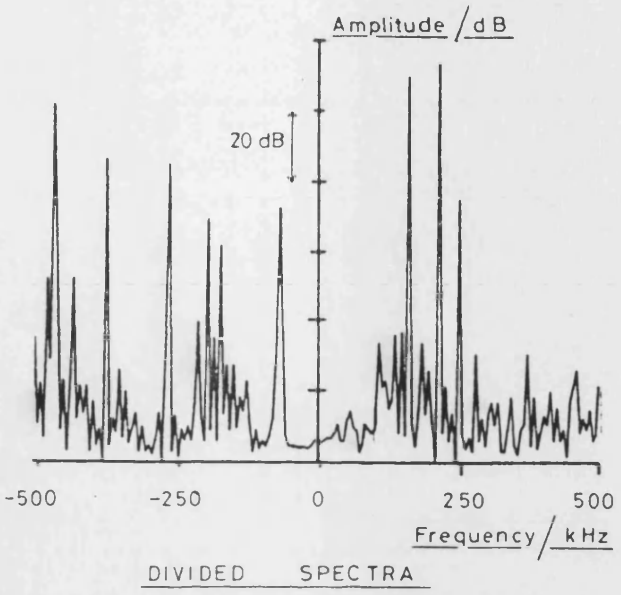

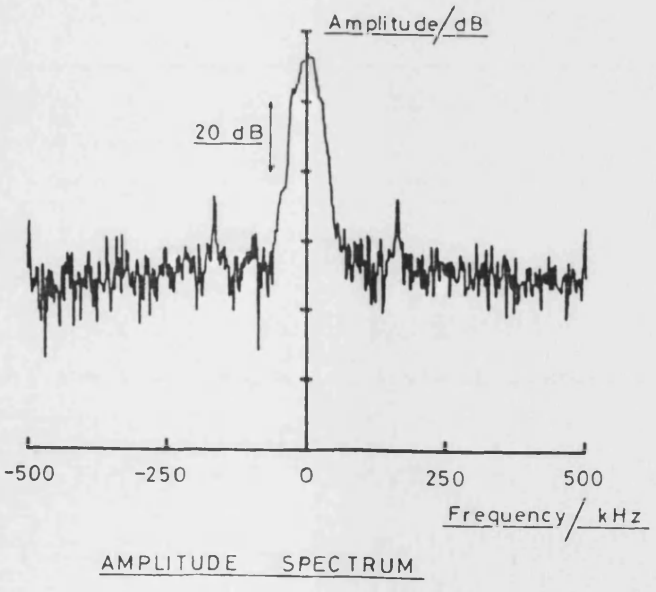

FREQUENCY DIVISION COMPARED WITH AMPLITUDE SPECTRUM

Figure 6.2.1

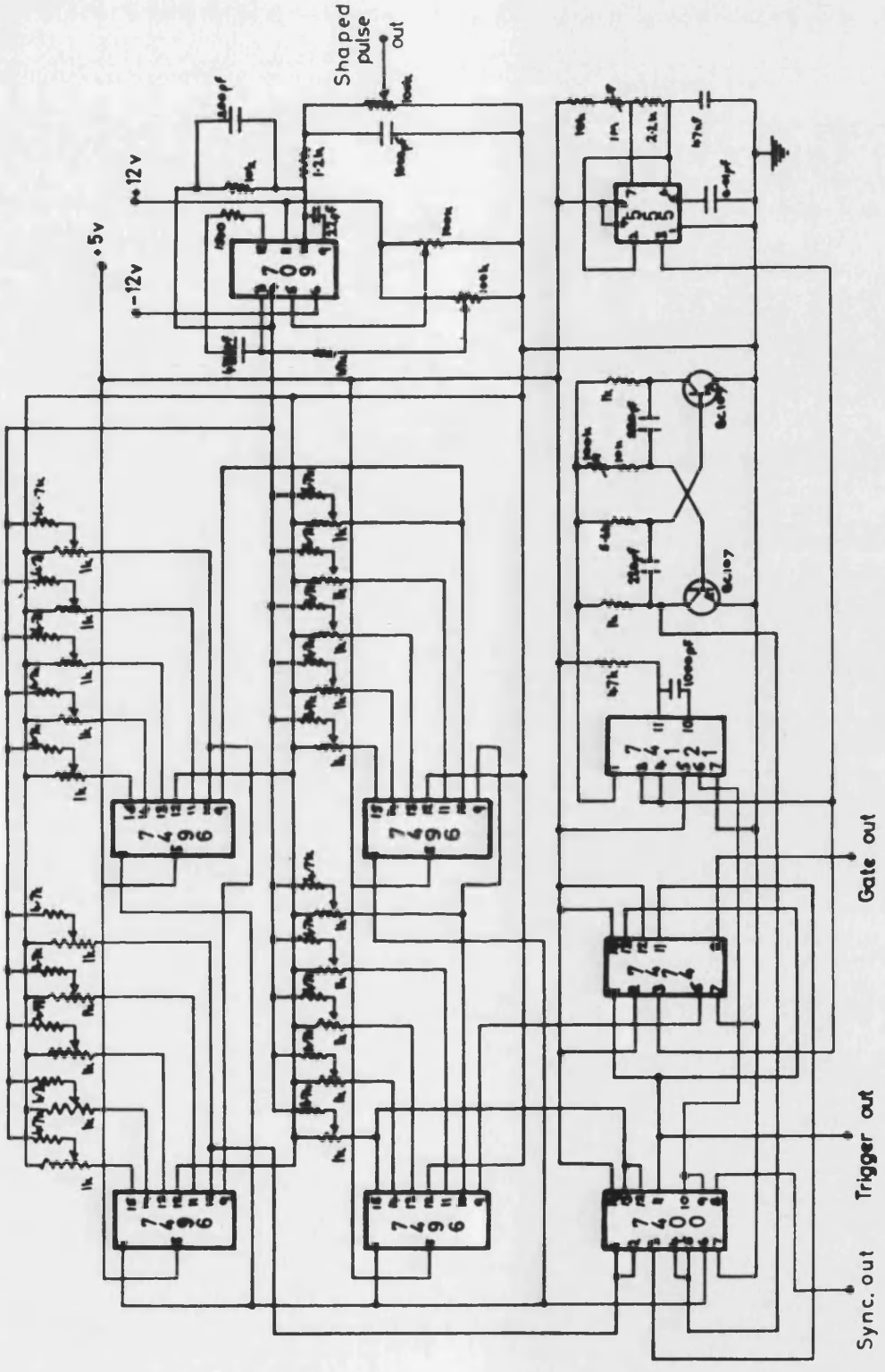

SHAPED PULSE GENERATOR

Figure A.1.1

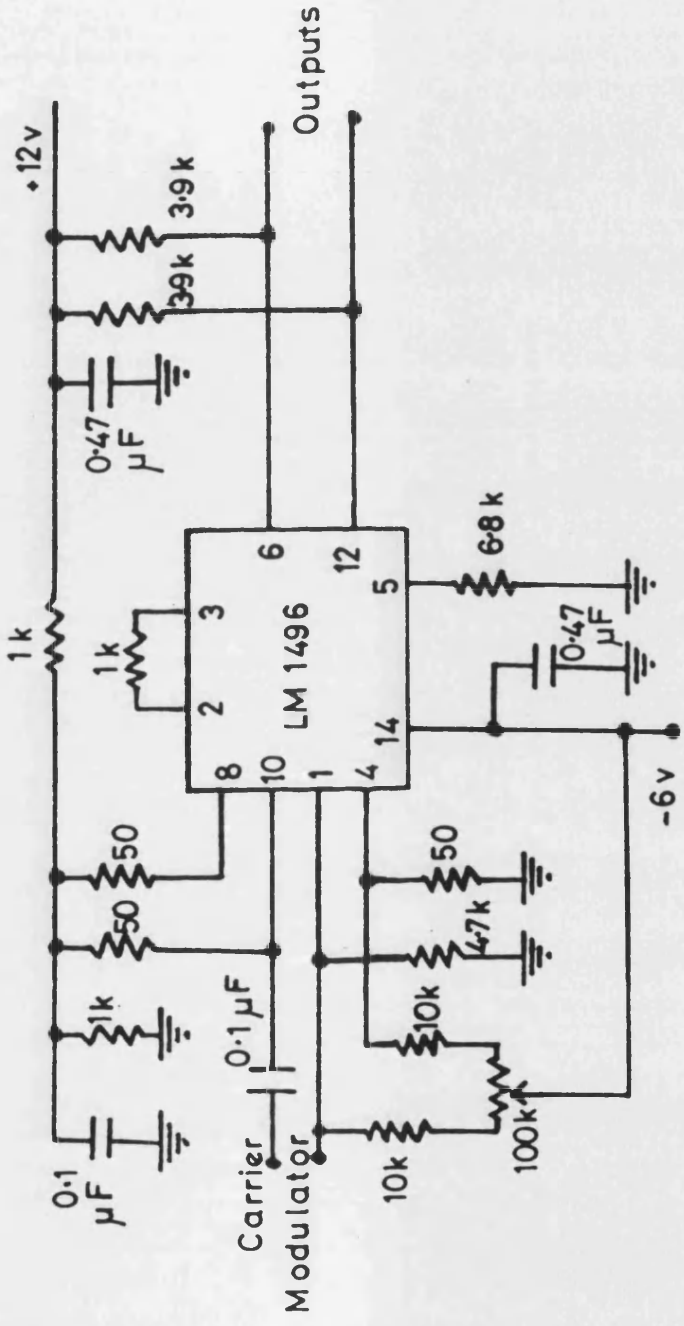

MODULATOR CIRUIT

Figure A.2.1

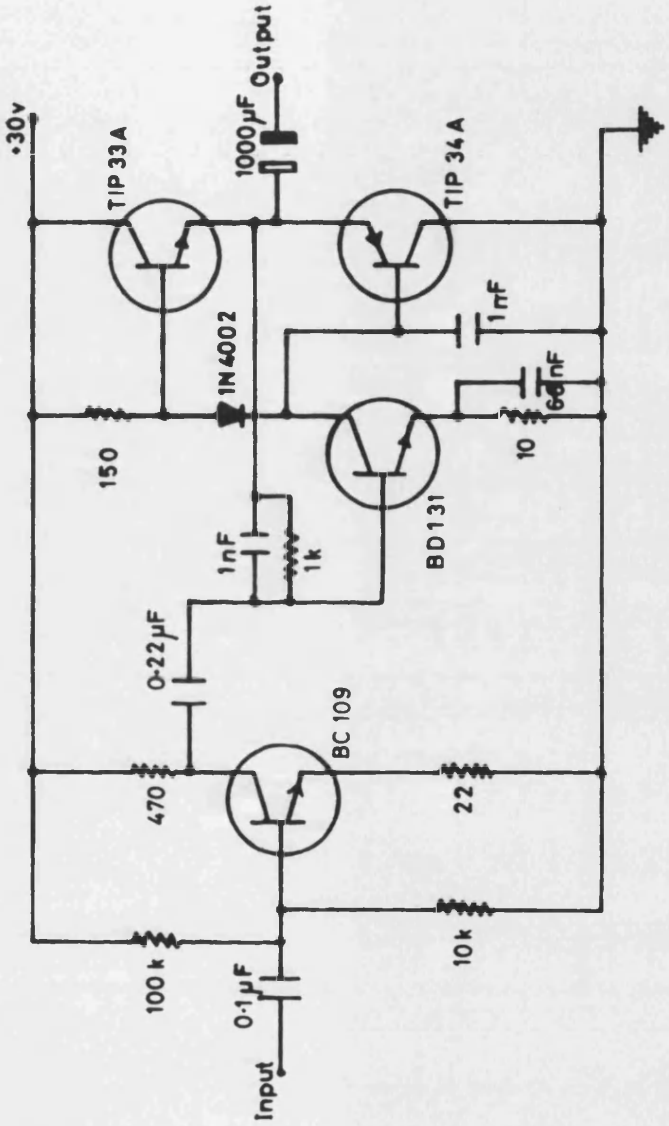

TRANSMITTING AMPLIFIER

Figure A.3.1

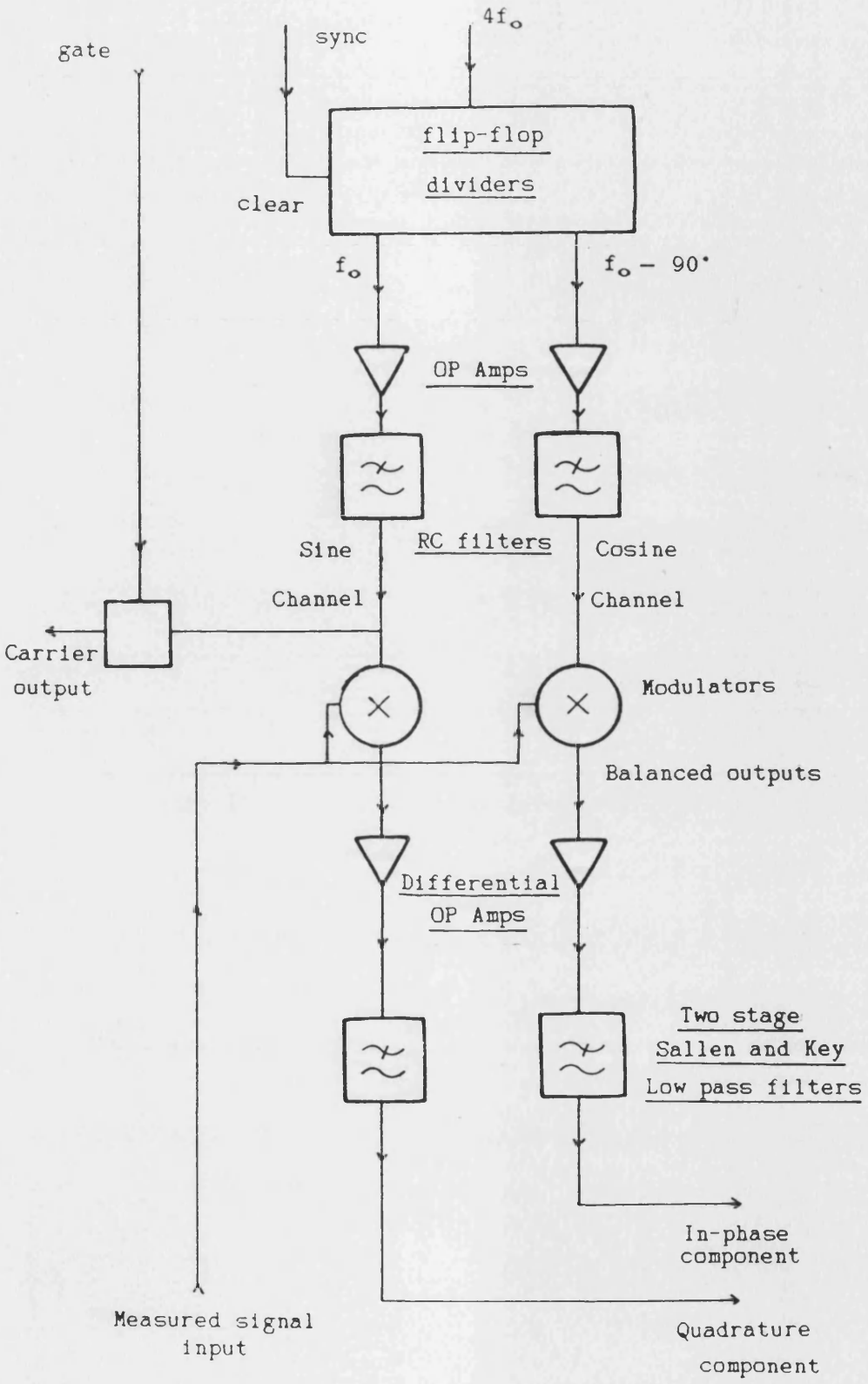

QUADRATURE DEMODULATION
BLOCK DIAGRAM

Figure A.4.1

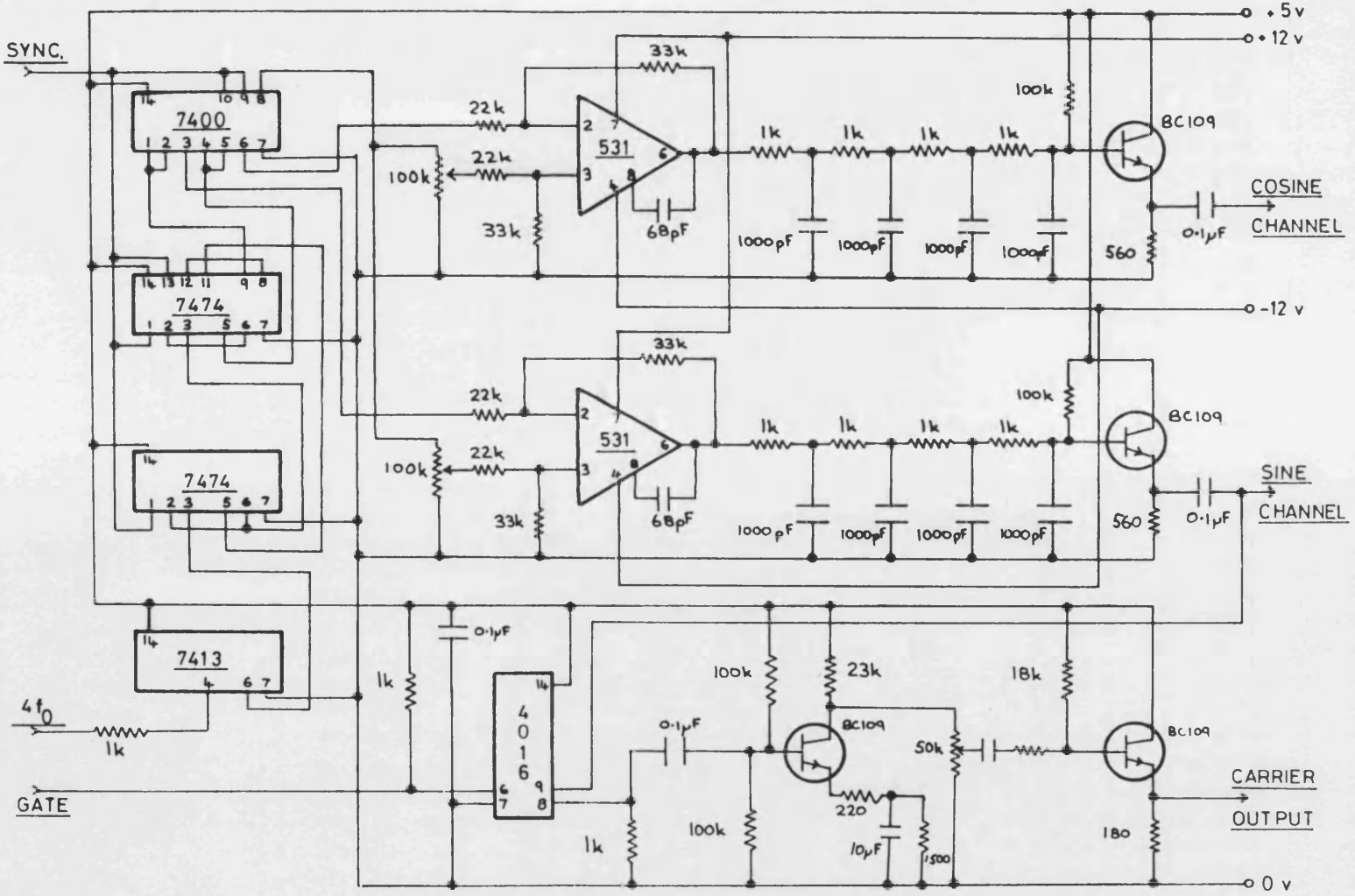

SINE AND COSINE GENERATION

Figure A.4.2

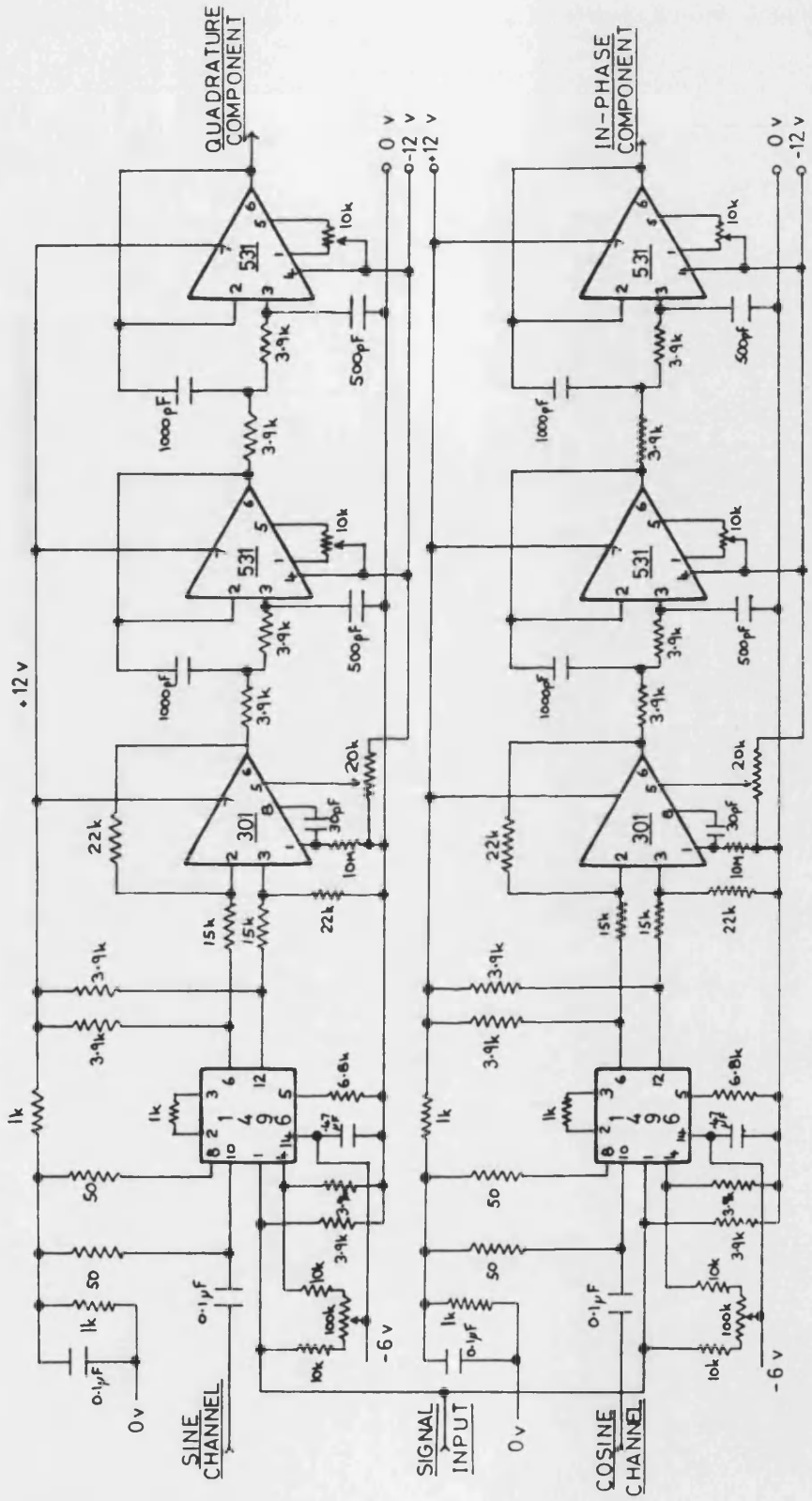

DEMODULATION AND FILTERING

Figure A.4.3

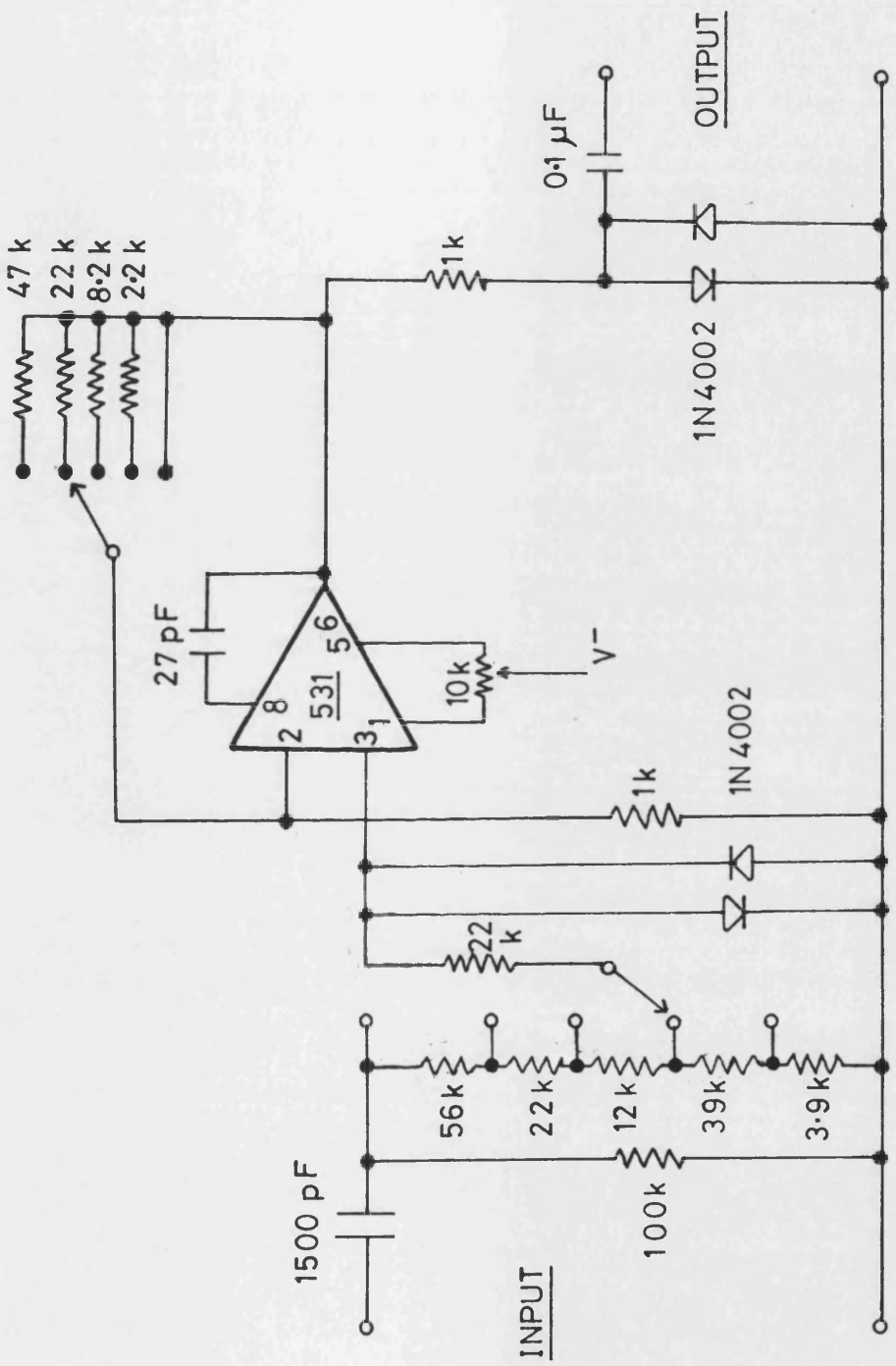

RECEIVING CIRCUIT

Figure A.5.1

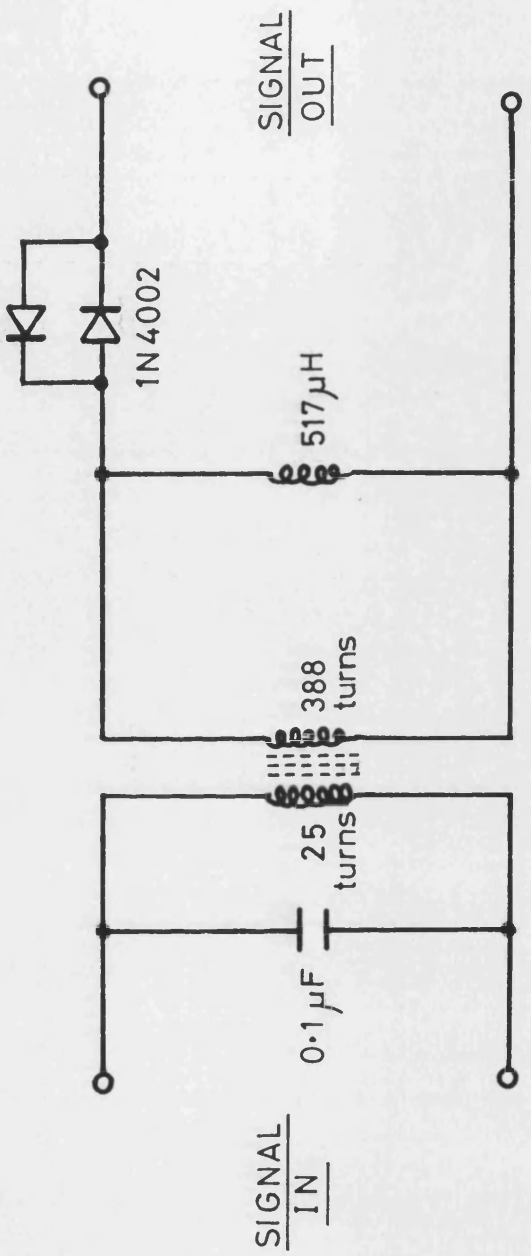

MATCHING TRANSFORMER

Figure A.6.1